# Sources, Interaction with Matter, Detection and Analysis of Low Energy Electrons

## SIMDALEE2017

Hotel Flamingo, Santa Margherita, Pula, Sardinia
September 18-22, 2017

Programme Schedule and Book of Abstracts

Edited by
Wolfgang S.M. Werner, Vytautas Astašauskas, Olga Ridzel

SOURCES INTERACTION WITH MATTER DETECTION AND ANALYSIS OF LOW ENERGY ELECTRONS 2

WWW.SIMDALEE2.NET

PEOPLE INITIAL TRAINING NETWORK
GRANT AGREEMENT 2013 | 606988

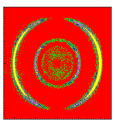

RoentDek Handels GmbH
Supersonic Gas Jets
Detection Techniques
Data Acquisition Systems
Multifragment Imaging Systems



SPECS™


FEI™

A.P.E. Research
NANOTECHNOLOGY

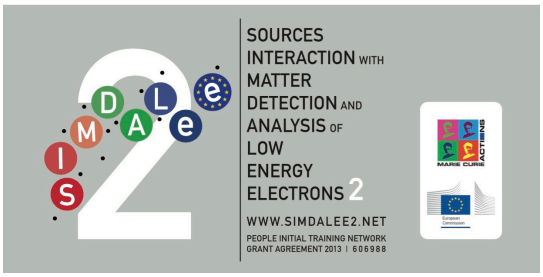



## Sponsors

| | |
|---|---|
| SPECS GmbH | www.specs.de |
| FEI | www.fei.com |
| EMS | www.eurmicsoc.org |
| IUVSTA | www.iuvsta.org |
| TESCAN | www.tescan.com |
| A.P.E. Research | www.aperesearch.com |
| RoentDek | www.roentdek.com |
| Vienna University of Technology | www.tuwien.ac.at |
| SIMDALEE2 | www.simdalee2.net |
| European Commission | ec.europa.eu/ |
| Marie Curie Actions | ec.europa.eu/research/mariecurieactions/ |

**SIMDALEE II consortium:**


## Table of Contents

## Welcome

Low Energy Electrons (LEE), how to create them, how to get rid of them, how to control them? Surprisingly, a subject in physics which is over a hundred years old, nowadays still poses challenges that are discussed in the community in a highly controversial fashion. In this connection, consider for example the simplest conceivable question one could ask in connection with electrons near solid surfaces: if one were to put a single electron with a certain kinetic energy inside a solid, how many will be ejected from the surface as a result? This essentially simple question of the Secondary Electron Yield (SEY) still awaits resolution.

On the other hand low energy electrons play an increasingly important role in many modern applications. For example low-energy SE may dramatically affect high-energy physics accelerators and storage rings through the multipacting phenomenon and the plasma-wall interaction in a fusion reactor. SE emission also plays a crucial role in the energy and charge balance of gaseous electronics such as plasma display panels or particle detection. In life sciences LEE are often the final product of ionising radiation interacting with biological tissue which actually induces DNA-damage. Hence the interaction of low energy electrons with matter is important for understanding tumour formation, but also therapy. Similarly, in semiconductor technology, in particular with the advent of VUV-lithography, the diffusion of LEE in matter represents a limiting factor. For the analysis of surfaces low energies are of increasing importance as well, as exemplified in a most impressive way in the Low Energy Electron Microscope (LEEM).

Since a number of fundamental questions regarding LEE need to be addressed to advance the applications mentioned above, the present meeting constitutes an ideal event since it brings together a number of renowned specialists in various fields related to these subjects using different approaches and focusing on different aspects such as Secondary Electron Emission and Electron-Solid Interaction, Correlation Spectroscopy on Surfaces using electron pairs, Photo- & Field-Emission, Electron Microscopy and Spectroscopy Scanning Probe Microscopy, Nanotechnology and Biomaterials their Interaction with LEE as well as Spin and Magnetism. The above considerations have given birth to the SIMDALEE2-consortium which is funded by the Research and Executive Agency of the European Commission through a Marie-Curie initial training network in the framework of which the present conference is organized.

The workshop venue provides an ideal ambient for intensive discussion among the participants on the above topics and on the basis of the abstracts compiled in this book it is to be expected that the workshop will provide a scientifically as well as socially exciting week.

The SIMDALEE2017 organising committee wishes all participants of the SIMDALEE2017 workshop a fruitful conference and an enjoyable stay in Sardinia.

Wolfgang Werner
Olga Ridzel
Vytautas Astašauskas
Ernst-Dieter Janotka

## Plenary Lecture

| | | |
|---|---|---|
| Ernst Bauer | US | Low Energy Electron Microscopy |

## Invited Speakers

| | | |
|---|---|---|
| Roberto Cimino | I | Low-Energy Secondary Electron Yield (LE-SEY) of conductive surfaces |
| Anika Schlenhoff | D | Spin-polarized Scanning Field Emission Microscopy and Spectroscopy of Non-collinear Spin Textures and Atomic- Scale Magnets |
| Roland Feder | D | Creation of entangled electrons by scattering at surfaces |
| Frank Oliver Schumann | D | Frontiers in low energy electron pairs emission |
| Isabel Montero-Herrero | E | Secondary electron emission |
| Gerd Schönhense | D | Rapid 3D Mapping of Fermi Surface, Fermi Velocity and Spin Texture |
| Peter Schattschneider | A | Magnetic Circular Dichroism in EELS |
| Leonhard Grill | A | Imaging and manipulation of single molecules by scanning probe microscopy: Wires, switches and motors |
| Andrew Bass | CAN | Low energy electron induced synthesis and degradation in simple molecular solids and biomolecular targets |
| Christopher Chantler | AUS | Novel Plasmon-Coupling Theory of the Electron Inelastic Mean Free Path |

## Organising Committee

| | |
|---|---|
| Wolfgang Werner | Ernst-Dieter Janotka |
| Vytautas Astasauskas | Olga Ridzel |
| | (Vienna University of Technology, A) |
| Sabrina Masur | (University of Cambridge, UK) |
| Alessandra Bellissimo | (Universita Roma Trè, I) |
| Marzia Fantauzzi | (University of Cagliari, I) |
| Ashish Suri | (University of York, UK) |

## Scientific Committee

| | |
|---|---|
| Prof. Wolfgang Werner | Prof. Mehmet Erbudak |
| Prof. Rafal Dunin-Borkowski | Dr. Ilona Müllerova |
| Prof. Giovanni Stefani | Prof. Antonella Rossi |
| Dr. Kevin Jensen | Prof. Jürgen Kirschner |

## Contact

| | |
|---|---|
| SIMDALEE2017 | Conference Office: |
| Verkehrs Büro Bussiness Travel | Mrs. Helene Perlini |
| Helene.Perlini@verkehrsbuero.at | tel:+43-664-6258214 (during SIMDALEE2017 ) |

http://www.iap.tuwien.ac.at/www/simdalee2017/index

## SIMDALEE2017 Venue

The venue of the conference is set in Santa Margherita di Pula, on the south tip of Sardinia. The Hotel Flamingo Resort has a congress centre consisting of two of the few beach hotels in South Sardinia directly by the sea, where you can find a beach with pure white sand which is only a few steps away from the rooms of the hotel.

### Address

Hotel Flamingo Resort
SS 195, Km 33,800
09010 Santa Margherita di Pula (Cagliari) Sardegna, Italia
http://www.hotelflamingosardinia.com

### Travel information

We advise all participants to plan their flight to Cagliari Airport, for it is by far the closest airport to the venue. The other two airports ( Alghero-Fertilia/Riviera del Corallo Airport Olbia-Costa Smeralda Airport) may be advantageous only if a vacation before or after the conference is scheduled.

Transport from Cagliari airport to the conference venue is most conveniently (and at a low price) done by means of the **shuttle service** which has been organised for the participants. Please visit http://www.iap.tuwien.ac.at/www/simdalee2017/travel for further information. Download complete and return the form for the shuttle service to Mrs Perlini and you will be picked up/brought back to Cagliari Airport.

The airport is located 7km northwest of Cagliari, transit from the airport to the city center takes only 10 to 15 minutes. **Buses** offer the cheapest option of transport with a one-way ticket costing approx. €1. There are two bus stations within Cagliari Airport. The first is located outside the arrivals area and buses operate from 8.40 in the morning to 11.30 at night. The second stage is outside the departures area. Here the first bus is at 5.20 am and a bus departs every half hour until 10.30 pm. Take bus line 160 for the city center. From the main bus station on Piazza Matteotti in Cagliari, ARST buses serve nearby Pula (€3, duration 50 minutes, departures hourly, bus line 129). We expect the reliability of the shuttle service organised by us to significantly exceed the quality of the bus service. While it is the cheapest option, it may be more tedious.

**Taxis** are available at the taxi ranks outside the terminal and are considerably more expensive than the shuttle service. The price for a one-way trip from the airport to the Hotel Flamingo range from: €60 - €90 (£55 - £70).

### Weather

The weather in Sardinia in September is usually still quite warm (15°C lows, 20-30°C highs) and relatively dry. Occasional precipitation is possible.

### Language

The workshop language is english.

### Insurance/Disclaimer

The organisers cannot accept any liability or responsibility for death, illness, or injury to the person or for loss of or damage to property of participants and accompanying persons which may occur either during or arising from the workshop. Participants are advised to make their own arrangements with respect of health and travel insurance.

## Social Programme

### Welcome reception

A welcome reception will take place before the plenary lecture on monday afternoon outside (if the weather permits it) on the lawn next to the pool area

### Get together & Whisky degustation

After dinner on monday an informal get-together will take place (at a location to be announced) during which the participants will have the opportunity to try out different types of (Scottish) whisky, from mild and clear aroma to heavily smoked medicinally peated ones.

### Excursion

A conference outing will be organised to visit one of the more than 3000 year old Phoenician settlements in Sardinia at the site of Nora. From there a short bus ride will take us to one of the most beautiful beaches of the island, Chia, where we will have a drink and a swim. Don't forget to bring your beach wear!!!

### Conference Dinner

On the evening after the conference excursion, gala-dinner with subsequent party will take place in the wild-duck restaurant in the eucalyptus forest between the Hotel Flamingo and the neighbouring hotel Pineta Mare.

## Scientific Programme

### Oral Presentations

Oral presentations have a duration of 15 min including discussion (30 min for invited talks). The lecture room has a PC (running windows) prepared for projection using a beamer. You can also bring your own laptop (e.g. an Apple Macintosh) and connect it to our system before the beginning of the session featuring your presentation. If you bring a file of your presentation instead (e.g. a powerpoint- or PDF-file) you should upload and test it well in advance of your presentation.

### Poster Presentations

A poster session will be held in the lecture room on Wednesday afternoon. Poster panels are A0 in size. Posters can be mounted on Tuesday and can be left hanging during the entire workshop. The presenting authors are encouraged to give a 1 min-/1 slide-"flash"-presentation about their posters before the Poster session starts.

# Scientific Programme

## Monday, September 18$^{th}$

| | |
|---|---|
| 12:00-13:00 | Lunch |
| 13:00-14:00 | Free time |
| 14:00 | Start Registration |
| 14:30-16:00 | SIMDALEE2-meeting |
| 16:30-17:00 | Welcome Reception |

**Session 0:** Scientific Perspective
Session Chair: *Wolfgang S. M. Werner*

---

| | |
|---|---|
| 17:00-17:10 | Opening address<br>*Wolfgang S. M. Werner* Institute of Applied Physics, Vienna University of Technology |
| 17:10-17:20 | Presentation of the EC-Marie Skłodowska Curie Programme<br>*Vojko Bratina, Research Executive Agency of the European Commission* |
| 17:20-18:30 | Plenary Lecture: Low Energy Electron Microscopy<br>*Ernst Bauer* Department of Physics, Arizona State University, Tempe, Arizona, USA |
| 18:30-19:30 | Free time |
| 19:30-20:30 | Dinner |
| 20:30-22:00 | Get-Together and (voluntary) Whisky degustation |

## Tuesday, September 19$^{th}$

**Session 1:** Inelastic mean free path/secondary electron yield
Session Chair: *Urs Ramsperger*

---

| | |
|---|---|
| 8:30-9:00 | **Novel Plasmon-Coupling Theory of the Electron Inelastic Mean Free Path**<br>*C. T. Chantler* School of Physics, The University of Melbourne, Melbourne, Vic, Australia |
| 9:00-9:15 | **Model sensitivity of Monte Carlo simulation of SEM images**<br>*K. T. Arat* Dept. of Imaging Physics, Delft University of Technology, Delft, the Netherlands |
| 9:15-09:30 | **What's next in Scanning Low Energy Electron Microscopy?**<br>*I. Müllerová* Institute of Scientific Instruments of the CAS, v. v. i., Brno, Czech Republic |
| 10:00-10:30 | Coffee-break |

**Session 2:** Secondary electron yield
Session Chair: *Ilona Müllerová*

---

10:30-11:00 **Low-Energy Secondary Electron Yield (LE-SEY) of conductive surfaces**
*R. Cimino* LNF-INFN, Frascati, Roma, Italy

11:00-11:15 **Investigation of the secondary electron yield of copper surfaces in particle accelerators**
*V. Petit, H. Neupert, E. Garcia Tabares, M. Taborelli, M. Belhaj, T. Paulmier* CERN, European Organization for Nuclear Research, Geneva, Switzerland

11:15-11:30 **Secondary Electron emission from graphene based materials**
*P. Riccardi* Dipartimento di Fisica, Universitá della Calabria and INFN- Gruppo collegato di Cosenza, Arcavacata di Rende, Cosenza, Italy

11:30-11:45 **Transmission electron yield simulations of tynodes**
*A. M. M. G. Theulings, J. Hidding, C. W. Hagen, H. van der Graaf*
Delft University of Technology, Delft, The Netherlands

12:00-13:00 Lunch

**Session 3:** Scanning probe microscopy
Session Chair: *Stefano Prato*

---

13:00-13:30 **Imaging and Manipulation of Single Molecules by Scanning Probe Microscopy: Wires, Switches and Motors**
*L. Grill* Department of Physical Chemistry, University of Graz, Austria

13:30-13:45 **STM and NC-AFM investigations of Graphene on Ir(111)**
*V. Simic-Milosevic, Y. Dedkov, A. Thissen* SPECS Surface Nano Analysis GmbH, Berlin, Germany

13:45-14:00 **Observation of Metal Nucleation on Freestanding Graphene by Means of LEEPS Microscopy**
*M. Lorenzo, C. Escher, T. Latychevskaia and H.-W. Fink* Department of Physics, University of Zürich, Zürich, Switzerland

14:00-14:15 **Charge-transfer plasmonics in self-organising metal-semiconductor-metal structures**
*B.J. Murdoch, A.J. Barlow, J.F. Portoles, S. Tardio, I.W. Fletcher, P.J. Cumpson* National EPSRC XPS Users Service (NEXUS), School of Mechanical and Systems Engineering, New-castle University, Newcastle upon Tyne, Tyne and Wear, UK

14:30-15:00 Coffee-break

**Session 4:** Coincidence spectroscopy
Session Chair: *Ottmar Jagutzki*

15:00-15:30 **Frontiers in low energy electron pair emission**
*F. O. Schumann* Max-Planck Institute of Microstructure Physics, Halle, Germany

15:30-15:45 **Low Energy Electron Emission Resulting from Auger Transitions Initiated by Deep Holes in the Valence Band of Graphene**
*A.H. Weiss, V.A. Chirayath, V. Callewaert, A.J. Fairchild, M.D. Chrysler, R.W. Gladen, S.K Imam, R. Saniz, B. Barbiellini, K. Rajeshwar, B. Partoens* The University of Texas at Arlington

15:45-16:00 **Spectra of correlated many-electrons systems: from a one- to a two-particle description**
*O. Gunnarsson, J. Merino, T. Schäfer, G. Sangiovanni, G. Rohringer, A. Toschi* Russian Quantum Center, Skolkovo, Moscow, Russia

16:00-16:30 Flash Poster Presentation

16:30-19:30 Free time

19:30-20:30 Dinner

20:30-22:30 **Session 5:** Poster Session

**Overlayer thickness determination based on XPS no-loss peaks ratio**
*V. Afanas'ev, P. Kaplya, D. Efremenko* National Research University "Moscow Power Engineering Institute", Moscow, Russia

**Principles of low energy electron interactions with simple molecular solids and condensed biomolecules**
*A. D. Bass and L. Sanche* Départment de Médecine Nucléaire et Radiobiologie, Faculté de Médecine et des Sciences de la Santé, Université de Sherbrooke, Sherbrooke, Québec, Canada

**Experimental investigation of electron emission yield of layered surfaces**
*M. Belhaj, S. Dadouch, D. Payan* ONERA-The French Aerospace Lab, Toulouse, France

**Unraveling relevance of the different electron generation mechanisms to the Total Electron Yield**
*A. Bellissimo, G. Stefani, H. Neupert, M. Taborelli* Dipartimento di Scienze, Universitá Roma Tre, Rome, Italy

**Spin Polarized Imaging with Scanning Field Emission Microscopy**
*G. Bertolini, L.G. De Pietro, O. Gürlü, D. Pescia, U. Ramsperger* Laboratory for Solid State Physics, EHT Zürich, Zürich, Switzerland

**Elimination of spherical and axial chromatic aberrations of the electron microscope lens**
*S.B. Bimurzaev, E.M. Yakushev* Almaty University of Power Engineering and Telecommunications, Almaty, Kazakhstan

**Comparative study of apparent barrier height and local surface potential by ambient scanning probe microscopy**
*M. Demydenko, A. Varlec, D. Cassese, D. Kostiuk, J. Ivanco, E. Majkova, S. De Monte, S. Prato* A.P.E. Research, Area Science Park, Basovizza Campus, Trieste, Italy

**Comparison of Low Energy Electron Emission Resulting from Deep Valence Hole Auger Transitions in Graphene on Cu, Highly Oriented Pyrolytic Graphite (HOPG), and Graphene on Si**
*A.J. Fairchild, V.A. Chirayath, S.K. Imam, M.D. Chrysler, R.W. Gladen, A.R. Koymen, A.H. Weiss* The University of Texas at Arlington, Arlington, USA

**Energy Spectrum of Low Energy Electrons Emitted from a Ag(100) Surface as a Result of NVV Auger Transitions**
*M. R.W. Gladen, P.V. Joglekar, K. Shastry, Q. Dong, S.L. Hulbert, R. A. Bartynski, W.S.M. Werner, A.H. Weiss* The University of Texas at Arlington, Arlington, USA

**Modelling entire XPS spectra of core-shell nanoparticles for the calculation of shell thicknesses and core radii**
*M. Hronek, H. Kalbe, J. Pseiner, C.J. Powell, W.S.M. Werner* Vienna University of Technology, Vienna, Austria

**A secondary electron emission empirical model**
*C. Inguimbert, J. Pierron, M. Belhaj, J. Puech* Onera, 2 av. Edouard Belin Toulouse, France

**The effect of structural disorder on the secondary electron emission of graphitic materials**
*R. Larciprete, L.A. Gonzalez, A. Di Trolio, D. R. Grosso, R. Cimino* LNF-INFN, Frascati, Roma, Italy

**Spin-Polarized Metastable Helium Atoms as a Probe of Surface Electronic and Magnetic Structure**
*A. Pratt, M. Kurahashi, Y. Yamauchi* Department of Physics, University of York, York, UK

**Cathodoluminescence of AlGaN/GaN Using Monte Carlo Simulation. Effect of Temperature and Compositional**
*A. Redha, L. Lazhar, N. Abdelkader* Thin Films and Interfaces Laboratory, University of Fréres Mentouri Constantine, Constantine, Algeria

**Low energy (1-50 eV) inelastic mean free path (IMFP) values estimated from experimental results using Monte Carlo calculations**
*O. Ridzel, W.S.M. Werner, V. Astašauskas*
Vienna University of Technology, Vienna, Austria

**Effect of axial aberrations on the degree of coherence in SEM**
*T. Řihaček, I. Müllerová* Institute of Scientific Instruments of the CAS, v. v. i., Brno, Czech Republic

**Investigation of the long-term behavior of the work function and the quantum efficiency of surfaces by photoelectron spectroscopy**
*K. Schönung, M. Wecker* Max Planck Institute for Nuclear Physics, Heidelberg, Germany

**The Bessel box Electron Energy Analyser in the Scanning Electron Microscope**
*A. Suri, S.P. Tear, C.G.H. Walker, A. Pratt, M.M. El Gomati* Dept. Electronics, University of York, Heslington, York, UK

**The variation in the Transport Mean Free Path for electrons at low energy for different atomic potential models**
*C.G.H. Walker, S.P. Tear, A. Pratt, M.M. El Gomati* Dept. Physics, University of York, Heslington, York, UK

## Wednesday, September $20^{th}$

**Session 6:** Scanning field microscopy
Session Chair: *Seyno Sluyterman*

---

08:30-09:00 **Spin-polarized Scanning Field Emission Microscopy and Spectroscopy of Non-collinear Spin Textures and Atomic-Scale Magnets**
*A. Schlenhoff* Institute for Nanostructure- and Solid State Physics, University of Hamburg, Germany

09:00-09:15 **Exact Eigenstates of a Nanoscopic Paraboloidal Emiter: A Calculation of Field Emission Quantities**
*A. Chatziafratis, G. Fikioris, J.P. Xanthakis* National Technical University of Athens, Electrical and Computer Engineering Department, Athens, Greece

09:15-09:30 **Scanning Field-Emission Microscopy with Polarization Analysis**
*U. Ramsperger, L.G. De Pietro, G. Bertolini, D.A. Zanin, H. Cabrera, J. Zhou, O. Gürlü, S. Nayir, A. Vindigni, T. Bähler, D. Pescia* Laboratory for Solid State Physics, ETH Zürich, Zürich, Switzerland

09:30-09:45 **Improving the accuracy of modelling field emission into vacuum**
*S. M. Masur, C. J. Edgcombe, G. Constantinescu, G. Csanyi, C. H. W. Barnes* Department of Physics, University of Cambridge

10:00-10:30 Coffee-break

**Session 7:** Nanotechnologies
Session Chair: *Maja Remskar*

---

10:30-11:00 **Principles of low energy electron interactions with simple molecular solids and condensed biomolecules**
*A. D. Bass, L. Sanche* Départment de Médecine Nucléaire et Radiobiologie, Faculté de Médecine et des Sciences de la Santé, Université de Sherbrooke, Sherbrooke, Québec, Canada

11:00-11:15 **Characterization of Cu nanoparticles via X-ray photoelectron spectroscopy in combination with theoretical calculations using SESSA**
*M. Sauer, A. Cognigni, L. Anteina, R. Zirbs, K. Schröder, A. Foelske-Schmitz* Analytical Instrumentation Center, Vienna University of Technology, Vienna, Austria

11:15-11:30 **Extracting information on the structure of core-shell nanoparticles from the inelastic background in XPS spectra**
*H. Kalbe, M. Hronek, C.J. Powell, W.S.M. Werner*
Vienna University of Technology, Vienna, Austria

12:00-13:00 Lunch

13:00-18:00 Excursion

18:00-19:30 Free time
19:30-22:30 Conference dinner

## Thursday, September 21$^{st}$

**Session 8:** Photoemission
Session Chair: *Christopher Walker*

---

08:30-09:00 **Rapid 3D Mapping of Fermi Surface, Fermi Velocity and Spin Texture**
*G. Schönhense* Institut für Physik, Johannes Gutenberg-Universität, Mainz, Germany

09:00-09:15 **Graphene-based field emission sources for electron microscopy and lithography**
*X. Shao, A. Srinivasan, W. K. Ang, A. Khursheed* Department of Electrical and Computer Engineering, National University of Singapore, Singapore

09:15-09:30 **X-Ray photoelectron spectroscopy of ionic liquids - from half cell measurements to in situ electrochemical XPS studies**
*A. Foelske-Schmitz, M. Sauer* Vienna University of Technology, Vienna, Austria

10:00-10:30 Coffee-break

**Session 9:** Transmission electron microscopy
Session Chair: *Rafal Dunin-Borkowski*

---

10:30-11:00 **Magnetic Circular Dichroism in Energy Loss Spectrometry**
*P. Schattschneider, S. Löffler* Institute of Solid State Physics, Vienna University of Technology, Vienna, Austria

11:00-11:15 **Model-based Iterative Reconstruction of Charge Density in the Transmission Electron Microscope**
*F. Zheng, V. Migunov, J. Caron, G. Pozzi, R. E. Dunin-Borkowski*
Ernst Ruska-Centre for Microscopy and Spectroscopy with Electrons and Peter Grünberg Institute, Forschungszentrum Jülich, Jülich, Germany

11:15-11:30 **Radiative transfer methods for electron spectroscopy**
*P. Kaplya, V. Afanas'ev, D. Efremenko* National Research University "Moscow Power Engineering Institute", Moscow, Russia

11:30-11:45 **Reflection Electron Energy Loss spectra of Highly Oriented Pyrolytic Graphite: role of anisotropic structure in plasmon excitations**
*M. Azzolini, T. Morresi, G. Garberoglio, L. Calliari, Y. Zhou, H. Zhang, K. Abram, N. Stehling, R. C. Masters, C. Rodenburg, N. M. Pugno, S. Taioli, M. Dapor* European Centre for Theoretical Studies in Nuclear Physics and Related Areas (ECT*-FBK) and Trento Institute for Fundamental Physics and Applications (TIFPA-INFN), Trento, Italy

12:00-13:00 Lunch

**Session 10:** Reflection energy loss electron spectroscopy/Time of flight spectroscopy
Session Chair: *Chris Edgcombe*

---

13:00-13:15 **Very low energy STEM / TOF system**
*B. Daniel, T. Radlička, J. Piňos, L. Frank, I. Müllerová* Institute of Scientific Instruments of the CAS, v.v.i., Brno, Czech Republic

13:15-13:30 **Electron Motion in the Electrostatic Field in the Near-Field Emission Electron Microscope**
*M. Oral, W. Werner, T. Radlička, J. Zelinka, D. Pescia, U. Ramsperger, G. Bertolini* Institute of Scientific Instruments of the CAS, Brno, Czech Republic

13:30-13:45 **Application of the Bandpass Filter for Secondary Electrons in SEM**
*F. Mika and I. Konvalina* Institute of Scientific Instruments of the CAS, Brno, Czech Republic

14:30-15:00 Coffee-break

**Session 11:** Coincidence spectroscopy
Session Chair: *Giovanni Stefani*

---

15:00-15:30 **Creation of entangled electrons by scattering at surfaces**
*R. Feder, H. Gollisch* Theoretische Festkörperphysik, Universität Duisburg-Essen, Duisburg, Germany

15:30-15:45 **On the relevance of plasmon assisted generation of secondary electrons**
*A. Bellissimo, A. Ruocco, M. Sbroscia, S. Iacobucci, G.M. Pierantozzi, G. Stefani* Dipartimento di Scienze, Universitá Roma Tre, Roma, Italy

15:45-16:00 **Measurements of electronic structure of insulators**
*V. Astašauskas, W. S. M. Werner, P. Kuksa, J. Pseiner, H. Kalbe, A. Bellissimo* Vienna University of Technology, Vienna, Austria

16:30-19:30 Free time
19:30-20:30 Dinner

## Friday, September 22$^{nd}$

**Session 12:** Secondary electron yield
Session Chair: *R. Cimino*

---

08:30-09:00 **Low-secondary electron emission yield of polarized surfaces**
*I. Montero, L. Olano, M.E. Dávila, I. Bretos, L. Calzada, R. Jiménez* Instituto de Ciencia de Materiales de Madrid (ICMM), CSIC, Madrid, Spain

09:00-09:15 **Measurement of electron backscattering yield at low incident energies**
*M. Belhaj, S. Dadouch, Th. Gineste, J. Puech* ONERA-the French Aerospace-Lab, Toulouse, France

09:15-09:30 **GEANT4 Study of the effect of the surface roughness on the Secondary Emission Yield**
*C. Inguimbert, J. Pierron, M. Raine, M. Belhaj, J. Puech* Onera, 2 av. Edouard Belin Toulouse, France

10:00-10:30 Coffee-break

10:30-12:00 Discussion

12:00-13:00 Lunch

# SIMDALEE2017 Abstracts

## Monday, September $18^{th}$

# Low Energy Electron Microscopy without and with spin polarization (LEEM and SPLEEM)

**Ernst Bauer**
*Department of Physics, Arizona State University, Tempe, Arizona, USA*

This talk addresses the two most important aspects of image formation in cathode lens electron microscopy such as LEEM and PEEM: resolution and contrast. Detection limit and information depth, will be discussed briefly too.

Resolution is mainly determined by the chromatic and spherical aberrations of the objective lens, with the chromatic aberration dominating at the lowest energies, and by the angular aperture used for imaging. Both aberrations can be compensated with an aberration corrector using an electron mirror with opposite aberrations. The best line resolutions reported in this manner for selected samples are 2.0 nm in LEEM [1] and 2.6 nm in CW laser UV-PEEM [2]. With pulsed illumination space charge effects reduce the resolution strongly; for XPEEM a best line resolution of 18 nm has been reported [3]. While LEEM has reached its resolution limits with about 2.0 nm, CW laser UV-PEEM combined with energy width control via Cs activation promises further improvements. Although there are worldwide already many aberration-corrected instruments, aberration correction is seldom used because it is too time-consuming and the high resolution is frequently not needed. Practical resolutions are, therefore, in the 5 nm to 10 nm range.

Contrast is mainly determined by the interaction of the electrons used for imaging with the sample and by the angular aperture used for imaging. In LEEM, diffraction by the periodic arrangement of atoms is the main source of contrast but phase contrast due to optical path differences or quantum well effects also play an important role. In SPLEEM ferromagnetism determines the contrast. UV-PEEM contrast is dominated by work function differences but densities of state and transition probabilities often play a role too. Photoionization cross sections determine chemical XPEEM contrast.

The detection limits in LEEM and UV-PEEM depend strongly upon the lateral distribution of the material (2D gas or 2D/3D crystals) and can be small fractions of a monolayer, similar to XPEEM and to difference images in magnetic imaging (SPLEEM, XMCD/LPEEM).

The information depth is in all methods generally determined by the inelastic mean free path, which at low energies can deviate strongly from the universal curve due to high densities of occupied and unoccupied states near the Fermi level. Alternately, when energy loss probabilities are low, elastic back scattering can determine the information depth.

All these statements will be illustrated with emphasis on LEEM and SPLEEM by examples such as Figs. 1 and 2 to the extent time allows.

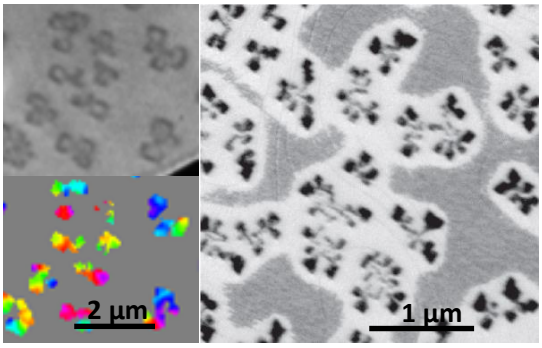


Figure 1. Small Fe crystallites. Left: SPLEEM sum and difference images; color: magnetization direction, E = 0.5 eV. Right: LEEM image, 9.0 eV [4]

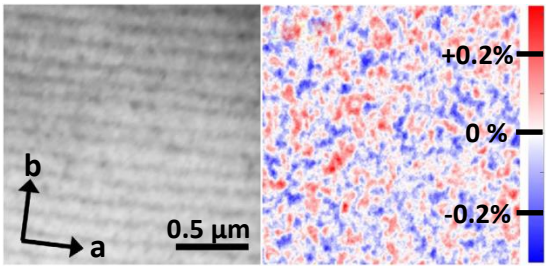


Figure 2. CW laser PEEM images of a $SrTiO_3$(100) surface. Left: raw image, right: difference image, showing magnetic domains in the metallic surface layer via MCD contrast; asymmetry values in % [5]

## References

[1] R.M. Tromp et al, Ultramicroscopy 127 (2013) 25
[2] T. Taniuchi et al, Rev. Sci.Instrum. 86 (2015) 023701
[3] Th. Schmidt et al, Ultramicroscopy 126 (2103) 23
[4] Y.R. Niu et al, Phys. Rev. B 95 (2017) 064404
[5] T. Taniuchi et al, Nature Commun. 7 (2016) 11781
[6] E. Bauer, Surface Microscopy with Low Energy Electrons, Springer, New York, 2014

E-mail: ernst.bauer@su.edu

# SIMDALEE2017 Abstracts

## Tuesday, September $19^{th}$

# Novel Plasmon-Coupling Theory of the Electron Inelastic Mean Free Path

**C T Chantler,[1,*] J D Bourke,[1]**
*[1]School of Physics, The University of Melbourne, Melbourne, Vic 3010, Australia*

**Synopsis** We present a new self-consistent model of inelastic electron scattering in condensed matter systems for accurate calculations of low-energy electron inelastic mean free paths (IMFPs) for XAFS, electron and particle transport and detector modelling. We develop a comparison to other techniques, and discuss new results for additional elements including zinc metal.

*Our model implements plasmon coupling mechanisms for the first time, in addition to causally-constrained lifetime broadening and high-precision density functional theory, and enables dramatic improvements in the agreement with recent high profile IMFP measurements.*

The accuracy of theoretical determinations of the electron inelastic mean free path (IMFP) at low energies is one of they key limiting factors in current XAFS modeling and Monte Carlo transport [1]. Recent breakthroughs in XAFS analysis show that there exist significant discrepancies between theoretical and experimental IMFP values [2], and that this can significantly impact upon extraction of other key structural parameters from both XANES and XAFS. Resolution of these discrepancies is required to validate experimental studies of material structures, and is particularly relevant to the characterization of small molecules and organometallic systems for which tabulated electron scattering data is often sparse or highly uncertain [3].

We have devised a new theoretical approach for IMFP determination linking the optical dielectric function and energy loss spectrum of a material with its electron scattering properties and characteristic plasmon excitations. For the first time we present a model inclusive of plasmon coupling, allowing us to move beyond the longstanding statistical approximation and explicitly demonstrate the effects of band structure on the detailed behavior of bulk electron excitations in a solid or small molecule [4]. This is a novel generalization of the optical response of the material, which we obtain using density functional theory [5].

We find that our developments dramatically improve agreement with experimental electron scattering results in the low-energy region (<~100 eV) where plasmon excitations are dominant. Corresponding improvements are therefore made in theoretical XAFS spectra and detector modelling.

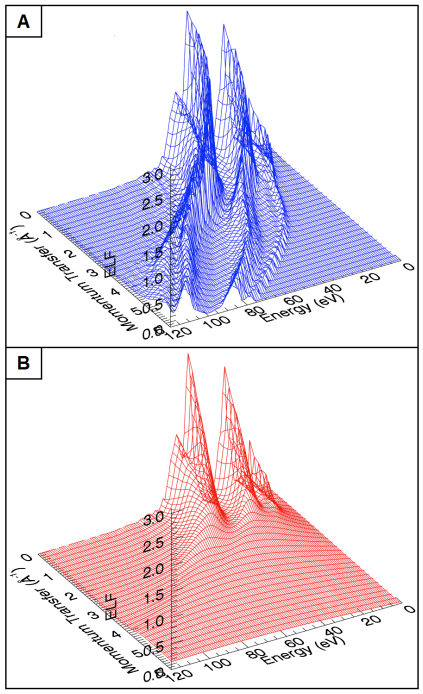


**Figure 1: The electron energy loss function (ELF)** of Mo. (A) is calculated **using a lossless Lindhard type model, while (B) utilises a self-consistent coupled-plasmon model.**

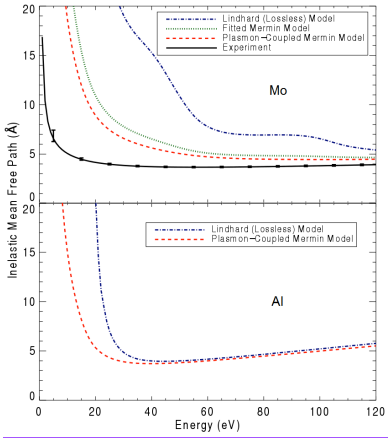


**Figure 2: Theoretical and experimental determinations of the electron IMFP for molybdenum and aluminium**

**References**

[1] J. D. Bourke and C. T. Chantler, *Phys. Lett. A* **360**, 702 (2007)

[2] J. D. Bourke and C .T. Chantler, *Phys. Rev. Lett.* **104**, 206601 (2010)

[3] C. T. Chantler, N. A. Rae, M. T. Islam, S. P. Best, J. Yeo, L. F. Smale, J. Hester, N. Mohammadi, F. Wang, *J. Synch. Rad.* **19**, 145 (2012)

[4] J. D. Bourke and C. T. Chantler, *J. Phys. Chem. Lett.* **6** 314 (2015); C T Chantler, J D Bourke, *J Phys CM* 27 (2015) 455901-1-7

[5] C. T. Chantler and J. D. Bourke, *J. Phys. Chem. A* **118** 909(2014); J D Bourke, C T Chantler, Y Joly, *J Synch Rad* 23 (2016) 551-559

E-mail: chantler@unimelb.edu.au

# Model sensitivity of Monte Carlo simulation of SEM images

**K.T. Arat,[1,*] C.W. Hagen[1]**

*[1]Dept. of Imaging Physics, Delft University of Technology, Lorentzweg 1, 2628CJ Delft, the Netherlands*

**Synopsis:** we studied the sensitivity of simulated scanning electron microscopy (SEM) images to the various model ingredients using an accurate, but slow simulator, based on state-of-the-art electron-matter interaction models, to identify the main ingredients to include in a reliable and fast SEM image simulator.

In SEM based inspection, it becomes more and more crucial to operate with optimized system parameters to handle the narrowed-down error margins in cases where resolution enhancement is required, 3D information needs to be extracted or buried structures are present. Monte Carlo simulations can be used to predict these parameters. However, to achieve the predictive power needed, such simulators preferably contain the most accurate interaction models, which unfortunately augment the computation time significantly. Alternatively, simulators with well-chosen approximate models, which are fast and still produce key effects of the fully rigorous models with a reasonable accuracy, can be very useful for certain applications.

Recently a full Monte Carlo simulator was developed at Delft University of Technology [1], based on first principle models. The inelastic scattering is based on dielectric function theory (DFT). The elastic scattering is based on the relativistic Mott cross-sections (> 200eV) and acoustic phonon cross-sections (< 100eV). Also, boundary-crossing of electrons is treated quantum mechanically and surface plasmons are taken into account. Moreover, the simulator runs on a GPU which decreases simulation times significantly. On the other hand, the semi-empirical Monte Carlo simulator based on Bethe's continuous slowing down approximation (CSDA), as described by Arat [2] et al. and developed by GenISys GmbH [3], is still faster, by almost an order of magnitude (see Figure 1-a). In Figure 1-b, the cross-section view of a silicon line sample is depicted. In Figure 1-c and 1-d, the SEM images of that Si line were simulated with the two simulators. The results look similar, yet quantitatively they are not the same. It is the goal of this work to use the 1st-principle code to investigate how sensitive the simulated results are to the various ingredients of the accurate model. The final goal is to identify the most important ingredients of the model such that a simplified, approximate model is obtained that can be used in a fast semi-empirical simulator. To that end, we 'switch off' parts of the model, e.g. phonon scattering, or surface plasmons, etc., and study the effect on the intensity profile of the simulated Si line. We discovered that the profiles are influenced most, among others, by the inclusion of quantum mechanical transmission of electron through interfaces, compared to classical interface transmission (see Figure 1-e). More details will be discussed at the conference.

E-mail: k.t.arat@tudelft.nl

**References**

[1] T. Verduin; et. al. "GPU accelerated Monte-Carlo simulation of SEM images for metrology", Proc. SPIE 9778, (April 21, 2016); doi:10.1117/12.2219160.

[2] K. T. Arat; et. al. "Electric fields in Scanning Electron Microscopy simulations", Proc. SPIE 9778, (April 21, 2016); doi:10.1117/12.2219182.

[3] "VirtualSEM" software developed by GenISys-GmbH in Taufkirchen, Germany

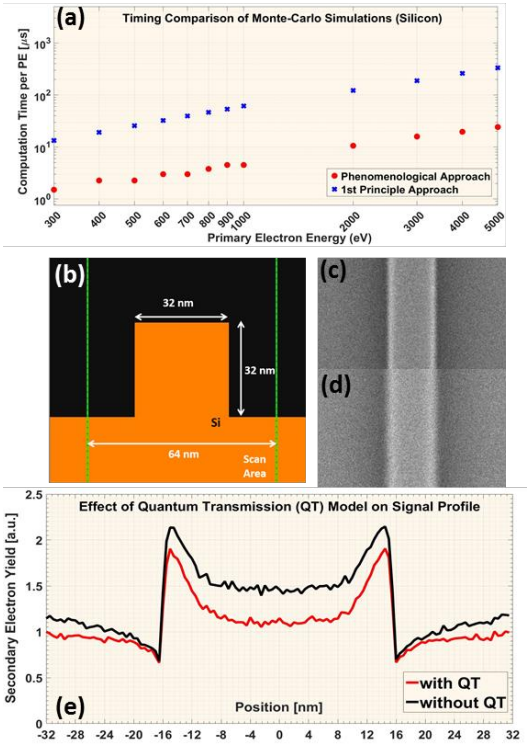


**Figure 1 - a) the computation time comparison shows that the semi-empirical approach on Intel Xeon CPU E5-1620v3 is roughly 10 times faster than 1st principle approach running on NVIDIA GTX480; b) the cross-section of sample geometry, a 32 nm x 32 nm infinitely long silicon line on top of a silicon wafer; simulation of the line by two different simulators c) the semi-empirical simulator and d) the 1st principle simulator; e) effect of quantum mechanical transmission through the silicon-material interface at 300 eV: red line is full Monte-Carlo simulation and black line is absence of quantum mechanical transmission model in the full simulation.**

# What's next in Scanning Low Energy Electron Microscopy?

**I. Müllerová, Š. Mikmeková, E. Mikmeková and L. Frank**
*Institute of Scientific Instruments of the CAS, v.v.i., Královopolská 147, 61264 Brno, Czech Republic*

**Synopsis** The optimum contrast can be found in the SLEEM for each specimen, when proper primary beam energy and the collection of the signal electrons by the detector align.

Thanks to the use of the Cathode Lens (CL) principle in Scanning Electron Microscope (SEM) [1], we can obtain high lateral resolution of several nm throughout the entire energy scale of the primary electron beam; say from 30 keV down to nearly zero landing energy. We call this instrument SLEEM (Scanning Low Energy Electron Microscope). The images in the reflected and even transmitted electrons are now available in this system. There is no atomic resolution nor is there sufficient coherence of the beam in the SLEEM as it is in the high energy Transmission Electron Microscope (TEM), or the coherence of the beam in LEEM [2]. Still, there are many advantages of the SLEEM in the comparison to the above mentioned instruments. With the SLEEM it is possible to observe contrast development throughout the large energy range in both reflected and transmitted signals. The final contrast of the image depends mainly on the energy of electrons which interacts with the specimen, the specimen itself, and the collection efficiency of the detector; which part of the energy and angular spectra of the emitted electrons will be collected. It is possible to find some optimum conditions for the above mentioned parameters for the observation of the maximum contrast of each specimen.

At optimum energy and with their complete angular distribution acquired, the backscattered electron (BSE) images offer enhanced information about crystalline structures thanks to contrast mechanisms that are otherwise unavailable. The example is shown in Figure. 1. Transmitted mode of the SLEEM is shown in Figure . 2. Individual graphene layers are visible at very low energies. The commercial multi-layered CVD graphebe (http://www.tedpella.com/) was used for this study. The efficiency of using low energies is finally demonstrated in Figure 3, comparing the 500 eV bright field SLEEM frame of the structure free of any heavy metal salts with a 10 nm section from the same prepared tissue observed in TEM at 80 keV. The image contrast at high energy is so low that assessment of the resolution becomes impossible. [3].

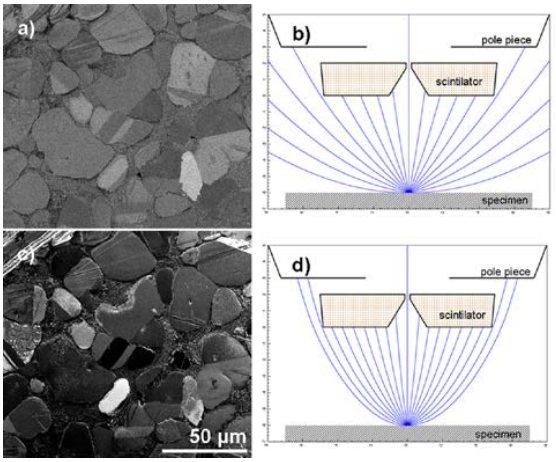


**Figure 1. SLEEM images of X210Cr12 steel obtained at energy 4 keV (a) and 1 keV (c), together with corresponding simulations of the BSE trajectories (b and d).**

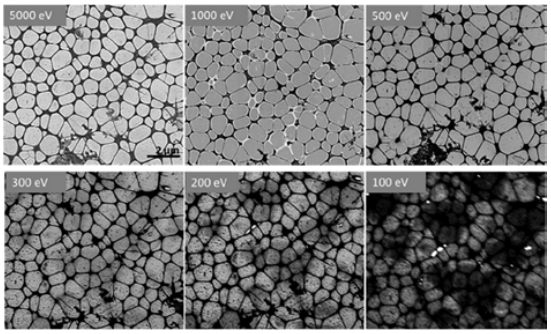


**Figure 2. Micrographs of multilayered graphene (3 to 5 layers) observed from 5000 eV to 100 eV.**

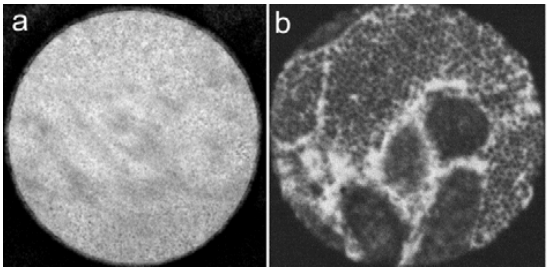


**Figure 3 Section of mouse heart muscle, not fixed with osmium tetroxide and not stained: 10 nm section imaged by conventional TEM at 80 keV (a), CL mode micrograph taken at 500 eV (b).**

## References

[1] I. Müllerová and L. Frank, Adv. Imaging Electron Phys. 128 (2003), p. 309-443.
[2] E. Bauer, Surface Microscopy with Low Energy Electrons, Springer Science and Business Media, New York (2014).
[3] This work was supported by project no: TE01020118 of the Technology Agency of the Czech Republic and by the European Commission for the Marie Curie Initial Training Network SIMDALEE2: Grant No. 606988 under FP7- PEOPLE-2013-ITN.

E-mail: ilona@isibrno.cz

# Low-Energy Secondary Electron Yield (LE-SEY) of conductive surfaces.

**R. Cimino,**[1,*]
[1]*LNF-INFN, P.O. Box 13, Frascati, Roma, Italy.*

The detailed study of the Secondary Electron Yield (SEY) of technical Surfaces for very low electron landing energies (from 0 to 30 eV) is a very important parameter in many fields of research, spanning from accelerator technology [1-3] to detectors, photon or electron-multipliers, high power microwave tubes, systems for satellite applications, radio-frequency cavities, optics for Extreme Ultraviolet lithography, etc. Some of the devices used in all those fields of research base some of their essential functionalities on the number of electrons produced by a surface when hit by other electrons, namely its SEY, and, in most cases, its very low energy behavior (LE-SEY).

Despite of such interest, the very low electron landing energy part of a SEY curve has been rarely addressed due to the intrinsic experimental complexity to control and measure very low energy electrons. In this talk, I will report on our recent studies to review the experimental methods used to study LE-SEY, solving the apparent controversy present in the literature regarding the different LE-SEY behavior between clean noble metals and their technical untreated surfaces [3]. It is now clear how SEY of all clean noble metals goes to very low values at impinging energies just above metal work function $W_f$, while their technical counterpart shows a significant LE-SEY value due to the enhancement of the reflected component [2] as due to the presence on the surface of various contaminants.

The LE-SEY sensitivity to surface composition suggests to use this technique to follow adsorption and desorption study. This has been done exposing at various gases a clean polycrystalline Cu surface held at low temperature (about 10 K) while following its SEY and LE-SEY. Indeed, it is shown that sub monolayer coverages of Ar (see Fig. 2) and CO [5] are sufficient to significantly modify the LE-SEY values. This suggests that non-metallic adsorbates can enhance low energy electron reflectivity [1]. LE-SEY and SEY have been also used to follow the subsequent thermal desorption and the comparison with TPD curves obtained with mass spectrometry is indeed very promising to promote SEY and LE-SEY as the ideal technique to follow electron stimulated induced desorption.

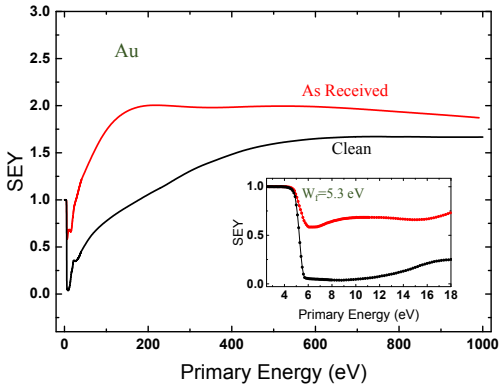


**Figure 1. Comparison between the SEY curves measured for clean (black line) and as received (red line) Au surfaces [4].**

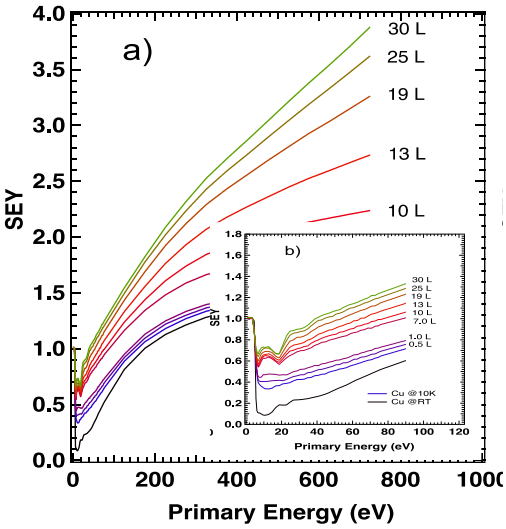


**Figure 2. SEY curves versus primary electrons energy as function of Ar dose. In the left panel (a) it is shown the behaviour in the complete region between 0 and 720 eV. In the right panel (b) it is presented an enlargement of the region between 0 and 90 eV [5].**

## References

[1] R. Cimino, T, Demma, Int. J. Mod. Phys. A 29, 1430023, 2014.
[2] R. Cimino et al. Phys. Rev. Lett. 93, 014801, 2004.
[3] R. Cimino et al. Phys. Rev. ST-AB 18, 051002, 2015.
[4] L.A. Gonzalez et al. Proc. Mucopin 2017.
[5] M. Angelucci et al. Proc. Mucopin 2017.

E-mail: Roberto.cimino@lnf.infn.it

# Investigation of the secondary electron yield of copper surfaces in particle accelerators

**V. Petit[1,2], H. Neupert[1], E. Garcia Tabares[1], M. Taborelli[1], M. Belhaj[2] and T. Paulmier[2]**
*[1]CERN, European Organization for Nuclear Research, 1211 Geneva 23, Switzerland*
*[2]ONERA, DPhIEE, 2. Av. E. Belin, 31000 Toulouse, France*

The phenomenon of electron cloud is one of the limitations to stable operation of beam and cryogenics in modern particle accelerators with intense positively charged beams, as LHC. The secondary electron yield (SEY) of the inner surface of the vacuum chambers steers the multiplication of impinging electrons and sets the threshold of beam charge and structure for the occurrence of electron cloud. Fortunately, for several materials used in the vacuum system of particle accelerators, in particular copper and stainless steel, the SEY and hence the intensity of the electron cloud, have been observed to decrease with the time of machine operation. This behavior is generally called conditioning or beam scrubbing. The mechanism of conditioning is not completely understood yet, neither at room temperature, nor in the cryogenic temperature range. Several studies indicate a modification of carbon on the surface and possibly an increase of carbon concentration [1, 2]

The present investigation consists of a series of measurements on parts extracted from the CERN accelerators and laboratory experiments aiming at giving an interpretation to these measurements.

In a laboratory setup equipped with X-ray Photoelectron Spectroscopy (XPS) and a SEY measuring system, the SEY measurements and surface composition analysis of vacuum parts which have faced the beam in one of the main LHC dipoles during the initial phase of run 2 were performed. In particular, the beamscreen of the dipole at several lengths along the magnet and the pumping slot shield along the beamscreen have been analyzed after prolonged (weeks) air exposure due to the extraction and dismounting from the hosting magnet. This makes particularly difficult the identification of conditioning, since air exposure partly cancels the effect. As a reference, a freshly cleaned and air exposed beamscreen surface has been also analyzed.

The beamscreen surface is made of colaminated copper on a stainless steel substrate. It can be divided in four different surfaces (figure 1) with respect to azimuth: top and bottom surfaces which are normal to the dipole magnetic field and are expected to receive most of the electrons from the electron cloud; an internal (with respect to the center of the machine) surface which does not receive synchrotron radiation; and an external surface with a sawtooth profile designed to absorb synchrotron radiation. The SEY of the copper surface has values between 1.60 and 1.80.

The pumping slot shields, made of copper beryllium alloy, are on top and bottom position behind the holes of the beamscreen and show conditioning. The difference of SEY between the parts exposed to the electron cloud through the pumping slots and the parts which remain masked, is about 0.1. Since this is above accuracy of the measurement this is interpreted as a memory of conditioning. The analysis of the surface chemical composition as well as a comparison with the reference sample are in progress and will be presented and discussed.

In parallel to these measurements, the behavior of as-received (chemically cleaned and passivated) Oxygen Free Electronic grade (OFE) copper under irradiation with electron beam at 250 eV at room temperature is investigated. The SEY decreases progressively, down to a value of 1.15 for a dose of $3.10^{-2}$ C/mm . The main change in the surface composition is a modification of the carbon C1s and Cu2p lines. We observe the vanishing of high binding energy components in C1s and a shift of intensity to lower binding energies. For the Cu2p line any $Cu^{II}$ contribution decreases with irradiation and finally vanishes. The decrease of SEY is ascribed to the modification of the carbon lineshape, since in contrast to some previous experiments no increase of carbon intensity occurs. The investigation of different surface treatments of OFE copper is in progress as well as the effect of deconditioning due to air exposure and will be presented and discussed.

## References

[1] R. Cimino, M. Commisso, D.R. Grosso, T. Demma, V. Baglin, R. Flammini and R. Larciprete, Phys. Rev. Lett. 109, 064801 (2012).
[2] C. Scheuerlein and M. Taborelli, J. Vac. Sci. Technol. A 20, 93 (2002).

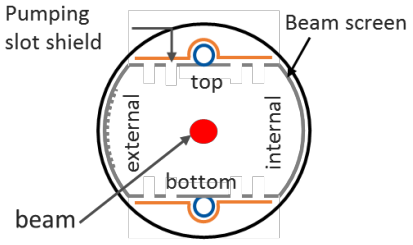


Figure 1. Schematics of beamscreen

E-mail: valentine.petit@cern.ch

## Secondary Electron emission from graphene based materials

P. Riccardi

*Dipartimento di Fisica, Università della Calabria and INFN- Gruppo collegato di Cosenza*
*Via P. Bucci cubo 33C, 87036 Arcavacata di Rende, Cosenza, Italy*
*e-mail: Pierfrancesco.riccardi@fis.unical.it;*

I will report on the use of the spectroscopy of secondary electrons as a probe for excited states of graphene based material. We report the observation of fine structures in the spectra of emitted electrons under the impact of $He^+$ and electrons with graphene on Ni(111). In the case of electron impact, the spectra are very sensitive to the crystalline quality of the sample and show several peaks, that reflect features in the density of conduction band states at corresponding energies above the vacuum level [1]. Experiments of keV $He^+$ ion impact show that excitation of valence electrons occur by electron promotion in close He-C collisions. This produces a high energy features that is attributed to the detection in vacuum of electrons promoted into conduction band states.

I will also present state of the art Density Functional Theory (DFT) calculations of the electronic band structure of graphene (1 to 6 layers), graphite and graphene adsorbed on Ni(111), focusing on the unoccupied energy levels up to 50 eV above the Fermi level. The results of the calculations are compared with available observations obtained in ARSEE experiment either performed by us or reported in the literature. ARSEE measurements show spectroscopic features that can be linked to energy states found in band structure calculations. The combined analysis of DFT calculations and ARSEE experiments demonstrates the role of 2D scattering resonances predicted in ref.4 in determining the secondary electron emission properties of graphene based materials.

References:

1. P. Riccardi, A. Cupolillo, M. Pisarra, A. Sindona, L.S. Caputi Appl. Phys. Letters 97 (2010) 221909
2. Riccardi P, A. Cupolillo, M. Pisarra, A. Sindona, and L. S. Caputi Appl. Phys. Letters 101 (2012) 183102
3. M. Pisarra, P. Riccardi, A. Sindona, A. Cupolillo, N. Ligato, C.Giallombardo, L. S. Caputi Carbon 77 (2014) 796
4. V.U. Nazarov, E.E. Krasovskii, V.M. Silkin, Phys. Rev. B **87**, 041405(R) (2013).
5. E. Kogan and V. U. Nazarov, Phys. Rev. B **85**, 115418 (2012).

# Transmission electron yield simulations of tynodes.

**Anne M. M. G. Theulings,[1,2,*] Johan Hidding,[3] Cornelis W. Hagen,[1] and Harry van der Graaf[1,2]**

*[1]Delft University of Technology, Lorentzweg 1, 2628 CJ Delft, The Netherlands*
*[2]Nikhef, Science Park 105, 1098 XG Amsterdam, The Netherlands*
*[3]Netherlands eScience Center, Science Park 140, 1098 XG Amsterdam, The Netherlands*

**Synopsis** Monte Carlo simulations are used to gain insight in the secondary electron emission of transmission dynodes, or tynodes, which consist of ultra-thin membranes. These simulations can be used to design tynodes with a high yield.

Photomultiplier tubes are widely used, despite their cost, size and the fact that they do not offer spatial resolution and are influenced by magnetic fields. It would be a great advantage to miniaturise a photomultiplier tube, by placing a stack of transmission dynodes, or tynodes, on top of a CMOS pixel chip, and capping the whole with a photocathode [1]. This way excellent spatial resolution and time resolution, per individual soft photon, are obtained. A tynode consists of an ultra-thin membrane. A crucial parameter to make the multiplier work is a high *total transmission electron* yield (TTY) of the tynodes, of at least 4. Just like the reflection yield, the TTY depends on the particular material used. However in the case of ultra-thin membranes, the TTY depends on the membrane thickness. A maximum TTY is expected for a certain optimum membrane thickness.

Monte Carlo simulations are used to aid the tynode design. The simulator used is an adapted version of the Kieft and Bosch code, especially developed to model the low-energy interactions of electrons with matter and accurately tracks secondary electrons inside the material [2]. The models used in this simulator are expanded and the calculation of the cross sections is made modular, which facilitates easy exchange of cross section models. The original simulator contains models for elastic scattering, inelastic scattering, and interface crossing. These processes are schematically shown in Fig. 1. Our model expansion includes newly calculated Mott cross sections, taking solid state effects into account [3], surface plasmons, trapping, and both the transversal as well as the longitudinal acoustic phonon branches instead of only the longitudinal mode as in the original simulator. This last extension made it possible to remove an absorption process at the surface, which had no physical explanation, from the original code. It is noted that charging is not taken into account, yet.

Once the material for a tynode is determined, based on a sufficiently large TTY, the Monte Carlo simulations can be used to determine the optimum tynode thickness. This is done by simulating the total transmission yield curve depending on the primary energy for a certain membrane thickness. The TTY will have a maximum at a certain energy, the maximum TTY specific for this membrane thickness. By repeating this for different membrane thicknesses, the dependence of the maximum TTY on the membrane thickness is determined. The maximum TTY will also show a maximum, the thickness where this maximum is reached is the optimum membrane thickness for the material in question.

The Monte Carlo simulations can also give insight in the difference between electron emission in reflection and in transmission mode by determining the shape of the electron cloud in thin membranes and in bulk samples of the same material. These and more results will be discussed at the conference.

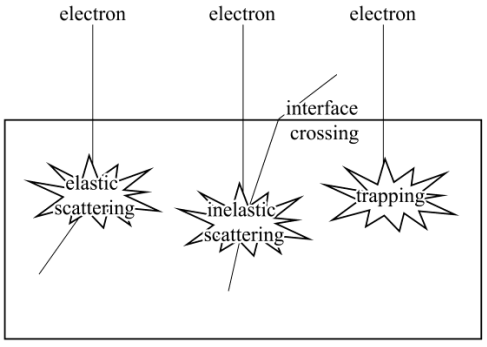


**Figure 1. The four different processes that can happen to an electron inside the material are: elastic scattering, inelastic scattering, interface crossing, and trapping (included in the model expansion).**

## References

[1] H. van der Graaf, *et. al.*, *NIM A* **847** (2016) 148-161.
[2] E. Kieft, E. Bosch, *J. Phys. D: Appl. Phys.* **41** (2008), 215-310.
[3] F. Salvat, A. Jablonski, C. J. Powell, *Comp. Phys. Comm.* **165** (2005) 157-190.

E-mail: a.theulings@nikhef.nl

# Imaging and Manipulation of Single Molecules by Scanning Probe Microscopy: Wires, Switches and Motors

**Leonhard Grill**
***Department of Physical Chemistry, University of Graz, Austria***
*(www.nanograz.com)*

Scanning tunneling microscopy is not only a useful method to study surfaces and adsorbates with high spatial resolution, but represents also a powerful tool to characterize molecules spectroscopically [1] and to manipulate matter at the atomic level [2-3]. This field, often named "Single-Molecule Chemistry", gives deep insight into physical and chemical processes at the level of individual molecules. Typically, tunneling electrons of very low energy are used to excite molecules electronically or vibrationally.

In this talk various examples of functional molecules, ranging from molecular wires to molecular switches and machines that are studied by scanning tunneling microscopy (STM) under ultrahigh vacuum conditions will be discussed. Their properties are investigated by tunneling microscopy and spectroscopy and via the controlled manipulation, i.e. triggering of the molecular function.

Molecular wires [4] or molecular nodes with different conjugation pathways [5] can be fabricated from specifically designed molecular building blocks that are connected to two-dimensional networks or one-dimensional chains. In the case of molecular switches, fundamental insight into the proton transfer is obtained by spectroscopically studying single porphycene molecules at a surface. It turns out by isotope substitution of the inner hydrogen atoms in the molecular cavity that the process is triggered by exciting the NH (or ND) vibration of the molecule [6]. The switching rate can be tuned up and down by only one single atom in the vicinity of the molecule. This effect can be extended to molecular assemblies where cooperative effects in single molecules are directly observed. Hence, the proton transfer in one molecules does not only depend on the presence of the neighbor molecule, but also on the arrangement of the hydrogen atoms in its center [7].

Molecular isomerization processes can also be used to trigger a molecular motor where the lateral translation of molecular machines on a surface can be enhanced by light of specific wavelengths that match the absorption properties of the molecule [8]. By comparing molecules with and without a motor unit, the enhanced motion can be directly assigned to the motor that is incorporated in the molecules.

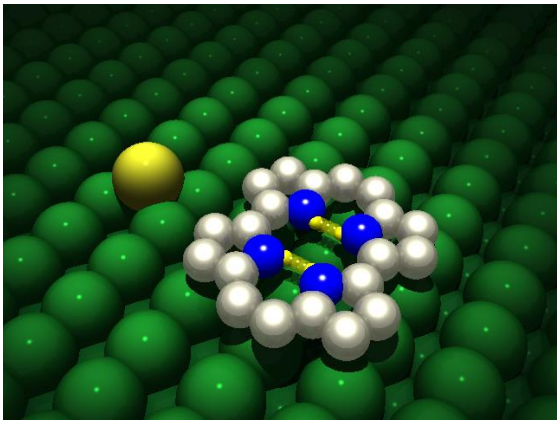

**Figure 1. Schematic view of the proton transfer within a porphycene molecule, modified by a single copper atom in its vicinity [7].**

**References**

[1] W. Ho, J. Chem. Phys. **117** (2002) 11033.
[2] D. M. Eigler et al., Nature **344** (1990) 524.
[3] L. Grill, J. Phys.: Cond. Matt. **20** (2008) 053001.
[4] C. Nacci et al., Nature Comm. **6** (2015) 7397.
[5] C. Nacci et al., Angew. Chem. Int. Ed. **55** (2016) 13724.
[6] T. Kumagai et al., Phys. Rev. Lett. **111** (2013) 246101.
[7] T. Kumagai et al., Nature Chem. **6** (2014) 41.
[8] A. Saywell et al., ACS Nano **10** (2016) 10945.

E-mail: leonhard.grill@uni-graz.at

# STM and NC-AFM investigations of Graphene on Ir(111)

**Violeta Simic-Milosevic,[1,*] Yuriy Dedkov,[2] and Andreas Thissen[1]**
*[1] SPECS Surface Nano Analysis GmbH, Voltastrasse. 5, 13355 Berlin, Germany*
*[2] Universität Konstanz, Universitätsstraße 10, 78464 Konstanz, Germany*

STM and nc-AFM results of graphene layers on Ir(111) are presented. With its stability and productivity the SPM Aarhus 150 is the ideal instrument for investigating lattice mismatched surfaces, like graphene/Ir(111). Microscopy experiments were performed in constant current / constant frequency shift (CC/CFS) and constant height (CH) modes, exploiting a combination of the STM and NC-AFM capabilities of the SPM Aarhus 150 system. We found that in STM imaging the electronic contribution is prevailing compared to the topographic one and the inversion of the contrast can be assigned to the particular features in the electronic structure of graphene on Ir(111). Contrast changes observed in constant height AFM measurements are analyzed on the basis of the energy, force, and frequency shift curves, obtained in DFT calculations, reflecting the interaction of the W-tip with the surface and are attributed to the difference in the height and the different interaction strength for high-symmetry cites within the moirè unit cell of graphene on Ir(111). The presented findings are of general importance for the understanding of the properties of the lattice-mismatched graphene/metal systems especially with regard to possible applications as templates for molecules or clusters.

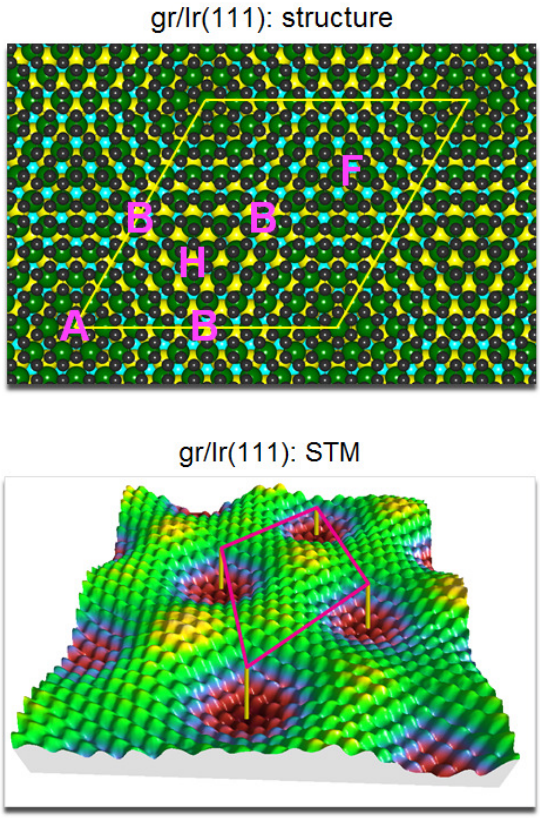


**Figure 1. Graphene-moiré structure on Ir(111), theory and experimental result.**

## References

[1] E. N. Voloshina et al., Sci. Rep. **3**, (2013) 1072.
[2] Y. S. Dedkov and E. N. Voloshina, Phys. Chem. Chem. Phys. **16**, (2014) 3894.

E-mail: Violeta.Simic-Milosevic@specs.com

# Observation of Metal Nucleation on Freestanding Graphene by Means of LEEPS Microscopy

**M. Lorenzo,* C. Escher, T. Latychevskaia and H.-W. Fink**
*Department of Physics, University of Zurich, Winterthurerstrasse 190, 8057 Zurich, Switzerland*

The Low-Energy Electron Point Source (LEEPS) microscope is a lens-less setup based on Dennis Gabor's proposition of holography in the year 1948 [1]. An ultrasharp field emission point source [2] emits a bright divergent beam of coherent electrons with kinetic energies in the range of 50-250 eV, corresponding to wavelengths of 0.17-0.08 nm. The interference between the electron reference wave and the wave elastically scattered off the sample, produces a hologram on the detector [3].
We have recently developed a new LEEPS microscope with improved mechanical stability that allows investigating the adsorption of metals on freestanding graphene. Thanks to the high transparency (>70%) to low-energy electrons, graphene is a suitable substrate for LEEPS investigations [4-5]. Moreover, low-energy electrons are particularly sensitive to electric fields, therefore this kind of microscopy allows resolving the charge of a single adsorbate on graphene with elementary charge precision [6].
Here I present studies on metal nucleation and growth on freestanding graphene by means of the LEEPS microscope. Metals are evaporated on the graphene sample in-situ, allowing for real time recording of cluster growth with a temporal resolution of $3x10^{-2}$s.
Among the growth of metal on graphene, the adsorption of alkali metals is of particular interest because of their highly polar bond. Alkali metals adsorb on graphene donating their *s* electron, which gets delocalized. The signature of the positively charged ion is a bright spot on the detector, whose intensity is related to the amount of charge. Along with these studies I also discuss the alkali intercalation between two graphene layers.

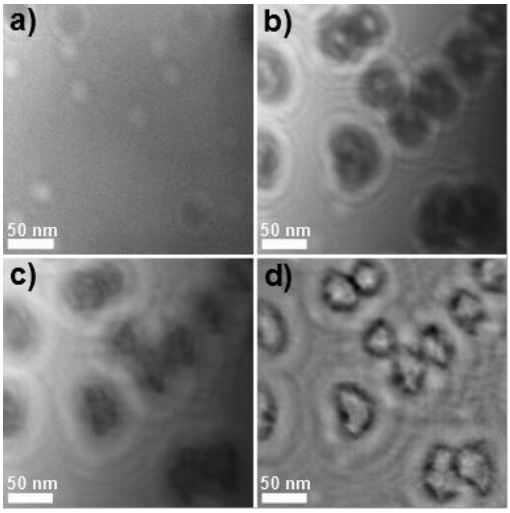


**Figure 1. (a) Hologram of clean freestanding graphene. (b) Hologram of palladium clusters on freestanding graphene and its amplitude (c) and phase reconstructions (d). Holograms are acquired with 55eV electrons. The reconstruction algorithm is reported in [7].**

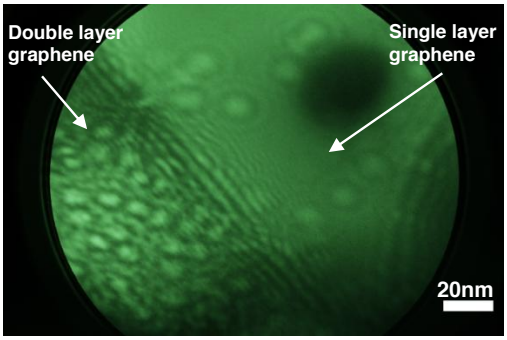


**Figure 2. Hologram of cesium intercalation between double layer graphene. The kinetic energy of the electrons is 66eV.**

## References

[1] D. Gabor, Nature **161** (1948) 777.
[2] H.-W. Fink, W. Stocker, H. Schmid, J. Vac. Sci. Technol. B. **8** (1990) 1323.
[3] H.-W. Fink, W. Stocker and H. Schmid, Phys. Rev. Lett. **65** (1990) 1204.
[4] J. Y. Mutus, L. Livadaru, J. T. Robinson, R. Urban, M. H. Salomons, M. Cloutier and R. A. Wolkow, New J. Phys. **13** (2011) 063011.
[5] J.-N. Longchamp, T. Latychevskaia, C. Escher and H.-W. Fink, Appl. Phys. Lett. **101** (2012) 113117.
[6] T. Latychevskaia, F. Wicki, J.-N. Longchamp, C. Escher and H.-W. Fink, Nano Lett. **16** (2016) 5469.
[7] T. Latychevskaia and H.-W. Fink, Appl. Opt. **54** (2015) 2424.

E-mail: marianna@physik.uzh.ch

# Charge-transfer plasmonics in self-organising metal-semiconductor-metal structures

**B J Murdoch[*1], A J Barlow[2], J F Portoles[1], S Tardio[1], I W Fletcher[1] and P J Cumpson[1]**

*[1] National EPSRC XPS Users' Service (NEXUS), School of Mechanical and Systems Engineering, Newcastle University, Newcastle upon Tyne, Tyne and Wear, NE1 7RU, UK*

*[2] Centre for Materials and Surface Science (CMSS), Department of Chemistry and Physics, La Trobe University, Melbourne, Victoria 3086, Australia*

**Synopsis** When the space between two metallic nanoparticles becomes conductive a charge transfer can take place that gives rise to a recently discovered class of plasmon. These so-called charge transfer plasmons have been demonstrated to be sensitive to the conductance of the interparticle junction [1].

Until now, charge transfer plasmonics has been studied in two main scenarios – firstly, where the dimer is bridged by a metallic nanowire or substrate [1] and, secondly, where the dimers are within quantum tunnelling proximity [2].

We have observed charge-transfer plasmons from photoconductively-coupled plasmonic nanoantenna comprising metallic nanoparticles on a semiconductor substrate. We utilise the self-organising behaviour of In metallic nanoparticles produced by preferential sputtering of phosphorus atoms in InP to create metal-semiconductor-metal structures. The optical response of these structures has been investigated by reflection electron energy loss spectroscopy and photoluminescence spectroscopy. By altering the optical pump power, we can actively control the conductive-coupling between In nanoparticles and tune the wavelength of the observed charge-transfer plasmons. These observations are in excellent agreement with the theoretically proposed model of photoconductively-coupled metal-semiconductor-metal systems. The devices presented have been demonstrated to be suitable for visible wavelength surface enhanced Raman spectroscopy [3] and, also, potentially offer a route to ultrafast, compact and active all-optical switches [4].

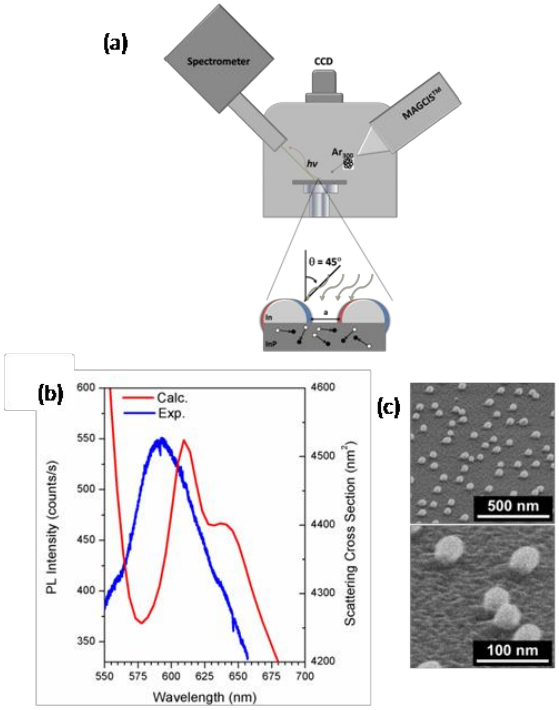


**Figure 1. (a) Experimental set-up for *in situ* fabrication and characterisation of self-organising In-InP structures. (b) Photoluminescence and simulated scattering cross section due to charge transfer plasmon. (c) Helium ion microscope images of self-organising In-InP metal-semiconductor-metal structures.**

## References

[1] F. Wen, Y. Zhang, S. Gottheim, N. S. King, Y. Zhang, P. Nordlander, and N. J. Halas, ACS nano **9** (6), 6428 (2015).
[2] R. Esteban, A. G. Borisov, P. Nordlander, and J. Aizpurua, Nature communications **3**, 825 (2012).
[3] B. J. Murdoch, J. F. Portoles, S. Tardio, A. J. Barlow, I. W. Fletcher, and P. J. Cumpson, Applied Physics Letters **109** (25), 253105 (2016).
[4] N. Large, M. Abb, J. Aizpurua, and O. L. Muskens, Nano letters **10** (5), 1741 (2010).

E-mail: billy.murdoch@ncl.ac.uk

# Frontiers in low energy electron pair emission

**F.O. Schumann**
*Max-Planck Institute of Microstructure Physics, Weinberg 2, 06120 Halle, Germany*

**Synopsis** Coincidence spectroscopy reveals relevant time scales leading to electron emission at surfaces. We use in these studies the effect of double photoemission and ion neutralization.

The availability of intense and short light pulses has opened up a new and active research field. This allows to address fundamental questions on the time evolution of the electron dynamics leading to electron emission.
We demonstrate in our studies that electron pair emission from surfaces holds the promise to unravel the time scale of electron dynamics. This can be achieved without atto-second light sources.
Specifically we studied the Auger decay following the emission of core-electron due to photon absorption. With coincidence spectroscopy, we demonstrate an extensive energy sharing between the Ag 4p photoelectron and the NVV Auger electron exceeding 10 eV. This energy width provides access to the time scale of the emission process. We convert this to a timescale of 60 as over which the fluctuations takes place. This value is fair agreement with the theoretical calculation of the time-scale to fill an exchange-correlation hole.[1]
The neutralization of ions near a surface is known to be efficient process and leads to electron emission via Auger-type processes. Specifically, the neutralization of $He^{2+}$ ions makes available the double ionization energy.
We demonstrate that the neutralization of a single $He^{2+}$ ion near an Ir(100) surface leads to the emission of an electron pair. Via coincidence spectroscopy we give evidence that a sizable amount of these electron pairs originate from a correlated single step neutralization of the ion involving a total of 4 electrons from the metal. These correlated electron pairs cannot be explained in the common picture of two consecutive and independent neutralization steps. We infer a characteristic time scale for the correlated electron dynamics in the metal of 40-400 as.[2]

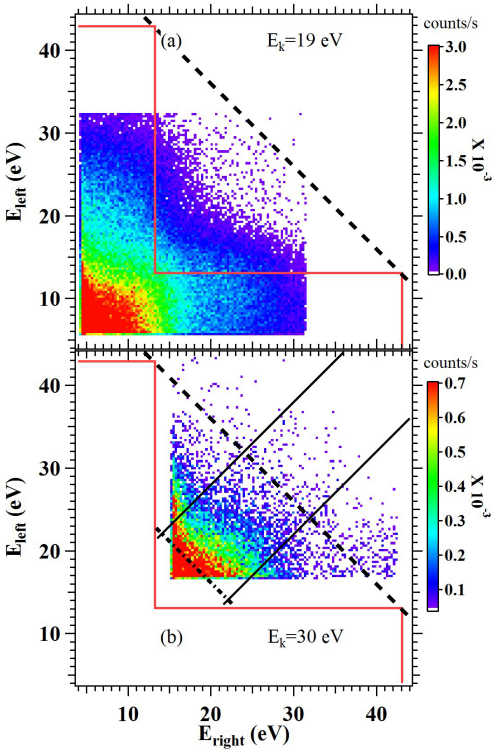


**Figure 1. 2D-Energy distributions from a Ir(100) surface due to $He^{2+}$ neutralization.**

## References

[1] Z. Wei, F.O. Schumann, C.H. Li, L. Behnke, G. Di Filippo, G. Stefani, and J. Kirschner, Phys. Rev. Lett. **113**, 267603 (2014).
[2] C.-H. Li, C. Tusche, F.O. Schumann, and J. Kirschner, Phys. Rev. Lett. **118**, 136402 (2017).

E-mail: schumann@mpi-halle.de

# Low Energy Electron Emission Resulting from Auger Transitions Initiated by Deep Holes in the Valence Band of Graphene

**A. H. Weiss, [1,*] V A Chirayath,[1] V Callewaert,[2] A J Fairchild, [1] M D Chrysler, [1] R W Gladen, [1] S K Imam, [1] R Saniz, [2] B Barbiellini, [3] K Rajeshwar, [1] and B Partoens[2]**

*[1]The University of Texas at Arlington*
*[2]Universiteit Antwerpen, Belgium*
*[3]Northeastern University, Boston, USA*

**Synopsis** We report the observation of low energy electrons emitted as a result of an Auger transition initiated by the creation of deep hole in the valence band created by positron-electron annihilation.

Here, we report the direct measurement of the energy spectra of electrons emitted from graphene as a result of the decay of deep holes in the valence band. These measurements were made possible by eliminating competing backgrounds by employing low energy positrons to create valence band holes by annihilation. Similar processes are thought to make important contributions to the low energy photo-electron and secondary electron spectrum in many molecules and solids [1-4]. However, measurements of the energy spectrum and efficiency with which electrons are emitted in this process remain elusive due to large unrelated backgrounds. A low energy positron beam (1.25 eV) was used to deposit the positron on single layer graphene on a Cu substrate and the low energy peak was designated as VVV following the X-ray notation. Calculations show that the PAES signal stems almost entirely from the top graphene layer due to the trapping of positrons in the image potential well on the surface of graphene. The spectrum of low energy electrons associated with the VVV Auger transition of single layer graphene on Cu was compared to spectra obtained from multilayer graphene on Cu and the implications of an observed shift of the spectrum to lower energy as the thickness of the graphene overlayer is increased will be discussed. Our experimental results, supported by first-principles calculations, indicate that between 80% and 100% of the deep valence band holes in graphene are filled via an Auger transition.

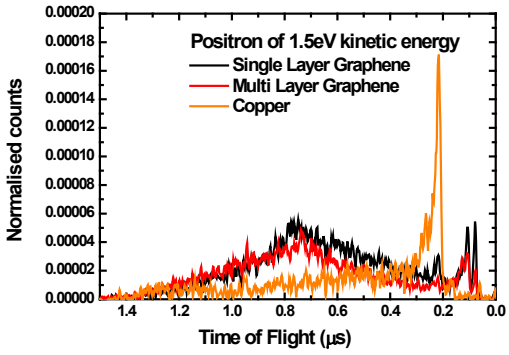


**Fig.1. The TOF-positron annihilation induced Auger electron spectra (PAES) obtained from single layer and multi-layer graphene (on polycrystalline Cu substrate) and from clean polycrystalline Cu. The broad peak at ~1.65 μs (~4 eV) in the PAES spectrum obtained from Graphene corresponds to electrons emitted by the VVV Auger transition.**

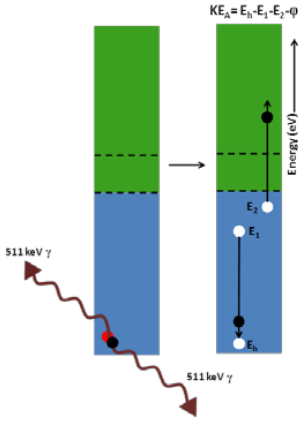


**Fig.2. Schematic representation of the VVV Auger transition.**

## References

[1] Jahnke, T., et al., Ultrafast energy transfer between water molecules Nature Physics 6, 139-142 (2010). https://doi.org/10.1038/nphys1498
[2] Melanie Mucke, et al., A hitherto unrecognized source of low-energy electrons in water Nature Physics 6, 142-146 (2010). https://doi.org/10.1038/nphys1500
[3] Berglund, C. N. & Spicer, W. E. Photoemission studies of Copper and Silver: Experiment Phys. Rev 136 , A 1044-A 1064, (1964). https://doi.org/10.1103/PhysRev.136.A1044.
[4] Willis, R. F., Fitton, B., Painter, G.S. Secondary electron emission spectroscopy and the observation of high energy excited states in graphite: Theory and experiment Phys. Rev. B 9, 1926-37 (1974). https://doi.org/10.1103/PhysRevB.9.1926.

E-mail: weiss@uta.edu

# Spectra of correlated many-electrons systems: From a one- to a two-particle description

O. Gunnarsson[1], J. Merino[2], T. Schäfer[3], G. Sangiovanni[4], G. Rohringer[5,*], and A. Toschi[3]

[1]*Max-Planck-Institut für Festkörperforschung, Heisenbergstraße 1, D-70569 Stuttgart, Germany*
[2]*Departamento de Física Teórica de la Materia Condensada, IFIMAC Universidad Autónome de Madrid, Madrid 28049, Spain*
[3]*Institute of Solid State Physics, Vienna University of Technology, A-1040, Austria*
[4]*Institute of Physics and Astrophysics, University of Wurzburg, D-97070 Würzburg, Germany*
[5]*Russian Quantum Center, Business-center "Ural", 100A, Novaya street, Skolkovo, Moscow, 143025, Russia*

State-of-the art spectroscopic techniques allow for a comprehensive understanding of one-electron excitations in various physically interesting and/or technologically relevant materials. While for weakly-correlated systems the corresponding *one-particle* spectral function $A(\omega, \boldsymbol{k})$ contains essentially all information about their physical properties the situation is much more complicated in the presence of strong electronic correlations. In fact, in the latter case different theoretical treatments often lead to very different explanations of the origin of specific features in the spectrum. A typical example is the pseudogap in the cuprates, i.e., the momentum-selective suppression of spectral weight at the Fermi level (see Fig. 1), which has been related to spin, charge or (d-wave) pairing fluctuations by different authors. This ambiguity about the underlying physical mechanism at work can be overcome by considering *two-particle* correlation functions as they are able to describe the collective modes of the system and can be also related to certain ground state properties of the system. For the specific case of the pseudogap in correlated (single-orbital) lattice system this procedure coined fluctuation diagnostics [1,2] allowed us (1) to identify antiferromagnetic spin fluctuations as microscopic origin of this spectral feature which (2) can be related to the formation of a resonating valence bond ground state in the system.

**ARPES:**

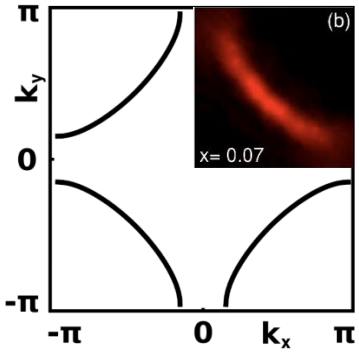


*Yoshida et al., PRB **74**, 224510 (2006).*

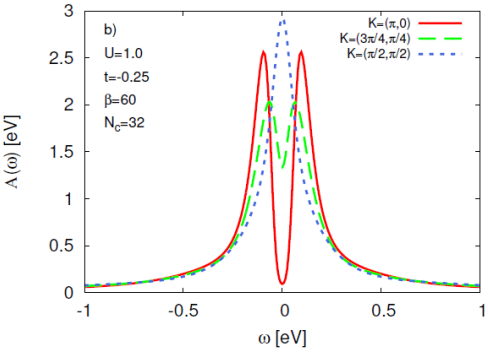


Figure 1: Upper panel: Spectral weight of the cuprate compound $La_{2-x}Sr_xCuO_4$ (x=0.07) at $E_F$. One can clearly see the pseudogap behavior at $k = (0, \pi)$ and $(\pi, 0)$. Taken from Ref. [1]; Lower panel: Frequency dependence of the spectral function of the two-dimensional half-filled Hubbard model obtained by dynamical cluster approximation. For $k = (0, \pi)$ a gap at the Fermi level ($\omega = 0$) is clearly visible. Taken from [2].

## References

[1] O. Gunnarsson, T. Schäfer, J. P. F. LeBlanc, E. Gull, J. Merino, G. Sangiovanni, G. Rohringer, and A. Toschi, Phys. Rev. Lett. 114, 236402 (2015).

[2] O. Gunnarsson, J. Merino, T. Schäfer, G. Sangiovanni, G. Rohringer, and A. Toschi, in preparation.

*Email: grohringer@gmail.com

# SIMDALEE2017 Poster Presentations

## Tuesday, September $19^{th}$

# Overlayer thickness determination based on XPS no-loss peaks ratio

**Viktor Afanas`ev[1], Pavel Kaplya, Dmitry Efremenko[2]**
*[1]National Research University «Moscow Power Engineering Institute», Krasnokazarmennaya 14, Moscow, Russia*
*[2]Deutsches Zentrum für Luft- und Raumfahrt (DLR), Institut für Methodik der Fernerkundung (IMF), 82234 Oberpfaffenhofen, Germany*

**Synopsis** Electron spectroscopy, invariant imbedding, XPS, EAL

X-ray photoelectron spectroscopy (XPS) is attracting considerable interest in surface science and is employed in commercial surface analytical instruments. While qualitative analysis of a XPS spectrum is relatively simple, quantitative analysis is more challenging since the quantification of no-loss peak areas in terms of atomic concentrations is required [1]. The elastic and inelastic scattering cross-sections of electrons at energies 100-1000 eV are of the same order. For lower energies the elastic scattering cross-section increases. Despite this, the majority of electron transport models (e.g. the straight line approximation (SLA)) used for XPS does not provide a rigorous treatment of elastic scattering processes. Instead, semi-empirical corrections are proposed replacing inelastic mean free paths (IMFPs) with so-called effective attenuation lengths (EALs).

In this work, a numerical technique is described, in which the no-loss XPS peaks are modeled by using the radiative transfer equation (RTE). The solution of RTE relies on the discrete ordinate method with matrix exponential [2]. It is suitable for any given singe scattering phase function. No additional assumptions on electron transport in solids are required. The RTE-approach is especially efficient for simulating the isotropization process of an electron beam. A new method for overlayer thickness determination from XPS spectra is proposed. It is based on computing lookup tables for no-loss peak ratios as a function of overlayer thickness by means of the RTE-solver. It provides results for a set of incident and sighting angles and, therefore, is extremely fast. For instance, the computational time required for creating the lookup table for a set of 64 incident and 64 sighting angles is less than 1 minute. Figure 1 illustrates the areas of no-loss XPS peaks for Ni overlayer on Au substrate. The RTE-approach (blue line) is validated against Monte-Carlo simulations (red circles). The agreement within 2 % is obtained. Note that the computations do not involve artificial parameters such as EAL.

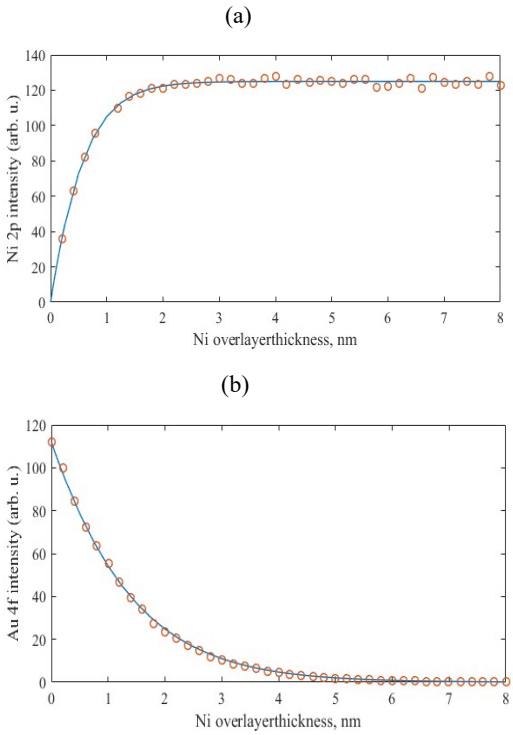


**Figure 1. XPS $Ni_{2p}$ (a) and $Au_{4f}$ (b) no-loss peak intensity gross with Ni sputtering on gold substrate compared to Monte-Carlo results from [3]**

## References

1. Hofmann S. Auger and X-ray Photoelectron spectroscopy in material Science. Springer-Verlag Berlin Heidelberg. 2013.
2. 2. Efremenko D.S., Molina Garcia V., Gimeno Garcia S., Doicu A. J. Quant. Spectr. Rad. Transfer. [accepted] DOI: 10.1016/j.jqsrt.2017.02.015.
3. Jablonski A., Zemek J. Surf. Interf Analysis. **41** (2009) 193.

Email: pavel@kaplya.com

# Principles of low energy electron interactions with simple molecular solids and condensed biomolecules

**Andrew D. Bass*** **and Léon Sanche**
***Départment de Médecine Nucléaire et Radiobiologie, Faculté de Médecine et des Sciences de la Santé, Université de Sherbrooke, Sherbrooke, Québec, J1H5N4, Canada.***

**Synopsis** We review the basic mechanisms of interaction of low energy electrons with atomic, molecular and bio-molecular targets in the condensed phase

Low energy electrons (LEEs) have energies of less than a few tens of eV and are encountered in numerous natural and technological settings. Large numbers of secondary electrons with these energies are produced when high-energy ionizing radiation interacts with a condensed medium, [1] and thus play an important role in energy transfer and any subsequent radiation chemistry. Dependent on the medium, the interactions of LEEs are relevant to understanding diverse phenomena encountered in fields such as radiobiology [2], astro-chemistry [3] and nano-fabrication [4]. The transport properties of LEEs and the nature of their interactions with condensed molecules can be studied by irradiating nano-scale samples with energy selected electron beams and monitoring electron-induced phenomena with techniques such as Low Energy Electron Transmission Spectroscopy (LEET), High Resolution Electron Energy Loss Spectroscopy (HREELS), X-ray Photoelectron Spectroscopy and Mass Spectrometry, particularly by the Electron Stimulated Desorption (ESD) of fragment charged and neutral species [2,5]. As in the gas-phase, electron-molecule interactions at the lowest energies (< 20 eV) are often dominated by the formation of transient negative ions (TNI) that modulate electronic and vibrational excitation and can induce dissociation via dissociative electron attachment (DEA) and autoionization when the target is left in a dissociative state [6]. Such dissociations can drive the synthesis of new chemical species [7]. In thin films, electron transport is often dominated by their structural and interface properties. Using examples drawn from 30+ years of study in the Sherbrooke laboratory, we illustrate how via their transport and reactions, LEEs can initiate significant chemical change in condensed-phase targets ranging from simple molecular solids to complex bio-molecules such as DNA.

E-mail: Andrew.Bass@USherbrooke.ca

## References

[1] S. M. Pimblott and J. A. LaVerne, Radiat. Phys. Chem. **76**, 1244 (2007).
[2] E. Alizadeh and L. Sanche, Chem. Rev. **112**, 5578 (2012).
[3] M. C. Boyer, et al., Surf. Sci. **652**, 26 (2016).
[4] R. M. Thorman, R. Kumar T. P., D. H. Fairbrother, and O. Ingólfsson, Beilstein J. Nanotechnol. 6, 1904 (2015).
[5] A. D. Bass and L. Sanche, in *Charg. Part. Phot. Interact. with Matter* (CRC Press, 2003).
[6] E. Alizadeh, S. Ptasińska, and L. Sanche, in *Radiat. Eff. Mater.*, edited by W. A. Monteiro (InTech, 2017).
[7] C. R. Arumainayagam, et al., Surf. Sci. Rep. **65**, 1 (2010).

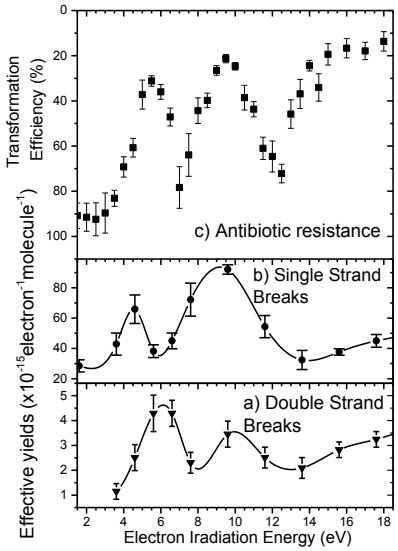


**Figure 1. The ubiquity of TNI: The yields of double (a) and single (b) strand breaks in electron-irradiated pGEM-3ZfL(−) plasmid DNA are modulated by TNI. The ability of these irradiated plasmids to confer antibiotic resistance to *E. coli* (c) is similarly affected. [Kouass-Sahbani et al, Chem. Phys. Lett. 6, 3911 (2015)**

# Experimental investigation of electron emission yield of layered surfaces

**M. Belhaj,[1,] S. Dadouch[1] and D. Payan[2]**
*[1]ONERA-The French Aerospace Lab, 31055 Toulouse, France*
*[2]CNES, 31055 Toulouse, France*

When a solid is hit by incident electrons, the energy transfer can result in the emission of secondary electrons (SE) and backscattered electrons (BSE). Electron emission (EE) is a physical phenomenon involved in several scientific and technical fields such as micro-analysis, particle accelerator space technology (spacecraft charging, Hall Effect Thrusters (HET), nuclear Physics. As the mean escape depth of the SE is of few nm, the electron emission properties of materials are highly dependent to the surface and the first nanometres subsurface. In previous study [1] we have observed that the evolution of the electron emission yield (EEY) of hydrocarbon/silver as function of the hydrocarbon thickness is difficult to interpret. The EEY decreases abruptly at the beginning of hydrocarbon film reduction to pass by a minim value then increase again to reach a steady state value when the entire hydrocarbon layer was removed. The interpretation of the result is made more difficult due to the lack of knowledge of exact composition of the hydrocarbon layer. Therefore, we conducted similar experiments on $SiO_2$/Si layer with well-known composition and material proprieties. We monitored the variations of the electron emission properties (EEY) and the surface composition (Auger Electron Spectroscopy) during step by step ion etching procedure.

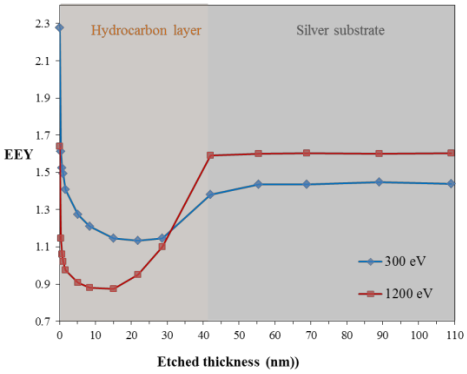


**Figure 1. Evolution of the EEY at 300 ev and 1200 eV of hydrocarbon/silver as function of the hydrocarbon thikness.**

[1] T. Ginestea, M. Belhaj, G. Teyssedre, J. Puech, J. Surf. Anal. **11** (2004) 99. Appl. Surf. Scien. **359** (2015) 398

E-mail: Mohamed.Belhaj@onera.fr

# Unraveling relevance of the different electron generation mechanisms to the Total Electron Yield

**Alessandra Bellissimo,[1,*] Giovanni Stefani,[1] Holger Neupert[2] and Mauro Taborelli[2]**
[1]*Dipartimento di Scienze, Università Roma Tre, Via della Vasca Navale 84, 00146, Rome, Italy*
[2]*CERN, European Organization for Nuclear Research, 1211 Geneva 23, Switzerland*

When a surface is bombarded with an electron beam electrons from the target are released yielding a characteristic energy distribution. Such electron spectrum depends on the microscopic properties of the bombarded target and is intrinsically linked to its band structure and geometrical arrangement. Although secondary electron emission (SEE) has been known and extensively studied [1,2] since over a century, there is still a lack of understanding on their generation-ejection mechanisms. A broad variety of technologies are based on Secondary Electrons (SEs), think of their role in visualizing sub-micron patterns in Scanning Electron Microscopy (SEM) or even their relevance in the patterning process itself (in Electron Beam Lithography). Materials used in technological devices need to be meticulously selected in order to achieve a goal-oriented performance. In some cases, the choice of a material is based on an intended enhancement of the Secondary Electron Yield (SEY), e.g. in particle detectors, whereas for other applications it is desirable to suppress this emission. The vacuum chambers of particle accelerators need to be coated by low-emitting materials thus to prevent (or limit) the electron cloud formation. With the advent of high-power lasers, e.g. Free Electron Lasers (FEL) the understanding of space charge effects due to the emission of SEs is also required. Knowledge about connection between microscopic electronic properties and Total Electron Yield (TEY) has been pursued by comparison of well-characterised metal and carbon surfaces, in various allotropic forms using two different experimental setups present at CERN [3,4]. The TEY, or σ, was measured as a function of the electron beam energy, $E_0$ and of the angle of incidence, Θ. The experiments were performed for each target within two different kinetic energy ranges – one going from 50eV up to 1800eV, whereas the other at lower kinetic energies ranging from 50eV and approaching landing energy ~0eV. Dependence of the electron yield on the angle of incidence of primary electrons (PEs) has been examined at both kinetic energy ranges. In the higher energy range the maximum of the total electron yield, $\sigma_{max}$ exhibits a shift towards higher primary energies and increases with the angle [3]. This effect appears to be more evident for well-ordered systems than in their polycrystalline or amorphous counterparts and can be therefore exploited to disentangle the contribution to the TEY due to the crystalline structure from the one arising due to the bandstructure. Furthermore an attempt to separate the contributions to the total yield of the reflected electrons (REs) and the ejected electrons (SEY) has been made by using a collector as a high-pass filter for electrons with kinetic energies >50eV. Measurements performed in the higher energy range (50-1800eV) show that the TEY curve is built up to ca. 84-91% by the sole ejected electrons, hence it becomes justifiable to approximate it as a SEY, or δ. On the other hand, it is already known that the reflectivity at low primary energies is dictated by the bandstructure of the irradiated material [6] and therefore dedicated effort was applied to the study of TEY response obtained starting from zero landing energy up to 25eV. When the kinetic energy of the primary electron approaches values in the range of the surface potential, the calibration of the measuring setup becomes critical. To this end, reliability of the employed methods will be also discussed into depth. The TEY curves shown in Fig.1 were acquired on nearly free electron metals (NFE) such as polycrystalline Al and Cu surfaces and on a layered electron gas (LEG) material as Highly Oriented Pyrolytic Graphite (HOPG), which also exhibits bi-dimensional crystalline order. It will be demonstrated that in addition to the possibility to investigate the TEY response at these low energies, this type of measurements enables to determine the workfunction of materials with an estimated resolution in the order of 10-100mV (note that high-resolution Kelvin probe methods reach 1-3mV). The evident differences between the TEY curves of the polycrystalline metallic surfaces and the in-plane ordered HOPG will represent a point of further discussion.

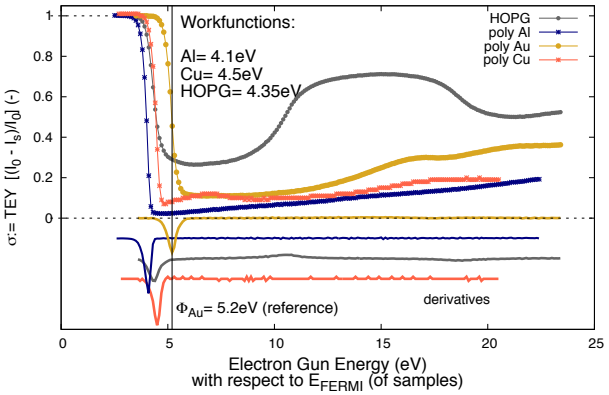


**Fig. 1** Series of low energy TEY of surfaces as indicated in the legend. σ=1, hence total reflectivity, is obtained as long as the primary electron energy is lower than the surface potential. The flexus of the curve indicates the value of the surface barrier and can therefore be used to measure the workfunction of the material.

## References

[1] H. Seiler, J. Appl. Phys., vol. 54, no. 11, pp. R1–R18, Nov. 1983.
[2] A. Shih, J. Yater, C. Hor, and R. Abrams, App. Surf. Sci., 111: 251–258, (1997).
[3] J.R.M. Vaughan, IEEE Trans. on el. devices, Vol. 36, No. 9 (1989).
[4] B. Iouri, N. Hilleret, and C. Scheuerlein. *Journal of Vacuum Science & Technology A: Vacuum, Surfaces, and Films* 18.3 (2000): 972-979.
[5] N. Hilleret, C. Scheuerlein, and M. Taborelli, Appl. Phys. A 76, 1085 (2003).
[6] H. Lüth *"Solid Surfaces, Interfaces and Thin Films"* (Graduate Texts in Physics) – chapter 4.4.1 - Springer Berlin Heidelberg (2010).

## Acknowledgments

Financial support by the FP7 People: Marie-Curie Actions Initial Training Network (ITN) SIMDALEE2 (Grant No. PITN 606988) is gratefully acknowledged.

* e-mail: bellissimo@fis.uniroma3.it

# Spin Polarized Imaging with Scanning Field Emission Microscopy

**G. Bertolini [1], L.G. De Pietro[1], O. Gürlü[1,2] , D. Pescia[1] and U. Ramsperger[1]**
*[1]Laboratory for Solid State Physics, EHT Zurich, Zürich, Switzerland*
*[2]Department of Physics, Istanbul Technical University, Istanbul, Turkey*

In a *Scanning Tunneling Microscope* (*STM*) retracting the tip from the sample by 5 to 100 *nm* and applying a suitable junction bias (-10 to -100 *V* tip bias) between them bring the tip-sample junction out of the tunnelling regime and the tip becomes a source of electrons due to field emission [1]. In this regime the electrons arriving from the tip to the sample cause the generation of secondary electrons on the sample surface, which can escape from the tip-sample junction. Such electrons may be collected by several means and analysed.
This technique is named as *Field Emission Scanning Probe Microscopy* [2]. The strong dependence of the physical properties of the secondary electrons on the nature of the sample surface makes complementary information accessible. Besides the emitted and absorbed current maps and the z-piezo displacement images of the surface, chemical and magnetic contrast with nanometer scale resolution can be achieved on the same region. We are currently aiming at detecting the spin polarization of the secondary electrons, for the purpose of magnetic imaging with nanometer resolution [3].

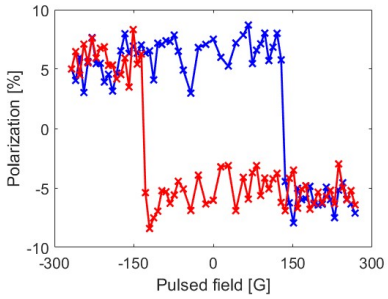


**Figure 1.** Hysteresis curve of secondary electrons polarization signal on 8 *ML* of Fe on W(110). Red and blue discern falling and raising field during the loop.

In this poster we present the magnetic hysteresis behavior observed on one in plane component of the polarization of secondary electrons escaped from a ferromagnetic thin film by *Scanning Field Emission Microscopy* (Fig. 1).

## References

[1] R. Young, J. Ward and F. Scire Rev. of Sci. Inst. 43, 999 (1972).
[2] D. A. Zanin et al. Proc. R. Soc. A 472 :20160475 (2016).
[3] R. Allenspach and A. Bischof Appl. Phys. Lett. 54, 587 (1989)

Furthermore we show the first result of spin polarized imaging of a 500*nm* x 500*nm* region previously scanned in *STM* regime (Fig. 2) despite the fact we had a polarization signal of only 5% on the secondary electrons collected.

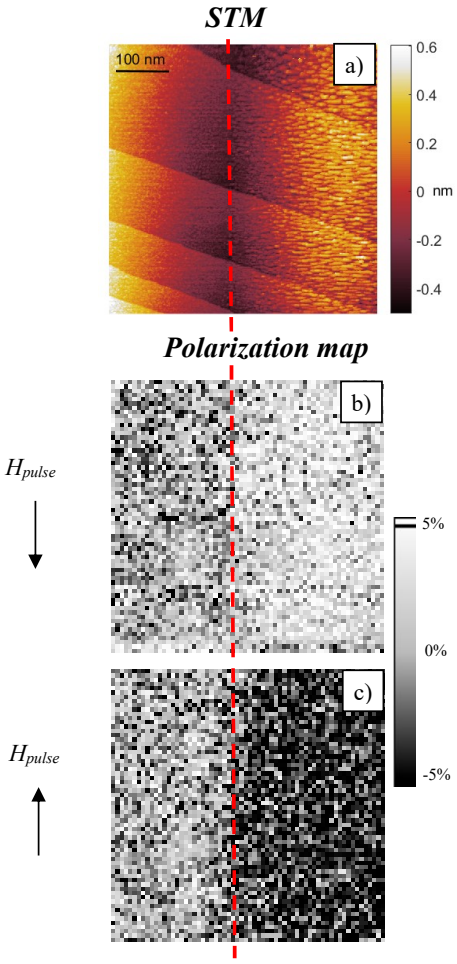


**Figure 2.** a) STM topografic image of 8 *ML* of Fe on W(110) as a wedge. The dash line separates the two regions, Fe on the right and W on the left. b) Secondary electrons polarization mapping of the same region after application of a magnetic pulse in the down direction. Fe appears white. c) Secondary electrons polarization mapping of the same region after application of a magnetic pulse on the up direction. Fe appears black. In both cases W is grey.

E-mail: bertolig@ethz.phys.ch

# ELIMINATION OF SPHERICAL AND AXIAL CHROMATIC ABERRATIONS OF THE ELECTRON MICROSCOPE LENS

**S.B. Bimurzaev[1], E.M. Yakushev[2]**
*[1]Almaty University of Power Engineering and Telecommunications, Almaty, Kazakhstan*
*[2]Institute of Nuclear Physics, Almaty, Kazakhstan*

A new electron-optical scheme of the electron lens aberrations corrector by means of the electrostatic mirror, based on the special focusing mode, in which the planes of Gaussian images of the lens and the mirror coincide with each other and pass through the center of curvature of the deflection magnetic field formed by the round magnetic poles was suggested in [1]. With this location of the magnetic deflector with respect to the electron lens and electron mirror, the magnetic field does not introduce any additional aberrations. The task of calculating the aberration corrector is considerably simplified and mainly reduced to the calculation of the electron mirror, spherical and (or) axial chromatic aberrations of which are equal in magnitude and opposite in sign to the corresponding aberrations of the electron lens.

This paper shows that creation of a relatively simple aberration corrector of the lens of transmission electron microscope (TEM) is principally possible. Operation of the corrector is demonstrated by numerical calculations on the example of correction of the main aberrations of the lens-mirror system consisting of the well-known objective lens with a bell-shaped distribution of the axial magnetic fields and the electrostatic mirror with rotational symmetry. Two simple models of the corrector are considered: in the first, to correct aberrations of the objective lens a two-electrode electrostatic mirror is used, and in the second, a three-electrode electrostatic mirror is applied. It is shown that using the two-electrode mirror it is possible to eliminate either spherical or chromatic aberration of the objective lens, without changing the value of its linear magnification. The three-electrode mirror enables us to simultaneously eliminate spherical and axial chromatic aberrations of the objective lens, which is especially valuable in the design of electron microscopes with extremely high resolution.

The main advantage of the considered aberration corrector is its ability to fully compensate spherical and axial chromatic aberrations of electron lenses of rotational symmetry, which, as we know, cannot be done by aberration correctors using multipole electric and magnetic fields.

## References

[1] Bimurzaev S.B. and Yakushev E.M., Electron lens aberration corrector. // WIPO Patent Application WO/2013/077715 A1 (2013).

E-mail: bimurzaev@mail.ru

# Comparative study of apparent barrier height and local surface potential by ambient scanning probe microscopy

**M. Demydenko[1,*], A. Varlec[1], D. Cassese[1], D. Kostiuk[2], J. Ivanco[2], E. Majkova[2] S. De Monte[1], S. Prato[1],**

*[1] A.P.E. Research, Area Science Park, Basovizza Campus, s.s. 14, Km 163.5 34149, Trieste, Italy*

*[2]Institute of Physics, Slovak Academy of Sciences, Dubravska cesta 9, 84511, Bratislava, Slovakia*

**Synopsis** The paper reports the approach of apparent barrier height and local surface potential analysis by scanning probe microscopy.

Scanning probe microscopy is an important and powerful method to study the nanostructured materials that allows to collect information about surface topography, phase separation, electrical and mechanical properties etc. However necessity to obtaining more complex information of the interested area is still important to improve the technique.

In this work we compare study of the apparent barrier height distribution and surface potential of gold film and nanoparticles of semiconductive and conductive material. To compare the proposed approaches the experimental setup was build based on ambient Scanning Tunneling Microscope (STM) and Kelvin Probe Force Microscope (KPFM), both produced by A.P.E. Research.

The apparent barrier height measurements provide information about spatial distribution based on dishomogeneity of the sample surface. The gold film on mica was taken as a reference sample, where the change in apparent barrier height (Fig. 1 b) on the atomic steps was measured simultaneously with topography (Fig. 1 a). During the measurement generated sinusoidal signal of small amplitude was used to modulate the tip-sample separation in the range of 4 Å. The oscillating frequency was chosen out of working range of STM amplifier to avoid additional noise of the topography signal. In the result a small response variation of current was measured using lock-in amplifier. In contrast to the Ref. [1] where similar technique was applied in UHV STM system our setup show stable and low-noise results in the ambient conditions.

The surface potential measurement was carried out on KPFM. The mapping of the work function by this technique was used as a reference method to compare the same functional characteristic of the material.

The study of the nanoparticles shows distribution of different types of nanoparticles on the substrate. Such additional information in combination with topography allows to analyze more in detail the sample.

The results of the measurements show a perspective of using the proposed technique with the existing scanning probe microscopes to obtain local information about different characteristics of nanoscaled systems. Our approach open the way to study the soft matter that is not suitable for vacuum systems however could be used in ambient conditions.

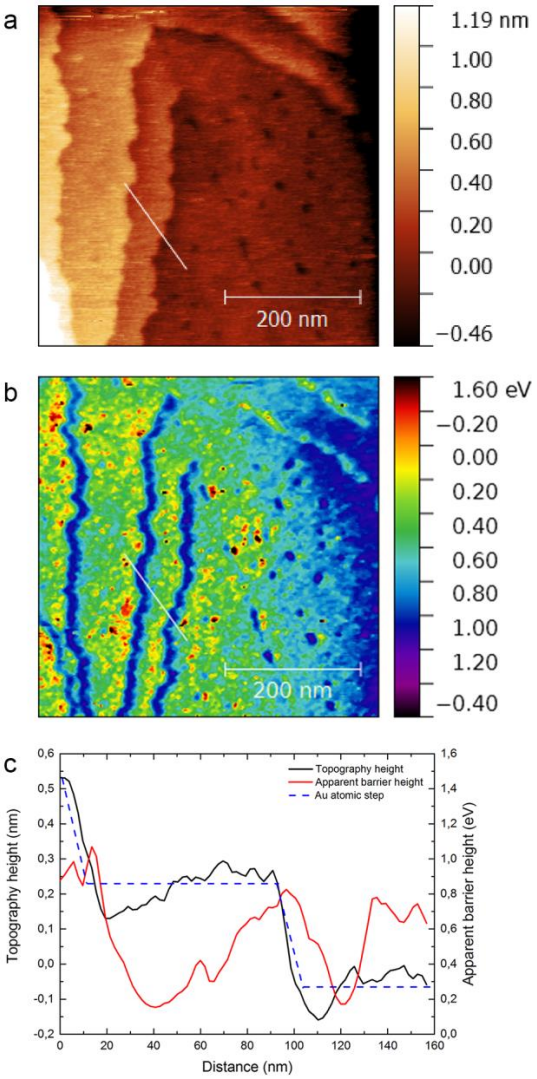


**Figure 1. STM image of gold film surface in constant current mode combined with modulation: topography (a), apparent barrier height distribution (b) and line profile (c).**

## References

[1] J. Jia at al. Phys. Rew. B. **58** (1998) 1193

## Acknowledgments

This project is supported by SIMDALEE2, FP7-PEOPLE-2013-ITN (Grant agreement N. 606988)

* E-mail: maksym.demydenko@aperesearch.com

# Comparison of Low Energy Electron Emission Resulting from Deep Valence Hole Auger Transitions in Graphene on Cu, Highly Oriented Pyrolytic Graphite (HOPG), and Graphene on Si

**A J Fairchild,[1,*] V A Chirayath,[1] S K Imam,[1] M D Chrysler,[1] R W Gladen,[1] A R Koymen,[1] and A H Weiss[1]**

*[1]The University of Texas at Arlington, Arlington TX 76019*

**Synopsis** We discuss the low energy electron spectra due to positron induced deep valence hole Auger relaxation in single layer graphene on Cu, multi-layer graphene on Cu, HOPG, and single layer graphene on Si.

Recently, our group at the University of Texas at Arlington (UTA) has directly measured the energy of electrons emitted as a result of the relaxation of deep valence holes in single layer graphene (SLG) on Cu, multi-layer graphene (MLG) on Cu, and HOPG. A low energy positron beam (1.5 eV) was used to initiate the Auger process through positron-electron annihilation. The energy was measured using time of flight (TOF) technique where the TOF was taken from the time difference between the detection of the 511 keV annihilation gamma ray, using a $BaF_2$ scintillator, and the detection of the Auger electron, using a micro-channel plate (MCP). A low energy peak was observed and following the X-ray notation was designated as a VVV Auger transition. The VVV Auger transition is initiated by a deep hole in the valence band which is filled by an electron from a higher valence level. The energy associated with this electronic transition is coupled to another valence electron which can have sufficient energy to leave the material. The kinetic energy of the emitted Auger electron is given by $KE = E_h - E_1 - E_2 - \varphi$, where $E_h$ is the energy level of the initial hole, $E_1$ and $E_2$ are the binding energies (with respect to the Fermi level) of the electronic states involved in the transition, and $\varphi$ is the work function. Therefore, electron emission due to VVV Auger transitions should be observable in any material that has a sufficiently wide valance band to allow deep hole filling, e.g. Si, Ge, Te and Se. Recently, we have compared the VVV spectra of MLG to SLG on Cu and a shift to lower energies was observed for MLG. In this report, we compare the VVV spectra of SLG on Cu, MLG on Cu and HOPG (Figure 1) to better understand this shift to lower energies and to investigate the influence that the number of graphene layers has on the VVV line shape. A reduction in intensity and a shift toward higher TOF (lower energy) of the VVV signal is observed as the number of graphene layers approaches graphite. Additionally, the VVV spectra of SLG on Cu and SLG on Si (100) are compared (Figure 2) to investigate the influence of the substrate on the VVV line shape. Lastly, the results of VVV experiments on Si (100) are presented and discussed.

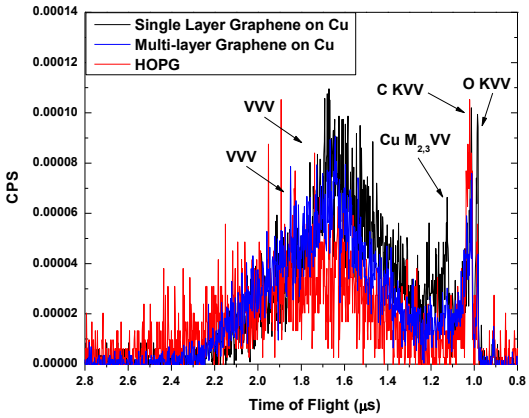


**Figure 1. The time of flight positron annihilation induced Auger electron (TOF-PAES) spectra from single layer and multi-layer graphene on Cu and HOPG. The inelastic tail of Cu $M_{2,3}VV$ has been subtracted.**

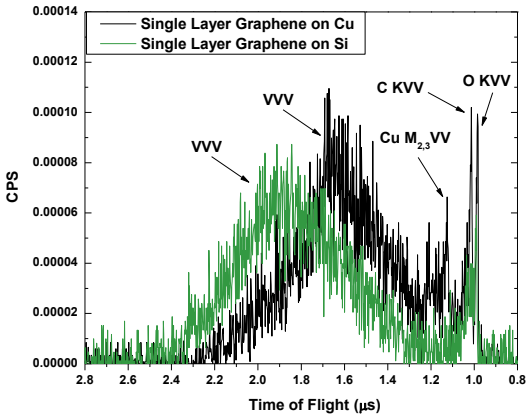


**Figure 2. The TOF-PAES spectra from single layer graphene on Cu and Si. The inelastic tail of Cu $M_{2,3}VV$ has been subtracted.**

E-mail: alexander.fairchild@uta.edu

# Energy Spectrum of Low Energy Electrons Emitted from a Ag(100) Surface as a Result of NVV Auger Transitions

**R.W. Gladen[1,*], P.V. Joglekar[1], K. Shastry[1], Q. Dong[2], S.L. Hulbert[2], R. A. Bartynski[3], Wolfgang S.M. Werner[4], and A.H. Weiss[1]**

*[1]The University of Texas at Arlington, USA*
*[2]Brookhaven National Laboratory, USA*
*[3]Rutgers University, Piscataway, NJ, USA*
*[4]Vienna University of Technology, Austria*

**Synopsis** A series of Auger-Photoelectron Coincidence measurements from Ag(100) were used to extract the part of the energy distribution of emitted electrons due solely to NVV Auger transitions. The extracted spectra are compared to detailed Monte-Carlo Calculations modeling transport and cascade processes.

Measurements are presented of the full energy spectra of electrons emitted from Ag(100) surface as a result of the NVV Auger transition, obtained using Auger Photoelectron Coincidence Spectroscopy (APECS), from which Auger-unrelated contributions have been subtracted. The experimental Auger spectra were obtained in time coincidence with the photo-emitted 4p core emissions for Ag. The large background contribution to the APECS spectrum, owing to Auger-unrelated processes in which the initial photon energy is shared by two or more valence band electrons, was determined by extrapolation from a series of coincidence measurements and subtracted from the APECS spectrum to obtain the energy distribution of electrons emitted solely as a result of NVV Auger transitions. The resulting spectrum also includes, in addition to Auger electrons emitted without energy loss, inelastically scattered Auger electrons and (possibly) electrons emitted as a result of multi-electron Auger decays. We observed that the spectral weight in the low energy tail (LET) in the APECS spectra is reduced by more than a factor of 2 after subtraction of the Auger-unrelated contributions. However, the intensity of the LET after this subtraction is still of the same order or larger than the integrated intensity in the Auger peak. The intensity of the remaining LET in the coincidence measurements is consistent with a Monte-Carlo model that includes the inelastic transport of both the Auger and photoelectrons.

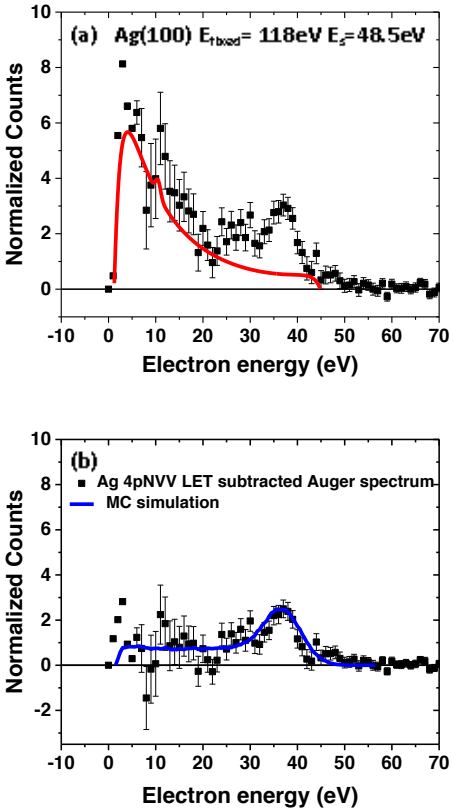


**Fig.1. Ag(100) photoelectron spectra (180 eV photon energy) taken in time coincidence with valence band emission (118 eV electron energy). (a) NVV coincidence Auger spectrum (symbols) and the estimated contribution from Auger-unrelated electrons (red curve) [1,2]. (b) spectrum in (a) after subtraction of the estimated contribution from Auger-unrelated scattering events (symbols) and the model spectrum obtained through a detailed Monte-Carlo simulation (blue curve) [1].**

## References

[1] Joglekar, et al. Energy Spectrum of Electrons Emitted as a Result of Core-Valence-Valence (CVV) Auger Transitions in Ag(100), to be published.
[2] Satyal, et al. Measurement of the background in Auger-photoemission coincidence spectra (APECS) associated with inelastic or multi-electron valence band photoemission processes, Journal of Electron Spectroscopy and Related Phenomena **195,** 66 (2014).

E-mail: randall.gladen@uta.edu

# Modelling entire XPS spectra of core-shell nanoparticles for the calculation of shell thicknesses and core radii

**M. Hronek[1*], H. Kalbe[1], J. Pseiner[1], C.J. Powell[2] and W.S.M. Werner[1]**
*[1]Vienna University of Technology, Vienna, Austria*
*[2]National Institute of Standards and Technology, Gaithersburg, United States of America*

The investigation of planar-layered samples as well as core-shell nanoparticles (CSNP) based on quantitative X-ray photoelectron spectroscopy (XPS) analysis provides valuable information about the chemical and structural properties of a sample. Particularly, the estimation of shell thicknesses of CSNP from XPS data is well established [1,2,3]. These methods only make use of the intensities of the main XPS peaks, but neglect the information contained in the shape of the inelastic background, which usually exhibits a far larger cumulative intensity than the narrow elastic peaks.

As was previously shown [4], it is possible to calculate planar layer thicknesses from the intensity of the background signals in relation to the peak intensities in XPS spectra. A novel approach for CSNP is presented based on the simulation of entire XPS spectra [1] and the comparison with experimental data. The simulation result is fitted to the measured spectrum with the shell thickness and core radius of the CSNP as fit parameters.

XPS spectra are calculated in a Monte-Carlo (MC) simulation of the electron trajectories [1]. The experimental spectrum is deconvoluted into the contributions of the individual XPS lines, which are then compared with the corresponding simulated partial spectra in a fitting routine. The background shape is modelled based on the partial loss intensities of inelastically scattered electrons, which are computed from the results of the MC simulations.

E-mail: martin.hronek@gmx.at

The electron energy loss is simulated over a wide range. Thereby, the single particle approximation used by all previous methods breaks down and disordered powders of nanoparticles are simulated instead. Furthermore, the change of the inelastic mean free path (IMFP) as a function of the changing electron kinetic energy must be accounted for.

For this study, a series of polymeric CSNP samples consisting of polytetrafluoroethylene (PFTE) cores and poly (methyl methacrylate) (PMMA) shells were investigated by XPS. The experimental results are presented along with fitted spectra from which shell thicknesses and core radii were determined.

**Thanks/Acknowledgement**

The funding from the 14IND12 Innanopart project by the EU through the EMPIR initiative is gratefully acknowledged.

**References**

[1] W.S.M. Werner et al., Nist Database for the Simulation of Electron Spectra for Surface Analysis, SRD 100, Version 2.0, National Institute for Standards and Technology (NIST), Gaithersburg, MD, USA, 2014
[2] H. Kalbe et al., J. Electron Spectrosc. Relat. Phenom. 212, 2016, 34-43
[3] A. Shard, J. Phys. Chem. C, 116(31), 2012, 16806-16813
[4] S. Tougaard, J. Vac. Sci. Technol. A 14, 1996, 1415-1423

# A secondary electron emission empirical model

**C. Inguimbert[1], J. Pierron[1], M. Belhaj[1], J. Puech[2]**
*[1]Onera, 2 av. Edouard Belin Toulouse, France*
*[2]CNES, 18 av. Edouard Belin Toulouse, France*

## Synopsis

In the past, many attempts have been made to elaborate models of electron Secondary Emission Yield [1-12]. Some models based on sophisticated theories exist [3-5], but they are often restricted to given targets studied under specific conditions. Some other models such as the probabilistics models developed by Furman [5] are difficult to apply. That's why simplistic approaches have been developed along the years [6-12]. They are based on very simplifying assumptions in order to get analytical compact formulas.

$$Y_{se}(E) = c_1 \cdot \int_0^{h_e(E)} \left| \frac{dE}{dh}(h) \right| \cdot e^{-c_2 h \cdot} dh \qquad (1)$$

Those kind of models postulate most of time a power law range/energy function $h_e(E)$ with a constant energy loss [6, 12]. These simple approaches give relatively satisfying results when fitting procedures are applied but it generally fails to reproduce faithfully experimental SEY curves [8, 9]. Some improvements, including more accurate physical mechanisms have been made [13]. But this is often detrimental to the simplicity of the models. This work proposes a semi empirical model built on the same theory as the Dionne formulation [8, 9] (equation (1)). But our approach is based on accurate range [14] and transmission η(r) probability expressions, deduced from a Monte Carlo analysis (OSMOSEE code [15-17]).

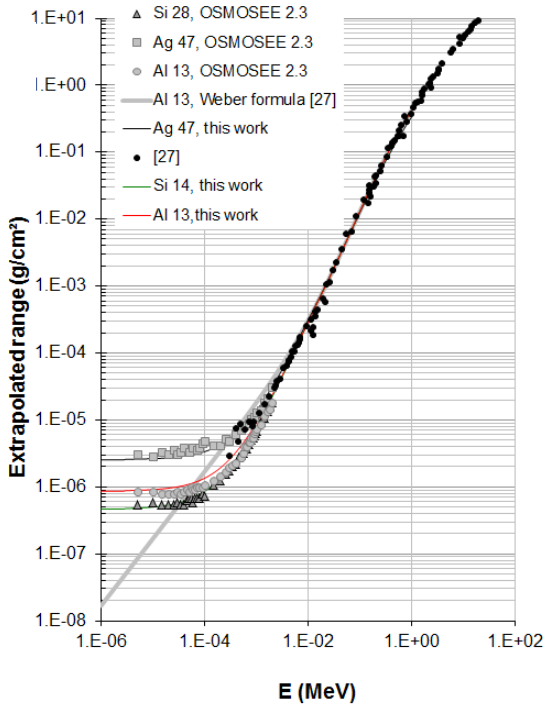


**Figure 1. Extrapolated range for incident electrons in Al, Si and Ag in the energy range [1 eV, 30 MeV].**

The range/energy function is demonstrated to be very different at low energy from the classically used power law expressions [14] (Figure. 1). It reaches a plateau region and does not tend to zero as predicted by the classical models [14]. These two functions, given for energies down to few eV, have been used to define an accurate expression of the secondary electron generation term. This ionizing dose expression, contrary to the commonly used constant energy loss function, has a typical shape that goes through a maximum. This particular form is demonstrated to have a direct impact of the shape of the SEY curve. The secondary emission yields given by this new model are in quite good agreement with experimental data obtained for two materials Ag, Al (Figure 2).

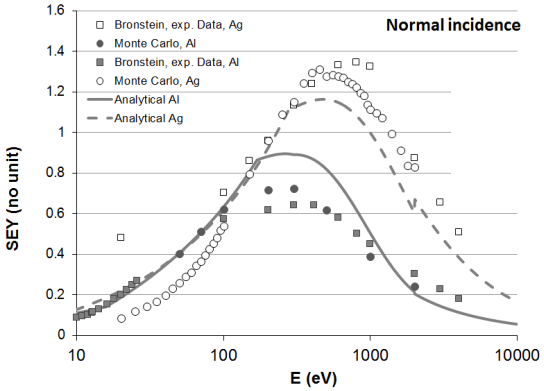


**Figure 2. Comparison of the SEY given by the model and the experimental data of Bronstein [28] and the calculation of the Monte Carlo code.**

## References

[1] H. Salow, Z. Tech. Phys. 21, 8 (1940),
[2] H. Bruining, 1954, Physics and Applications of Secondary Electron Emission, McGraw-Hill, New York.
[3] A.J. Dekker, 1954 Physica 21, 29.
[4] E .Schreiber, H .J .Fitting, 2002 J .Electron .Spectrosc .Rel.Phenom .124, 25
[5] Furman, M. A., & Pivi, M. T. F. 2002, Physical Review Special Topics-Accelerators and Beams, 5(12), 124404.
[6] Baroody EM. 1950, Phys. Rev. 78, 780
[7] Jonker JLH 1952 Philips Res. Rep
[8] Dionne G. F. 1973 J. Appl. Phys. 44 5361-5364
[9] Dionne G. F. 1975 J. Appl. Phys. 46 3347-3351
[10] Seiler H. 1983 J. Appl. Phys. 54 1-18.
[11] J .Cazaux, 2001, J .Appl .Phys .89, 8265.
[12] Lin, Y., & Joy, D. C. 2005, Surface and Interface Analysis, 37(11), 895-900
[13]J. Cazaux, 2003, Thin Solid Films, 434(1-2), 303-310.
[14] Inguimbert C & al. MULCOPIM2017 Conference, Netherland.
[15] Roupie J. & al.2013 J. of Phys. D: Appl. Phys. 46 1-9
[16] Pierron J. & al.2015 LEE2015 Conference Austria
[17] Pierron J. & al.2016 RADECS2016Conference Germany


E-mail: Christophe.Inguimbert@onera.fr

# The effect of structural disorder on the secondary electron emission of graphitic materials.

**R. Larciprete,[1,2] L.A. Gonzalez,[1] A. Di Trolio,[1,2] D. R. Grosso,[1] and R. Cimino[1]**
*[1]LNF-INFN, via E. Fermi 27, Frascati, RM, Italy*
*[2]CNR – Institute for Complex Systems, Via Fosso del Cavaliere 100, 00133 Roma, Italy*

Due to the low secondary electron yield (SEY) properties of $sp^2$ carbon the use of graphitic thin films is seen as an efficient solution to mitigate electron cloud phenomena in high energy particle accelerators and in space devices. However, when considering this kind of applications, important issues arise related to the level of structural quality of the graphitic layers necessary to guarantee a low SEY and to their stability once exposed for long time to hostile working conditions, i.e. electron, photon and ion bombardment.

In this study we faced both aspects. First, we investigated the effect that the level of crystalline ordering of ultrathin carbon layers has on their SEY properties [1]. To this aim we deposited amorphous C films on copper substrates and followed the $sp^3 \rightarrow sp^2$ structural reorganization and the coalescence of the $sp^2$ clusters into nanocrystalline graphite induced by thermal annealing while measuring in parallel the SEY of the samples (Fig.1). Then we focused on the opposite process by studying in highly oriented pyrolitic graphite (HOPG) the relation between SEY and the increasing structural disorder induced by subsequent cycles of $Ar^+$ ion bombardment at low kinetic energy (150 eV) (Fig.2) [2]. In this case the modification of the electronic and structural properties of HOPG were related to the changes observed in the SEY curves.

In both experiments we measured *in situ* the SEY curves from very low energies up to several hundreds of eV and used ultraviolet and X-ray photoelectron spectroscopy to acquire valence band and C1s core level spectra, respectively, whereas *ex situ* Raman spectroscopy was employed to determine the structural order in the near surface layer of the samples.

Our results demonstrated that the moderate structural quality obtained during the graphitization of the amorphous C layer is sufficient to achieve a considerable SEY decrease indicating that the formation of aromatic clusters of a few nanometers in size lowers the macroscopic SEY to the level of that of graphitic carbon with much higher structural ordering. On the other hand amorphization of HOPG was proved to be capable of modifying the shape of the SEY curve leaving, however, its maximal value relatively stable and low (<1.1).

Both evidences might be exploited for the design and the optimization of ultrathin coatings aimed at mitigating multipacting processes.

## References

[1] R. Larciprete, D. R. Grosso, A. Di Trolio, R. Cimino, Appl. Surf. Sci. **328** (2015) 356
[2] L. A. Gonzalez, R. Larciprete, and R. Cimino, AIP Adv. **6,** 095117 (2016)

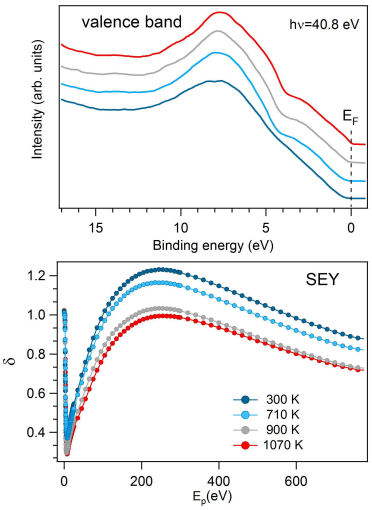


**Figure 1. (top) Valence band spectra and (bottom) SEY curves measured on the C films as a function of the annealing temperature.**

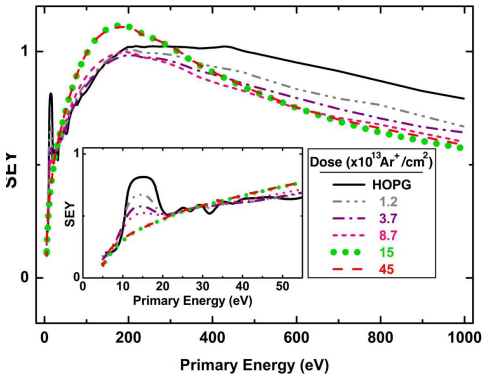


**Figure 2. SEY and LE-SEY (inset) curves measured on HOPG as cleaved (black line) and after the exposure to increasing doses of $Ar^+$ ions at 500 eV.**

E-mail: rosanna.larciprete@isc.cnr.it

# Spin-Polarized Metastable Helium Atoms as a Probe of Surface Electronic and Magnetic Structure

**Andrew Pratt,[1*] Mitsunori Kurahashi,[2] and Yasushi Yamauchi[2]**
*[1]Department of Physics, University of York, York YO10 5DD, UK*
*[2]National Institute for Materials Science, 1-2-1 Sengen, Tsukuba 305-0047, Japan*

**Synopsis** We outline the use of the surface analysis technique of spin-polarized metastable de-excitation spectroscopy to probe surface electronic and magnetic structure and review recent applications to technologically-relevant materials.

In this presentation, we review the use of a spin-polarized beam of metastable ($2^3S$) helium atoms to characterize surface electronic, chemical, and magnetic properties, especially those of materials relevant to future technological devices. Surface properties are often vastly different to the bulk of a material due to reduced dimensionality, unsaturated dangling bonds and relaxation and reconstruction of the bulk atomic structure. Hence, their understanding is critical to the design and operation of, for example, spintronic and organic spintronic devices. In particular, the role of surface and interfacial states in determining the efficiency of spin injection from a ferromagnetic (FM) metal into a non-magnetic solid has recently become increasingly clear [1].

When approaching a surface to within several angstroms, helium atoms, prepared in the long-lived metastable $2^3S$ state ($E_{He*}$ = 19.82 eV), may lose their energy via several de-excitation mechanisms. Depending on the conductivity of the sample, de-excitation will predominantly occur via direct Auger de-excitation or the two-step process of resonance ionisation followed by Auger neutralization (figure 1). This causes the emission of an electron which carries with it information on the surface electronic and magnetic properties. As the cross-section for this de-excitation is so large, there is no penetration of the atom below the topmost surface whatsoever (figure 2). The technique becomes magnetically active by electron-spin-polarizing the He $2^3S$ atoms to provide an extremely sensitive probe of the spin-resolved densities of state at the surface of a material.

Recent progress on the implementation of this technique will be given concentrating on three main areas: (i) novel methods used to intensify the helium beam, for example, by using methods of laser cooling [2]; (ii) the application of magnetic fields of up to 5 T to a sample during the acquisition of spectra [3]; (iii) the use of the technique in characterizing materials relevant to spintronic and molecular spintronic devices, for example, the spin polarization at the surface of FM oxides [4] and organic semiconductor-FM interfaces [5]. Comparisons will be made to other surface-sensitive techniques such as ultraviolet photoelectron spectroscopy (UPS) and future prospects will be reviewed including how the technique might be developed as a microscopy.

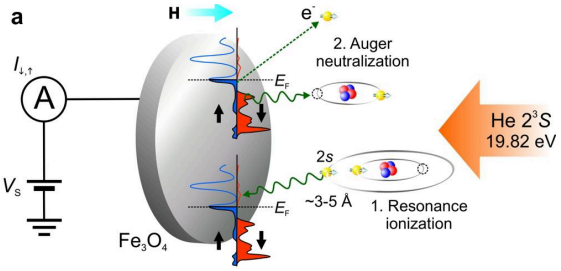


**Figure 1: Schematic of He $2^3S$ de-excitation at a ferromagnetic surface and the sample current method used to probe the spin-resolved density of states. De-excitation at the conducting $Fe_3O_4$ surface occurs via the two-stage process of resonance ionization followed by Auger neutralization.**

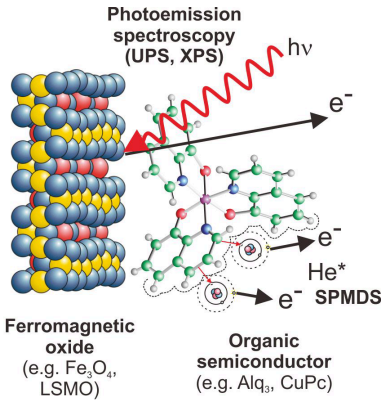


**Figure 2: A spin-polarized beam of metastable helium atoms (SPMDS) provides an extremely sensitive probe of spin-resolved surface electronic structure.**

## References

[1] V. A. Dediu *et al*., Nature Mater. **8**, 707 (2009); S. Sanvito, Nature Phys. 6, 562 (2010).
[2] A. Pratt and M. Jacka, J. Phys. D: Appl. Phys. **42**, 055308 (2009).
[3] M. Kurahashi, X. Sun and Y. Yamauchi, Phys. Rev. B **81**, 193402 (2010).
[4] A. Pratt, M. Kurahashi, X. Sun, D. Gilks and Y. Yamauchi, Phys. Rev. B **85**, 180409(R) (2012).
[5] A. Pratt, L. Dunne, X. Sun, M. Kurahashi and Y. Yamauchi, J. Appl. Phys. **111**, 07C114 (2012).

E-mail: andrew.pratt@york.ac.uk

# Cathodoluminescence of AlGaN/GaN Using Monte Carlo Simulation. Effect of Temperature and Compositional

**Aouati Redha[1,*], Legherib Lazhar[2], Nouiri Abdelkader[2]**

*[1]Thin Films and Interfaces Laboratory, University of Frères Mentouri Constantine, Constantine 25000, Algeria*

*[2]Department of physics, University of Oum-El-Bouaghi, Oum-El-Bouaghi, 04000, Algeria*

In this paper, a GaN cubic semi-conductor, AlGaN/GaN single-quantum well (SQW) and multi-quantum wells (MQWs) nanostructures of cubic phase with $Al_xGa_{1-x}N$ barriers and GaN quantum well (figure 1) have been studied using Monte Carlo calculations and cathodoluminescence (CL). A Monte Carlo calculation model is developed to describe the interaction of electron beam with GaN and their relate semiconductor, we demonstrate the influence of Al mole content (x) on penetration depth of electrons and CL intensity in GaN and AlGaN, penetration depth is increased with decreasing of the x mole fraction in the AlGaN simple, The effect of low-energy electron-beam (e-beam) irradiation of the cathodoluminescence in single quantum well (SQW) and multi-quantum wells of AlGaN/GaN structures has been studied. The cathodoluminescence signal CL is calculated in GaN and in their relate ternary taking into account compositional and confinement phenomenon within the quantum well of GaN, the diffusion length $L_d$ of generated carriers in GaN/AlGaN quantum well has been demonstrated.

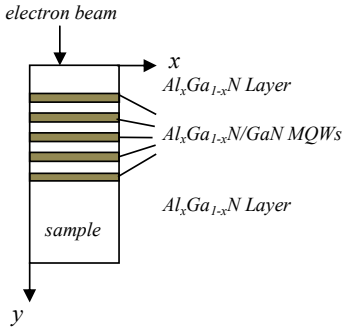


**Fig. 1 Schematic representation of $Al_xGa_{1-x}N$/GaN sample under an electron beam used in our cathodoluminescence simulation.**

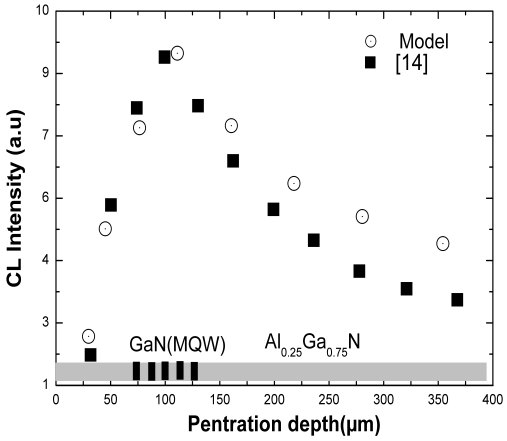


**Fig. 2 Comparison between our calculation model and other experimental model [1] for cathodoluminescence signal of $Al_{0.25}Ga_{0.75}N$/GaN multi-quantum wells simple. A schematic drawing of the sample is insetted at the bottom.**

## References

[1] D. J. As, S. Potthast, U. Köhler, A. Khartchenko and K. Lischka, Mat. Res. Soc. Symp. Proc. 743 (2003) L5.4.1

# Low energy (1-50 eV) inelastic mean free path (IMFP) values estimated from experimental results using Monte Carlo calculations

**O.Y. Ridzel,* W.S.M. Werner, V. Astasauskas**
*Vienna University of Technology, Vienna, Austria*

An extensive database of secondary electron yield (SEY) values (in the energy range between 10 eV and 10 MeV) has been created from a literature search. As it is well known SEY values at any energy depend sensitively on the inelastic mean free path (IMFP) values, in particular below 50 eV. A Monte Carlo (MC) code has been developed to simulate the SEY values based on Mott cross sections for elastic scattering, linear response theory (based on empirical optical constants) to describe inelastic scattering and the commonly employed model for the surface barrier in terms of the inner potential and the work function of the solid. References [1] and [2] represent upper and lower extreme IMFP-values. Variation of the IMFP in between these extreme values during the MC simulation and a comparison with the literature data [1,2] give us a realistic estimate for the IMFP values at energies below 50 eV. The presentation will contain first results of this study.

## References

[1] Tanuma, S., Powell, C. J. and Penn, D. R. (1994), Calculations of electron inelastic mean free paths. V. Data for 14 organic compounds over the 50–2000 eV range. Surf. Interface Anal., 21: 165–176.
[2] C. T. Chantler and J. D. Bourke, The Journal of Physical Chemistry A 2014 118 (5), 909-914.
[3] A. K. Fazlul Haque, M.M. Haque, M. Atiqur R. Patoary, et. al., Electron impact secondary electron emissions from elemental and compound solids, Vacuum, 2017 141, 192-209, http://dx.doi.org/10.1016/j.vacuum.2017.04.004.

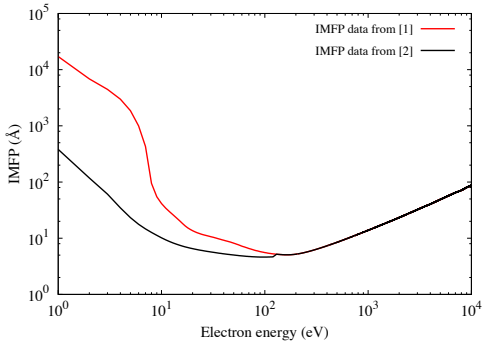


**Fig. 1 IMFP as a function of electron energy for Ag**

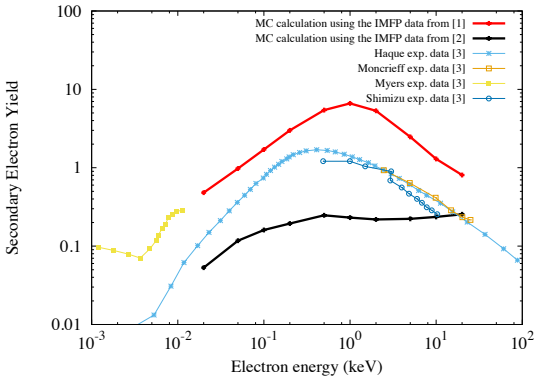


**Fig. 2 Electron impact SEY as a function of incident energy for Ag**

## Acknowledgement

Financial support by the FP7 People: Marie-Curie Actions Initial Training Network (ITN) SIMDALEE2 (Grant No. PITN 606988) is gratefully acknowledged

E-mail: ridzel@iap.tuwien.ac.at

# Effect of axial aberrations on the degree of coherence in SEM

**Tomáš Řiháček[1,*] and Ilona Müllerová[1]**
*[1]Institute of Scientific Instruments of the CAS, v. v. i., Brno, Czech Republic*

**Synopsis** We study the influence of axial aberrations on the degree of coherence in a scanning electron microscope. The effect of the chromatic aberration turns out to be important, especially for energies below a few keV, and this threshold depends upon geometrical parameters of the optical system.

Shaping and structuring of a beam in an electron microscope [1] became an interesting way of finding new applications in the last decade. A common method of doing this is electron diffraction on artificially made nanostructures, typically a grating. From the very nature of this process, it is clear that coherence of the primary beam is an important characteristic, which must be taken into consideration.

This condition is well described by a *(complex) degree of coherence* (between points $\mathbf{r}_1$, $\mathbf{r}_2$) defined as

$$\gamma(\mathbf{r}_1,\mathbf{r}_2) = \frac{\langle \psi^*(\mathbf{r}_1,t)\psi(\mathbf{r}_2,t)\rangle}{\sqrt{\psi^*(\mathbf{r}_1,t)\psi(\mathbf{r}_1,t)}\sqrt{\psi^*(\mathbf{r}_2,t)\psi(\mathbf{r}_2,t)}},$$

which depends upon many parameters of the optical system. The most substantial influence is commonly ascribed to the source size, whereas aberrations are usually omitted in (scanning) transmission electron microscopes ((S)TEM). On the other hand, scanning electron microscopes (SEM) are seldom employed for this purpose. In these systems, one sometimes have to bend the parameters into very contrived configurations and aberrations thus may reach considerable values, and must be therefore taken into account.

While spherical aberration is not very important, chromatic aberration turns out to be critical, notably when low energies are considered. Diameter of an area where $1 \geq \gamma \geq 0.88$ is sometimes called *coherence patch*.

We consider a finite source emitting a paraxial spherical wave, which is focused by a thin lens with chromatic aberration coefficient $Cc$ with respect to the image plane; see Figure 1. For a lens with $Cc = 0$, the coherence patch is given by [2]

$$d_{\mathrm{coh}} \approx \frac{0.16\overline{\lambda}}{\alpha},$$

where $\overline{\lambda}$ is electron mean wavelength.

By a direct calculation we show that the above-mentioned formula does not hold for a high chromatic aberration and low energy (below 2 keV in this case; this threshold depends upon geometry of the optical system).

The coherence patch is thus considerably reduced, as shown in Figure 2. However, the coherence patch may still remain sufficient to perform the diffraction in SEM, even at energies below 0.5 keV.

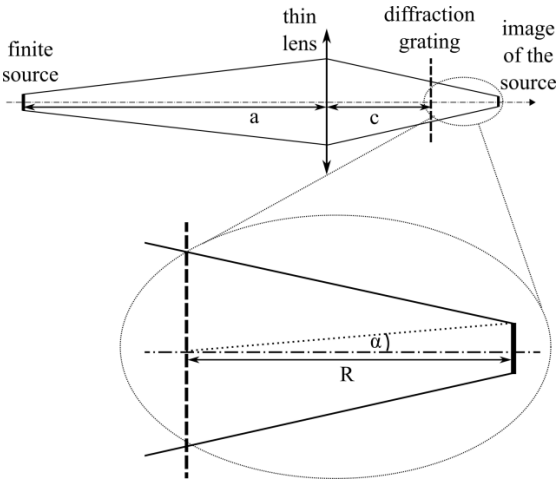


**Figure 1. Optical setup. For this example we take $\alpha = 1\ \mu$rad, $a = 100$ mm, $c = 20$ mm and $R = 40$ mm.**

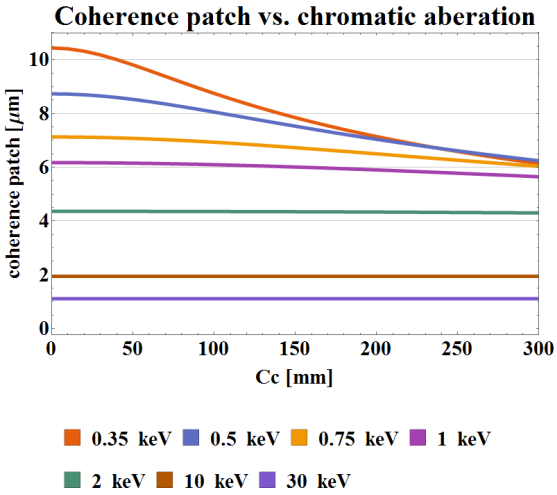


**Figure 2. Effect of chromatic aberration on coherence patch for primary beam energy of 0.35 - 10 keV and energy spread of 1 eV.**

## References

[1] J. Verbeeck et al., C. R. Phys. **15** (2014) 190–199.
[2] M. Born and E. Wolf, "Principles of Optics: Electromagnetic Theory of Propagation, Interference and Diffraction of Light", New York 1999, pp. 593.
[3] This work was supported by the project no: TE01020118 of the Technology Agency of the Czech Republic and by the European Commission for the Marie Curie Initial Training Network SIMDALEE2: Grant No. 606988 under FP7- PEOPLE-2013-ITN.

E-mail: rihacek@isibrno.cz

# Investigation of the long-term behavior of the work function and the quantum efficiency of surfaces by photoelectron spectroscopy

**Kerstin Schönung,[1,*] Matthias Wecker[2]**
*[1]Max Planck Institute for Nuclear Physics, Saupfercheckweg 1, 69117 Heidelberg, Germany*
*[2]Karlsruhe Institute of Technology, Institute for Technical Physics, Hermann-von-Helmholtz-Platz 1, 76344 Eggenstein-Leopoldshafen*

The KArlsruhe TRItium Neutrino experiment (KATRIN) [1] will perform a model-independent measurement of the effective neutrino mass. The measurement is performed by examining the β-electron energy spectrum of a gaseous molecular tritium source (WGTS). Due to ionization processes in the tritium source a cold plasma is generated in the WGTS. To achieve the desired sensitivity of 0.2 eV/c (90 % C.L.) the plasma potential of this cold plasma must be temporally and spatially stable within 10 meV.

One possible determinant of the plasma potential is a gold-coated stainless steel plate called Rear Wall (Fig. 1). The Rear Wall is located at the rear end of the tritium source. The work function of the Rear Wall has been optimized over several years in order to keep the homogeneity within $\sigma < 10$ meV over its approximately 130 cm surface. However, due to the plasma properties of the tritium source the Rear Wall only determines the plasma potential if the potential difference between the stainless steel tube walls enclosing the plasma and the Rear Wall is between 50 mV and -100 mV. This results in a stability requirement on the Rear Wall work function of better than 10 meV within a KATRIN measurement run. For that reason changes of the work function of both, the tube walls and the Rear Wall must be investigated. In addition the impact of a vacuum atmosphere (Fig. 2), heating, UV irradiation and exposure to a hydrogen atmosphere are of particular interest in this investigation. Knowing about these possible changes enables to compensate for them in the later experiment.

Furthermore it might be possible that positive ions generated in the tritium source cause a positive charging. This would cause an inhomogeneous plasma potential and therefore a non-tolerable systematic uncertainty for KATRIN. To prevent this charging it is planned to compensate for these ions through photoelectrons generated at the Rear Wall surface. However, if the number of emitted electrons is too high or too low, the intended quasi-neutrality of the plasma potential cannot be met. Because of this a detailed knowledge of the quantum efficiency of the Rear Wall surface and its stability is essential.

E-mail: kerstin.schoenung@mpi-hd.mpg.de

A setup which addresses not only the investigation of the stability of the work function but also of the quantum efficiency by photoelectron spectroscopy has been built up. The contribution presents the basic setup as well as first results performed with the setup.

This work is supported by BMBF (05A14VK2).

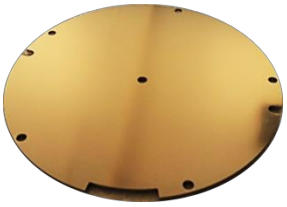

**Figure 1. Photograph of the gold-coated surface of the Rear Wall**.

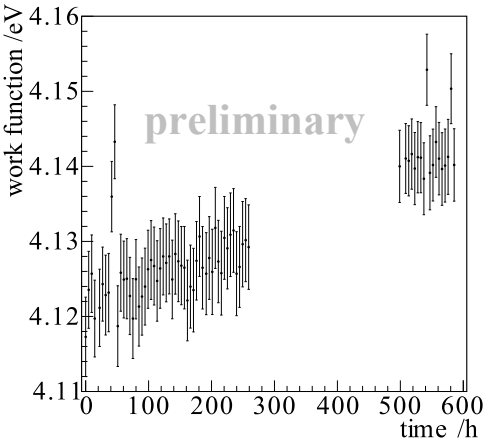


**Figure 2. Work function changes in vacuum. The sample has been heated up to 80 °C for about 2 days prior to the presented time interval.**

## References

[1] KATRIN Collaboration, "*FZKA report"*, **7090** (2004).

# The Bessel box Electron Energy Analyser in the Scanning Electron Microscope

**A. Suri,[1,*] S.P. Tear,[2] C.G.H. Walker,[2] A. Pratt,[2] and M.M. El Gomati[1,3]**
*[1]Dept. Electronics, University of York, Heslington, York, YO10 5DD, UK*
*[2]Dept. Physics, University of York, Heslington, York, YO10 5DD, UK.*
*[3]York Probe Sources 7 Harwood Rd, York, YO26 6QU*

**Synopsis** Simulations and experimental characterisation of a Bessel box electron energy analyzer to be used in scanning electron microscopes (SEM) are presented.

Advancements in the field of the SEM have been one of the major nano technology enablers. This has enabled us to control and manipulate the materials at the nano scale. In the conventional SEM, Everhart-Thornley (ET) has been proven to be an effective detector [1]. It is able to collect secondary electrons owing to the positive bias on its input-grid but in doing so it fails to conserve energy and angular resolved information. This information pertaining to the secondary electrons is essential for understanding the material under study. We propose the use of the Bessel box (BB) electron energy analyser (EEA) [2] for electron detection in the SEM. It has a simple cylindrical geometry with a central electrode and two endcap electrodes. The endcap electrodes incorporate apertures aligned with the BB optic axis. The voltages on these electrodes enable the BB to act as a band pass filter (Figure 1a). SIMION 8.1 [3] simulations are performed to assess its performance. The BB is operated in retarding field configuration in which the central cylinder and output electrode are shorted together and are biased negatively. The input electrodes along with the anode collector are grounded. Electron energies less than the peak pass energy are repelled back by the retarding fields inside the BB. For electron energies higher than the peak pass energy, the BB is unable to focus the electrons at the output aperture and therefore only a narrow band of energies are detected. Figure 1b shows the detected electrons (yellow) for a set of incident angles and electron energies. This angular dependence of the BB beyond the peak pass energy defines the effective acceptance angle of the device. We have fabricated and characterised a prototype of such a BB with 10 mm x 10 mm aluminium plates. A 5mm thick plate is used for the central Bessel cylinder with 0.2 mm thickness for the i/o and anode electrodes. This assembly is mounted to a dedicated ultra-high vacuum (UHV) chamber which is furnished with a tunable hot cathode electron gun. The retarding field is established using a high voltage power supply (Kepco OPS 2000) which is controlled using a low voltage DC power supply (Keithley 2460). The band-pass filtering action is demonstrated in figure 1c. Wherein, a peak energy of 1534 eV is experimentally determined for a retarding voltage of -1500 V. The simulated peak-pass energy for the system was calculated at 1530 eV for the BB biased at -1500 V (with a 0.5° angular dispersion in the primary beam fired at 8.5° to the optical axis). Furthermore, a linear relationship between peak-pass energies and the BB voltages is established by simulated and experimental results as shown in the figure 1d.

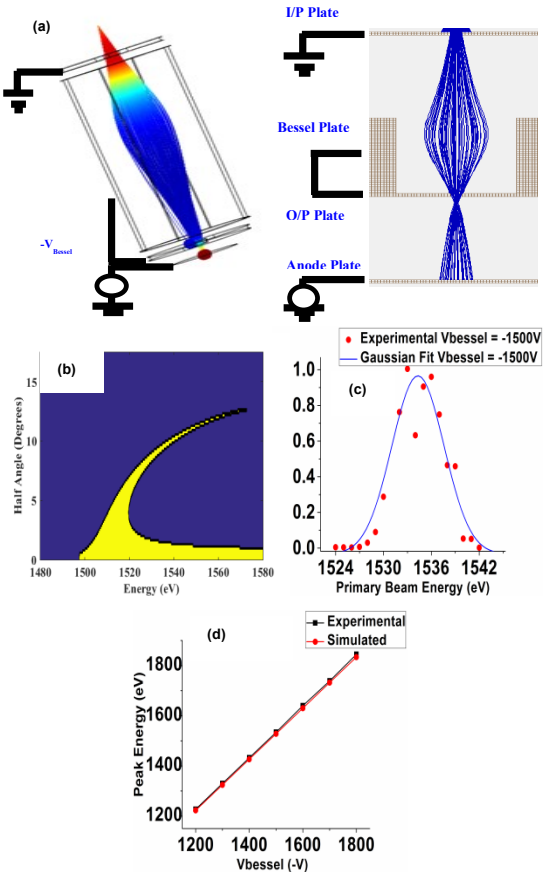


**Figure 1 (a) The Bessel box geometry and its band–pass filtering action, (b) Simulations showing effective acceptance angle of the BB beyond the peak-band pass energy. Yellow = electron detected, blue = electron not detected. (c) An experimental peak pass energy of 1534eV is obtained for the BB biased at -1500 V. The points are estimated with 10% accuracy. This peak-pass energy can be tuned linearly by varying the Bessel voltage, as demonstrated for simulated and experimental results (d).**

## References

[1] Everhart and Thornley, J. Scien. Inst. 37 (1960) p246–p248.
[2] G. Schiwietz, et al., J. Elec. Spec. Rel. Phen. 203 (2015) p51–p59.
[3] Dahl, D. Int. J. Mass Spec. 200 (2000) p1.

* E-mail: ashish.suri@york.ac.uk

# The variation in the Transport Mean Free Path for electrons at low energy for different atomic potential models.

**C.G.H. Walker,[1] S.P. Tear,[1] A. Pratt,[1] and M.M. El Gomati[2,3]**
*[1]Dept. Physics, University of York, Heslington, York, YO10 5DD, UK*
*[2]York Probe Sources Ltd., 7 Harwood Road, York, YO26 6QU, UK.*
*[3]Dept. Electronics, University of York, Heslington, York, YO10 5DD, UK*

**Synopsis** Calculated Transport Mean Free Paths for several elements using different atomic potentials and muffin tin radii are presented.

The Transport Mean Free Path (TMFP) plays a key role in the transport properties of electrons in solids [1,2] and is determined by $\lambda_{tr} = 1/(n\sigma_{tr})$ where n is the atom density and $\sigma_{tr}$ is the transport scattering cross-section given by:

$$\sigma_{tr} = \int_0^{\pi} \frac{d\sigma}{d\Omega}(1 - cos\theta)sin\theta d\theta \qquad (1)$$

where θ is the scattering angle and dσ/dθ is the differential elastic scattering cross-section. There is increasing interest in imaging with low energy electrons. Hence, a study of how the TMFP varies at low energy is timely. It is expected that the error in $\lambda_{tr}$ becomes larger as the electron energy reduces but up to now the size of this error has not been determined. Here, use of the ELSEPA [3] program has been employed to determine $\lambda_{tr}$ using 4 different types of atomic potential (AP) (Dirac-Hartree-Fock-Slater (DHFS), Thomas-Fermi-Dirac (TFD), Thomas-Fermi-Moliere (TFM) and Dirac-Fock (DF)). $\lambda_{tr}$ was determined from 10eV to $10^3$ eV and is shown for the case of Cu in Fig. 1. Variations reach a factor of ~5 below ~200eV between the different APs investigated.
Studies have also been made varying other parameters such as adding a muffin tin to the calculation so as to better simulate the case of electrons within a solid and then varying the radius of the muffin tin (-20%, -10%, +10% and +20%) around the standard radius [4]. The DF atomic potential was used. Results are shown in Fig. 2. Deviations between the different calculations start at lower energy than for the various APs, but can reach up to ~x10 for 10 - 25eV electrons. These results should be borne in mind when using Monte Carlo calculations of electron transport in solids. Results from other elements and varying other parameters will be presented.

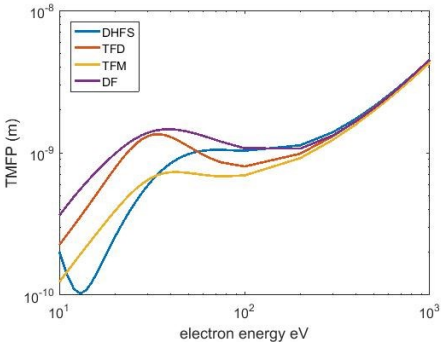


Figure 1. Transport mean free path for Copper for various atomic potentials.

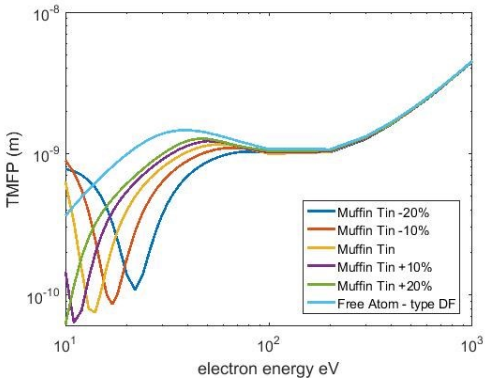


Figure 2. TMFP for Copper using Muffin Tins of various radii compared with the TMFP for the free atom. Dirac-Fock potential used in all cases.

**Acknowledgements**
The authors would like to thank J.A.D. Matthew for useful discussions.

E-mail: christopher.walker@york.ac.uk

**References**

[1] J. Matthew, et al. J. Elec. Spec. Rel. Phen. **85** (1997) 205.
[2] W. Werner et al. Surf. Sci. Lett. **268** (1992) L319.
[3] F. Salvat, et al., Comp. Phys. Comm. **165** (2005) 157.
[4] J.C. Slater, J. Chem. Phys. **41** (1964) 3199.

# SIMDALEE2017 Abstracts

# Wednesday, September $20^{th}$

# Spin-polarized Scanning Field Emission Microscopy and Spectroscopy of Non-collinear Spin Textures and Atomic-Scale Magnets

**Anika Schlenhoff**
*Institute for Nanostructure- and Solid State Physics, University of Hamburg, Germany*

**Synopsis** Spin-polarized low-energy electrons field-emitted from an SPM probe tip are used to resolve non-collinear spin textures with near-atomic spatial resolution. This novel spin-sensitive local probe technique can also be used to study the microscopic details of the interaction of low-energy electron spins with atomic-scale magnets.

Electrons can be extracted from a solid by a strong electric field, thereby generating an emission current. When using an atomically sharp needle, a point-like source of free electrons is realized, and for a magnetic emitter the electron beam becomes spin-polarized. A very local injection of these low-energy electrons is achieved when the field-emitting probe tip approaches a magnetic surface down to nm distance in a scanning probe microscopy setup. Subsequent scanning allows for magnetic imaging by spin-polarized field emission conductance measurements [1].

This novel spin-sensitive local probe technique, here referred to as *spin-polarized scanning field emission microscopy* (SP-SFEM), can be used to resolve non-collinear spin textures with near-atomic spatial resolution. Magnetic samples can be thereby as thin as possible, as demonstrated by tracing the profile of atomic-scale magnetic domain walls in a single atomic layer of Fe on W(110) [2]. Magnetic maps of the non-collinear inhomogeneous spin spiral in the Fe double layer on W(110) [3] are recorded at increasing tip-sample distances of up to 13 nm without losing magnetic resolution, thereby demonstrating the high spatial locality of this imaging technique. Corresponding laterally resolved spectroscopy data for electron energies from 100 meV to 20 eV reveal sensitivity to the respective local rotational angle of the spin momentum of the sample's spin spiral.

Spin-polarized scanning field emission microscopy can also be used to study the interaction of spin-polarized low-energy electrons with local magnetism providing insight into the underlying microscopic details. Resonantly injecting a spin-polarized field-emission current into magnets, consisting of only about 50 iron atoms on a W(110) surface, generates considerable Joule heating and spin-transfer torque, thereby severely affecting the thermally driven magnetization reversal [4]. The switching frequency is increased due to phonon generation, and a lifetime asymmetry develops with increasing emission current, most likely driven by Stoner excitations. On a quasistable nanomagnet, a spin-polarized emission current of a few nA already triggers magnetization reversal, thereby evidencing the high impact of low-energy electron spins on atomic-scale magnets.

E-mail: aschlenh@physnet.uni-hamburg.de

Our experiments thus demonstrate the capabilities of spin-polarized scanning field emission microscopy for magnetic imaging and controlled magnetization switching on the atomic scale at nm distances.

## References

[1] A. Kubetzka, M. Bode, and R. Wiesendanger, Appl. Phys. Lett. **91**, (2007) 012508.
[2] M. Pratzer, H. J. Elmers, M. Bode, O. Pietzsch, A. Kubetzka, and R. Wiesendanger, Phys. Rev. Lett. **87**, (2001) 127201.
[3] S. Meckler, N. Mikuszeit, A. Preßler, E. Y. Vedmedenko, O. Pietzsch, and R. Wiesendanger, Phys. Rev. Lett. **103**, (2009) 157201.
[4] A. Schlenhoff, S. Krause, A. Sonntag, and R. Wiesendanger, Phys. Rev. Lett. **109**, (2012) 097602.

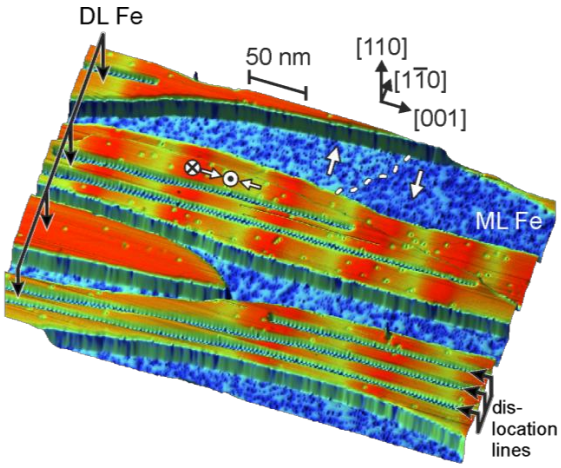


**Figure 1. Magnetic imaging using spin-polarized field emission: SP-SFEM topography and magnetic map of 1.5 AL Fe/W(110), revealing the non-collinear inhomogeneous spin spiral on the Fe double layer (DL) and magnetic domains on the Fe monolayer (ML). The relative magnetization directions are indicated. ($U$ = 4.6 V, $I$ = 2 nA, $T$ = 41 K.)**

# Exact Eigenstates of a Nanoscopic Paraboloidal Emiter: A Calculation of Field Emission Quantities

A. Chatziafratis, G. Fikioris and J.P. Xanthakis*
National Technical University of Athens, Electrical and Computer Engineering Department, Athens 15700 Greece

The Fowler –Nordheim (FN) theory of field-emission has served the scientific community for about 60 years. But from the mid-1990s it was becoming clear that it was not valid for highly curved surfaces even with the enhancement factor correction in it. There have been many works which have contributed to the establishment of a new theory of field-assisted emission from highly curved emitters such as Jensen et al [1], Edgcombe [2], Forbes et al [3] and Xanthakis & Kyritsakis [4, 5]. The common characteristic of these works is that they tackle only the transmission coefficient (and its angle dependence) outside the emitting tip i.e. they assume that, inside the emitter and at each angle θ to the axis of the tip, a locally planar wave impinges on the barrier.

However, just as the nanoscopic nature of the emitting tip alters the barrier shape outside, so it alters the supply of electrons inside the emitting material. For truly nanoscopic emitters (radius of curvature=R=1-5nm) this effect is expected to be significant. In this paper we calculate the eigenstates of a paraboloidal tip (see figure 1) exactly i.e. without the use of the JWKB theory. These are found to be (after separation of variables in Schroedinger equation) the regular Whittaker functions $M_{\kappa,\mu}(z)$, having applied the condition that they should be finite at η=0. Furthermore, applying the boundary condition of vanishing wavefunction at the emitter surface $\eta_o$ we get

$$\Psi_\eta(\eta_o) = \frac{1}{\sqrt{\eta_o}} M_{-\frac{iC}{\sqrt{E}},\frac{m}{2}}\left(i\sqrt{E}\eta_o\right) = 0$$

Hence we can find, for any given value of the energy E, the possible quantum numbers (also separation constant) $C_v$, with m being an integer. We note that if the 'soft-wall' Bohr-Sommerfeld quantization condition were used to obtain the $C_v$'s (as is sometimes done in connection with the JWKB) their values would in great error, as is seen in figure 2.

From the eigenstates we now calculate the incident current density (ICD) and we find it to behave very differently from the simple arithmetic factor of the planar FN theory, not shown here due to lack of space. Furthermore, the parallel to the barrier velocity –a crucial factor for the formation of the spot size of electron beams– is found to go to zero at the emitter apex in sharp contrast again to the FN theory (see figure 3). Experimental evidence for that is available; the spot size of the Near-Field Scanning Electron Microscope developed at ETH [6] fits very accurately this theory, see figure 4. To the best of our knowledge, this is the first exact calculation of such quantities for a nanoscopic tip.

**Acknowledgements**
This work is supported by the European ITN Project SIMDALEE2 under contract number 606988.

**References**

[1] JD Zuber, KL Jensen and TE Sullivan JAP 91, 9379 (2002)
[2] CJ Edgcombe PRB 72, 045420 (2008)
[3] RG Forbes JVST B 31, 032201 (2013)
[4] A Kyritsakis and JP Xanthakis Ultramicroscopy 125, 24 (2013)
[5] A Kyritsakis and JP Xanthakis Proc R. Soc 471, 20140811 (2015)
[6] DA Zanin, H Cabrera et al Advances in Imaging and Electron Physics, 170, 277 (2012)

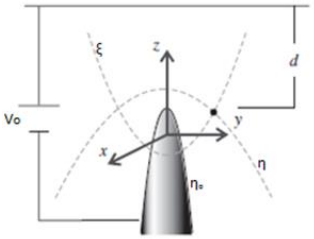


**Figure 1.** *Geometry used in our calculations.*

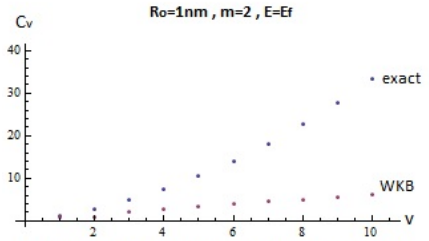


**Figure 2.** *Quantum numbers $C_v$ calculated exactly and by the Sommerfeld-BohrJWKB technique.*

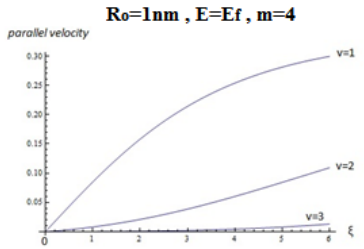


**Figure 3.** *Parallel velocity with respect to the ξ coordinate (i.e. angle to the normal)*

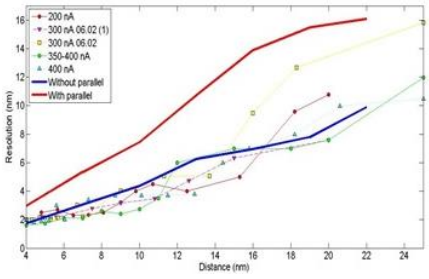


**Figure 4.** *Spo-size of the NFESEM beam calculated with zero initial parallel velocity (blue line) and with the traditional Cartesian FN value (red line)*

Email:jxanthak@central.ntua

# Scanning Field-Emission Microscopy with Polarization Analysis

**U. Ramsperger, L.G. De Pietro, G. Bertolini, D.A. Zanin, H. Cabrera, J. Zhou, O. Gurlu, S. Nayir, A. Vindigni, T. Bähler, and D. Pescia**

***Laboratory for Solid State Physics, ETH Zurich, 8093 Zurich, Switzerland***

Scanning Field-Emission Microscopy (SFEM) is based on STM technology, but instead of imaging in a tunneling regime the tip is retracted by some tenths of nanometers away from the sample surface and imaged in a field emission regime. In order to generate a field emission current a negative voltage is applied to the tip, which is kept constant as well as the distance between tip apex and sample during the scanning of the surface. In contrast to the tunneling technique SFEM produces secondary electrons out of the sample, which can be analyzed by different detectors such as SED, energy analyzer or spin polarimeter. With this novel technique we have shown a secondary electron contrast of 30% between a clean W(011) surface and monoatomic Fe islands on top of it and that the lateral resolution can be as high as 1 nm [1]. An energy analysis of these secondary electrons has revealed that a large amount of them are "truly" secondary with respect to the elastic scattered electrons.

Recent spin analysis with a Mott polarimeter has shown that these secondary electrons are carrying the magnetic signature of the sample. Hysteresis loop measurements of eight monolayers Fe on top of W(011) measured with the SFEM method demonstrate a typical magnetic behavior for that model magnetic sample. These measurements are confirmed with an in situ scanning electron microscope (SEM) revealing the very same magnetic signature (Fig.1).

The method of SFEM with polarization analysis (SFEMPA) enables the mapping of magnetic samples with high lateral resolution in principle as high as 1 nm. First results will be presented and compared with the method of SEM with polarization analysis (SEMPA).

**References:**

[1] Zanin DA, De Pietro LG, Peter Q, Kostanyan A, Cabrera H, Vindigni A, Bähler Th, Pescia D, Ramsperger U. 2016 *Thirty per cent contrast in secondary-electron imaging by scanning field-emission microscopy*.
Proc. R. Soc. A472: 20160475

E-mail: ramsperger@phys.ethz.ch

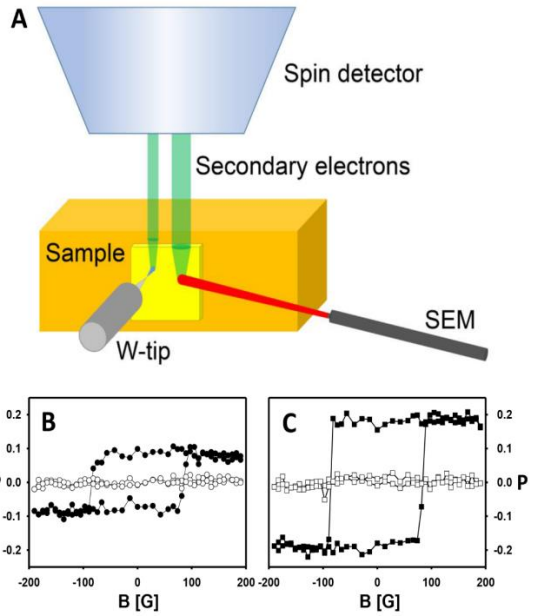


**Figure 1. A) Schema of the SFEMPA and SEMPA setup. For SEMPA measurements the primary electron beam of the SEM (red) hits the sample (yellow) and produces secondary electrons (green), which are analyzed in the spin detector. For SFEMPA measurements, the primary electrons (blue) are extracted from the W-tip. These electrons generate secondary electrons (green) out of the sample, which are analyzed in the same spin detector. All measurements have been done under ultra high vacuum (UHV) conditions and at room temperature.**

**B) Hysteresis loops of 8 ML of Fe on top of W(011) measured with the technique of SFEMPA. The Fe film shows a 20% polarization (black circles) in the in-plane direction, whereas the out of plane polarization is 0% (white circles). The tip sample distance is 100 nm and the voltage applied to the tip V = -62 V.**

**C) Hysteresis loops of the same sample as B), but this time measured with the technique of SEMPA. The in plane polarization amounts to 40% (black squares), while the out of plane is 0% (white squares). In B) and C) the coercivity is the same.**

# Improving the accuracy of modelling field emission into vacuum

**S. M. Masur[1], C. J. Edgcombe[1]*, G. Constantinescu[1], Gabor Csanyi[2], Crispin H. W. Barnes[1]**

[1]*Department of Physics, University of Cambridge*
[2] *Department of Engineering, University of Cambridge*
*cje1@cam.ac.uk*

Carbon nanotubes (CNTs) and structures of similar geometry are being investigated widely for possible uses in near field emission microscopy, large-area field emission displays [1] and other applications. For this purpose, it is desirable to give accurate predictions of the emission area, current density and electron energy distribution when immersed in electric fields. Conventional Fowler-Nordheim (FN) theory is often used and assumes a uniform electric field and a single electron energy. However, FN theory is inaccurate when applied to real emitters such as CNTs, where the radius of curvature of the emitting surface may be as small as the thickness of the potential barrier. Therefore, it is important to develop a new field emission theory for nano-sized emitters.

Recently a closed (10,10) CNT in applied field has been modelled at Cambridge by use of the DFT code ONETEP [2] (Fig. 1), developed as a linear-scaling alternative to plane-wave codes such as CASTEP. ONETEP uses non-orthogonal localised basis functions and is thus capable of calculating non-periodic and pointed structures such as CNTs. Its solution time scales linearly with number of atoms, making it suitable to provide quantitative theoretical predictions for problems involving thousands of atoms [2]. To address the problem of multi-scaling in field emission, we used a Poisson solver to calculate the classical potential distribution near the emitter apex for a certain background field. The potential then provided the boundary conditions for the DFT calculations with a smaller mesh spacing. For our first calculations, we found the classical potential distributions near a perfectly conducting rod of length 200nm in applied fields of zero and 12.5 Vμm$^{-1}$.

The resulting potentials differ from the approximate analytical form assumed hitherto, especially near the wells formed by carbon atoms. Also, the barrier is thinnest not on the axis of the nanotube but where the surface curvature is greatest, at about 45 degrees to the axis. Thus, the emitted current density is likely to be strongest in the same direction, though the trajectories will be pulled rapidly more parallel to the axis by the accelerating field. The local direction of maximum emission in practice is thus likely to depend strongly on the physical shape of the apex of the emitter.

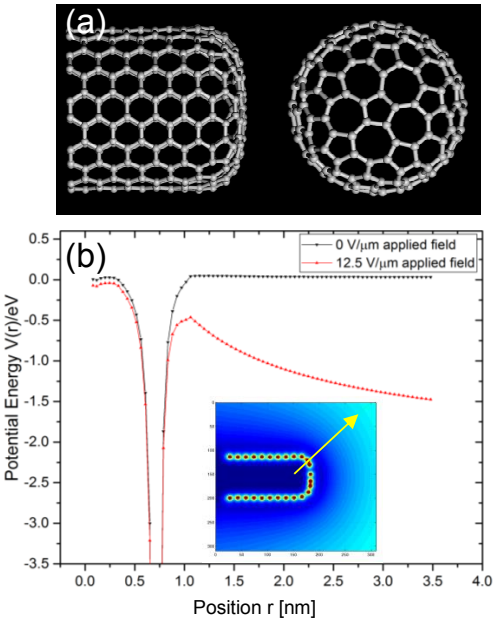


**Figure 1: (a) Structure of a closed (10,10) carbon nanotube; (b) Potential in applied fields of zero and 12.5 Vμm-1 along the line indicated in the inset; Inset shows potential distribution in applied field of 12.5 Vμm-1.**

**Acknowledgment**
This project has received funding from the People Programme (Marie Curie Actions) of the European Union's Seventh Framework Programme FP7/2007-2013/ under REA grant agreement n 606988.

**References**

[1] Lee, et al., Proc. 3rd Specialist Meeting on Amorphous Carbon (Mondovi), Diamond and Related Materials 10(2), 265-270 (2001)
[2] Skylaris, Haynes, Mostofi & Payne, J Chem Physics 122, 084119 (2005)

# Principles of low energy electron interactions with simple molecular solids and condensed biomolecules

**Andrew D. Bass*** **and Léon Sanche**
*Département de Médecine Nucléaire et Radiobiologie, Faculté de Médecine et des Sciences de la Santé, Université de Sherbrooke, Sherbrooke, Québec, J1H5N4, Canada.*

**Synopsis** We review the basic mechanisms of interaction of low energy electrons with atomic, molecular and bio-molecular targets in the condensed phase

Low energy electrons (LEEs) have energies of less than a few tens of eV and are encountered in numerous natural and technological settings. Large numbers of secondary electrons with these energies are produced when high-energy ionizing radiation interacts with a condensed medium, [1] and thus play an important role in energy transfer and any subsequent radiation chemistry. Dependent on the medium, the interactions of LEEs are relevant to understanding diverse phenomena encountered in fields such as radiobiology [2], astro-chemistry [3] and nano-fabrication [4]. The transport properties of LEEs and the nature of their interactions with condensed molecules can be studied by irradiating nano-scale samples with energy selected electron beams and monitoring electron-induced phenomena with techniques such as Low Energy Electron Transmission Spectroscopy (LEET), High Resolution Electron Energy Loss Spectroscopy (HREELS), X-ray Photoelectron Spectroscopy and Mass Spectrometry, particularly by the Electron Stimulated Desorption (ESD) of fragment charged and neutral species [2,5]. As in the gas-phase, electron-molecule interactions at the lowest energies (< 20 eV) are often dominated by the formation of transient negative ions (TNI) that modulate electronic and vibrational excitation and can induce dissociation via dissociative electron attachment (DEA) and autoionization when the target is left in a dissociative state [6]. Such dissociations can drive the synthesis of new chemical species [7]. In thin films, electron transport is often dominated by their structural and interface properties. Using examples drawn from 30+ years of study in the Sherbrooke laboratory, we illustrate how via their transport and reactions, LEEs can initiate significant chemical change in condensed-phase targets ranging from simple molecular solids to complex bio-molecules such as DNA.

E-mail: Andrew.Bass@USherbrooke.ca

## References

[1] S. M. Pimblott and J. A. LaVerne, Radiat. Phys. Chem. **76**, 1244 (2007).
[2] E. Alizadeh and L. Sanche, Chem. Rev. **112**, 5578 (2012).
[3] M. C. Boyer, et al., Surf. Sci. **652**, 26 (2016).
[4] R. M. Thorman, R. Kumar T. P., D. H. Fairbrother, and O. Ingólfsson, Beilstein J. Nanotechnol. 6, 1904 (2015).
[5] A. D. Bass and L. Sanche, in *Charg. Part. Phot. Interact. with Matter* (CRC Press, 2003).
[6] E. Alizadeh, S. Ptasińska, and L. Sanche, in *Radiat. Eff. Mater.*, edited by W. A. Monteiro (InTech, 2017).
[7] C. R. Arumainayagam, et al., Surf. Sci. Rep. **65**, 1 (2010).

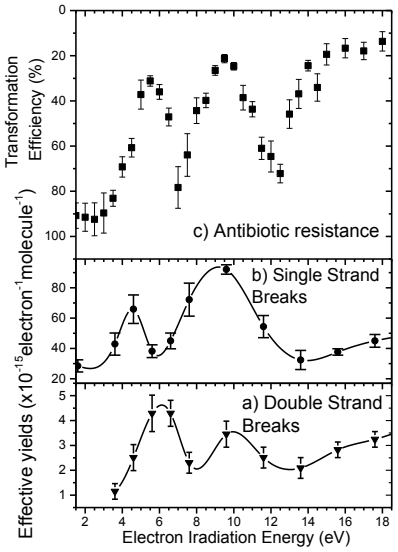


**Figure 1. The ubiquity of TNI: The yields of double (a) and single (b) strand breaks in electron-irradiated pGEM-3ZfL(−) plasmid DNA are modulated by TNI. The ability of these irradiated plasmids to confer antibiotic resistance to *E. coli* (c) is similarly affected. [Kouass-Sahbani et al, Chem. Phys. Lett. 6, 3911 (2015)**

# Characterization of Cu nanoparticles via X-ray photoelectron spectroscopy in combination with theoretical calculations using SESSA

**Markus Sauer[1,*], Alice Cognigni[2], Liene Anteina[2], Ronald Zirbs[3], Katharina Schröder[2], Annette Foelske-Schmitz[1]**

*[1]Analytical Instrumentation Center, Vienna University of Technology, Getreidemarkt 9, 1060 Vienna, Austria*
*[2]Institute for Applied Synthetic Chemistry, Vienna University of Technology, Getreidemarkt 9, 1060 Vienna, Austria*
*[3]Group for Biologically Inspired Materials, Institute of Nanobiotechnology, University of Natural Resources and Life Sciences, Muthgasse 11, 1190 Vienna, Austria*

Copper nanoparticles (NP) have attracted great interest due to their unique properties which make them ideal candidates for applications in catalysis [1].

Within this study we have investigated the properties of nanoparticles produced in ionic liquid-aqueous micellar systems, which would provide a media for further coupling reactions.
Despite the protective stabilizing environment of the ionic liquid, several question like possible oxide/hydroxide-shell formation within the aqueous solution including parameters, e.g. coverage and thickness of these layers need to be addressed to understand NP behavior in possible applications.
Therefore, we have employed X-ray photoelectrons spectroscopy (XPS) in combination with theoretical calculations using the SESSA software package [2,3].

Cu NP were formed via chemical reduction of $CuCl_2$ using sodium borohydride or hydrazine in ionic liquid (1-alkyl-3-methyl-imidazolium chloride)/aqueous solutions [4,5].
Samples investigated in XPS were pre-characterized using dynamic light scattering and transmission electron microscopy where mean diameters have been found to be 5-6 nm and 4.6±1.4 nm respectively.

After the preparation process, samples were extracted from the solution in inert gas atmosphere.
Cu nanoparticles were subsequently transferred to ultra-high vacuum without prolonged exposure to air.

As shown in Figure 1 we have acquired Cu 2p and Cu LMM signals of the different NP and compared them to signals from high-purity planar Cu and Cu-oxide reference samples.
As Cu 2p signals show no traces of Cu(II), we determined the Cu(0)/Cu(I) ratios from the Cu LMM signals.

Subsequently, different over-layer thicknesses have been calculated using SESSA. Assuming homogeneous coverage, the thickness of the oxide layer can be determined in the sub-nm range with accuracy of one monolayer of oxide coverage.

We could evidence the formation of few atomic layers of oxides, which exhibit varying thickness due to changes in the fabrication process. These variations can distinctly influence the NPs properties when they are used in catalytic reactions, thus proving that XPS is an essential tool for NP metrology.

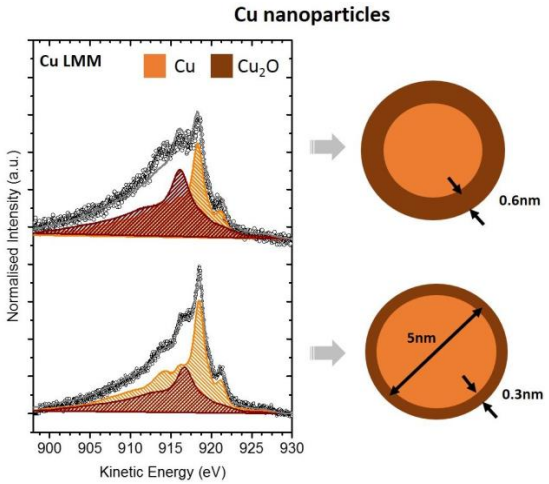


**Figure 1. Cu LMM Auger spectra of two differently prepared Cu nanoparticles with a mean diameter of 5 nm (Excitation of Auger signal via Al-Kα source)**

## References

[1] M.B. Gawande, A. Goswami, F.-X. Felpin et al., *Chem. Rev.* **116** (2016), 3722.
[2] J. Luczak, J. Hupka, J. Thörnig, C. Jungnickel, *Colloids Surf. A.* **329** (2008), 125.
[3] M. Blesic, M.H. Marques, N.V. Plechkova et al., *Green Chem.* **9** (2007), 481.
[4] W. Smekal, W.S.M. Werner, C.J. Powell, *Surf. Interface Anal.* **37** (2005), 1059.
[5] W.S.M. Werner, W. Smekal, C.J. Powell, NIST Database for the Simulation of Electron Spectra for Surface Analysis (SESSA); U.S. Department of Commerce/NIST: Gaithersburg, Maryland, 2016

[*]E-mail: markus.sauer@tuwien.ac.at

# Extracting information on the structure of core-shell nanoparticles from the inelastic background in XPS spectra

**H. Kalbe[1,*], M. Hronek[1], C.J. Powell[2], W.S.M. Werner[1]**
*[1] Vienna University of Technology, 1040 Vienna, Austria*
*[2] National Institute of Standards and Technology, Gaithersburg, MD 20899, USA*

Several methods are established for the estimation of shell thicknesses of core-shell nanoparticles from XPS peak intensities [1,2,3]. However, these methods completely discard the information that can be extracted from the shape of the inelastic background. A set of novel evaluation methods is presented and discussed that extend the capabilities of quantitative XPS for the investigation of CSNP samples.

It has already been established that the inelastic background signals can be utilised to estimate planar layer thicknesses [4]. Here, an accurate method is presented to retrieve the shell thickness as well as the core radius of CSNP from fitting simulated XPS spectra to experimental data by modelling the inelastic background with shell thickness and core radius as fit parameters. With the existing methods, accessible shell thicknesses are limited by the information depth of XPS experiments of typically 5-10 nm, but since the peak intensities of core signals are far surpassed by the background signal intensity for large shell thicknesses the background shape analysis shows promise to considerably extend the accessible shell thicknesses past the previous limit. Furthermore, the simultaneous calculation of the core radius was previously only possible for extremely small particles, less than 1 nm [2], which can possibly be extended to the calculation of core radii up to 10-20 nm.

In the presented method, the XPS spectra are calculated in Monte-Carlo simulations of the photoelectron trajectories [1]. To do this accurately, one has to account for the fact that the inelastic mean free path (IMFP) of the electrons changes over the wide range of energy losses that has to be simulated. The corresponding mathematical approach will be discussed.

Another extension to the existing XPS quantification models for CSNP that will be presented is the simulation of dispersed powders instead of single particles. Furthermore, the inclusion of eccentric cores and distributed shell thicknesses and core radii and their influence on the XPS spectrum will be discussed.

The funding from the 14IND12 Innanopart project by the EU through the EMPIR initiative is gratefully acknowledged.

**References**

[1] W.S.M. Werner et al., Nist Database for the Simulation of Electron Spectra for Surface Analysis, SRD 100, Version 2.0, National Institute for Standards and Technology (NIST), Gaithersburg, MD, USA, 2014
[2] H. Kalbe et al., J. Electron Spectrosc. Relat. Phenom. 212, 2016, 34-43
[3] A. Shard, J. Phys. Chem. C, 116(31), 2012, 16806-16813
[4] S. Tougaard, J. Vac. Sci. Technol. A 14, 1996, 1415-142

Email: henryk.kalbe@tuwien.ac.at

# SIMDALEE2017 Abstracts

# Thursday, September $21^{th}$

# Rapid 3D Mapping of Fermi Surface, Fermi Velocity and Spin Texture

**Gerd Schönhense**
*Institut für Physik, Johannes Gutenberg-Universität, 55099 Mainz, Germany*

**Summary** The 4D spectral function $\rho(E_B;\boldsymbol{k})$ of tungsten in the entire bulk Brillouin zone and 6 eV binding-energy ($E_B$) interval was acquired in ~3 hours thanks to a new multidimensional photoemission data-recording technique (combining full-field k-microscopy with time-of-flight parallel energy recording) and the high brilliance of the soft X-rays used. A direct comparison of bulk and surface spectral functions (taken at low photon energies) reveals a time-reversal-invariant surface state in a local bandgap in the (110)-projected bulk band structure.

Momentum microscopy is a novel way to perform ARPES via high-resolution imaging of the *Fourier plane* of a cathode lens. Combination with *time-of-flight* (ToF) energy recording using a delay-line detector (capable of >5Mcps) yields maximal parallelization. The $k_x,k_y$ field of view exceeds the first Brillouin zone, the energy range comprises several eV. Tunable soft X-rays allow variation of $k_z$ via direct transitions to free-electron-like final states, yielding ~$10^8$ resolved data points of the 4D spectral density function $\rho\,(E_B,k_x,k_y,k_z)$ (weighted by the photoemission cross section). Fermi surface and velocity distribution $\mathbf{v}_F(\boldsymbol{k}_F)$ (see Fig. 1a, from [1]), electron or hole conductivity, effective mass and inner potential can be obtained from $\rho$ by simple algorithms. In Fig. 1b,c (from [2]), the band features can be clearly distinguished by their surface and bulk character, encoded in green and red, respectively. Surface resonances appear in the mixed color yellow. Polarized light reveals the dichroism texture in a simple manner and an imaging spin filter exposes the spin texture.

Measurements for the prototypical high-Z *bcc* metal tungsten revealed the complete bulk and surface electronic structure, including the spin texture. The experiment uncovered a time-reversal invariant surface state with Dirac-like dispersion and spin texture. The surface state connects hole and electron pockets that would otherwise be separated by an indirect local bandgap. Its Dirac-like spin texture was confirmed by spin-filtered momentum imaging [3].

For the medium-Z *bcc* metal Mo sharp bulk ***k***-patterns are visible up to hν=1700eV, even for an oxidized surface. Vectorial spin detection permits acquisition of all four of the essential measurable quantities (intensity and three spin components, constituting the "complete" experiment [4]) with enormously increased speed.

Funded by BMBF

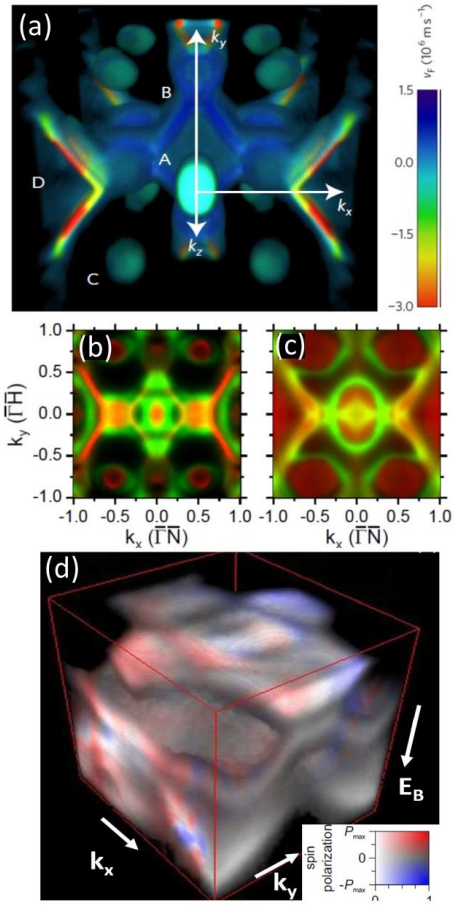


**Figure 1. (a) Fermi surface of tungsten, measured using high-brilliance soft X-rays from the storage ring PETRA III (beamline P04). The Fermi velocity is quantified by the color bar (in $10^6$m/s) (from [1]). (b,c) Superposition of the bulk (red) and surface spectral function (green), the latter measured at low photon energies at BESSY II (10m NIM). Constant energy slices for the Fermi level (b) and just above the Dirac crossing at $E_B$ = 1.1 eV (c) (from [2]). (d) Spin texture as measured using an imaging spin filter. Red and blue mark opposite spin orientation, see color bar (from [3]).**

## References

[1] K. Medjanik et al., *Nature Materials* DOI: 10.1038/ NMAT 4875 (2017).
[2] H.-J. Elmers et al., submitted.
[3] D. Kutnyakhov et al., *Sci. Rep*. **6** (2016) 29394.
[4] J. Kessler, *Comments Atom. Mol. Phys.* **10** (1981) 47.

E-mail: schoenhe@uni-mainz.de

# Graphene-based field emission sources for electron microscopy and lithography

**Xiuyuan Shao, Avinash Srinivasan, Wei Kean Ang and Anjam Khursheed***
*Department of Electrical and Computer Engineering, National University of Singapore, Singapore 117576*

Over the past decades, the extensive research work carried out on carbon-based cathodes for cold field emission, such as Carbon Nanotubes (CNTs), has not as yet, led to new viable electron sources for electron microscopy/lithography. Their most successful layout has typically been in form of dots arrays for large area field emission applications. Nano size emitter single point cathodes have proven to suffer from even more severe problems than conventional single crystal tungsten cathodes: unmanageably stringent UHV requirements, relatively large current stabilities, and rapid emission decay in periods as short as one to two hours, requiring regular flashing (Joule heating). These difficulties have prevented the widespread use of cold field emission electron sources for electron microscopy/lithography applications. The more stable and reliable Schottky field emission source is often used, despite it having a lower reduced brightness and a larger energy spread than cold field emission cathodes.

Recently, the research group at the National University of Singapore, led by A. Khursheed, has succeeded in using graphene field emission cathodes for electron microscopy/lithography applications. Stable field emission was obtained from a free-standing graphene ring structure, 5 µm in diameter and a wall thickness of around 3 nm [1], as shown in Fig. 1a. Emission currents (Figs. 1c and e) of around 30 µA have been obtained at a relatively low applied electric field strength (1.75 V/µm) in HV conditions ($5\times10^{-7}$ Torr). This ring-cathode emitter can directly image ring patterns, and has promising applications for electron beam lithography.

Another development is the discovery that under certain conditions, a graphene coated cathode-tip dramatically lowers the work function of graphene (by over a factor of 4), enabling it to both provide stable field emission at cathode-tip electric field strengths as low as 0.5 V/nm, an order of magnitude lower than conventional single crystal tungsten point cathodes. This makes it possible to both operate the cathode in HV conditions ($4\times10^{-8}$ Torr) and use relatively large cathode-tip sizes (micron sizes), over three time larger than conventional single crystal tungsten tip sizes, sizes that are comparable to the Schottky field emitter tip. Preliminary experimental results are shown in Figs. 1b, d and f. There is no obvious need for cathode-tip flashing. The reduced brightness calculations for these new graphene-based tips is comparable or better than that of conventional single crystal tungsten wire cathode cold field emission sources. These developments are expected to greatly extend the use of cold field emission electron sources for electron microscopy and lithography applications.

E-mail: eleka@nus.edu.sg

## References

[1] X. Shao, A. Srinivasan, Y. Zhao, and A. Khursheed, Carbon 110, 378 (2016). .

This research was funded the National Research Foundation (NRF), Singapore Competitive Research Programme (CRP) award # NRF-CRP13-2014-04 titled "Microfabricated Ring Carbon Nanotube electron/ion sources".

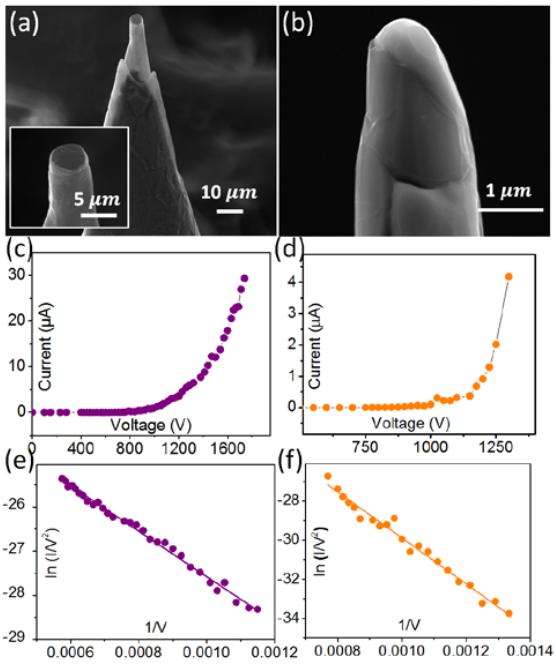


**Figure 1. (a) SEM image of a concentric graphene ring-cathode field emitter; inset at high magnification (ring diameter~ 5 µm, wall thickness~ 3nm). (b) SEM image of a graphene coated point cathode field emitter on sharpened Ni wire (tip radius~ 480nm). The dependence of the total emission current on extraction voltage for (c) a graphene ring cathode field emitter (anode-cathode spacing~ 1mm) and (d) a graphene coated point cathode field emitter (anode-cathode spacing~ 0.5 mm), and their F-N plot are shown in (e) and (f).**

**X-RAY PHOTOELECTRON SPECTROSCOPY OF IONIC LIQUIDS – FROM HALF CELL MEASUREMENTS TO IN SITU ELECTROCHEMICAL XPS STUDIES**

Annette Foelske-Schmitz, Vienna University of Technology
*annette.foelske-schmitz@tuwien.ac.at*
Markus Sauer, Vienna University of Technology

Key Words: Ionic Liquids, X-ray photoelectron spectroscopy, Electrochemistry, *in situ* EC XPS, Charging

X-ray Photoelectron Spectroscopy (XPS) investigations of the liquid/ultra-high vacuum (UHV) interface have been of fundamental interest for several decades. First experiments were performed by Siegbahn et al. in the 1970s [1]. The issue of evaporation of the liquid was overcome by use of differential pumping systems and a moving metal surface. In these and subsequent studies, charging was observed and XP spectra were commonly referenced to the C 1s line with respect to vacuum level [2]. Ionic liquids (IL) are particularly interesting to study the liquid/UHV interface as their negligible vapor pressure allows for XPS measurements without need of complex experimental setups. First XPS measurements of IL were performed in 2005 [3]. Charging was reported to occur and the C 1s line of aliphatic chains was suggested to be used as internal reference for charge correction [4].

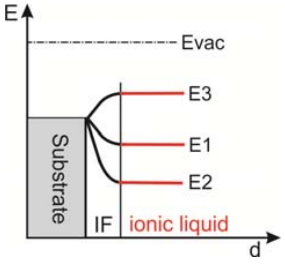


*Energy scheme explaining differences of BE by different potential drops within the electric double layer (IF).*

Foelske-Schmitz et al. investigated the charging phenomena in more detail and suggested that high surface area carbon supports may allow for determination of reliable binding energies (BE) without charging due to the high double layer capacitance of the support [5]. Same authors developed an *in situ* electrochemical (EC) XPS cell and measured the fundamental concept of electrochemical shift *in situ* for the first time [6]. Using that cell, significant charging was followed by recording the open circuit potential (OCP) of a platinum electrode in comparison to an activated carbon electrode under X-ray illumination of the IL electrolyte using a twin anode. The results further confirmed that the electrochemical double layer formed at the substrate/IL interface has to be considered when irradiating / measuring at the IL/UHV interface [7]. It is well established that the OCP reflects the potential difference between the bulk of an electrode and an electrolyte. The potential difference between both phases is constant as long as the interface is in dynamic equilibrium, however, expected to change if physical or chemical properties of the phases are changed (see Figure where E3 corresponds to lower BE and E2 corresponds to higher BE.).

Conversely, BE measurements may allow for determination of the OCP in one half-cell if significant charging of the IL caused by the X-ray induced photoemission can be excluded in course of the measurement. Since significant charging could not be observed by means of *in situ* EC XPS using a small spot monochromatic X-ray source directed to the bulk of the IL [8], we have further investigated double layer phenomena by means of XPS using a mono source. Recorded core level data of [EMIM][TFSI] on different substrates before and after 4h of irradiation indicates that significant charging does not occur in course of the measurement. Binding energies, however, were found to vary by 0.4 eV among the used substrates, thus confirming that the potential drop at the substrate/IL interface determines the BE values measured at the IL/UHV interface.

In the course of the presentation, recent XPS data of IL/UHV interfaces will be presented and elucidated by means of existing literature.

[1] H. Siegbahn, K. Siegbahn, *J. electron Spectrosc. Relat. Phenom.*, 1973, **2** 319
[2] R. Moberg, F. Bökman, O. Bohman, H.O.G. Siegbahn, *J. Am. Chem. Soc.*, 1991, **113**, 3663-3667
[3] E.F. Smith, I.J. Villar-Garcia, D. Briggs, P. Licence, *Chem. Commun.*, 2005, 5633-5635
[4] I.J. Villar-Garcia, E.F. Smith, A.W. Taylor, F. Qiu, K.R.J. Lovelock, R.G. Jones, P. Licence, *Phys. Chem. Chem. Phys.*, 2011, **13**, 2797-2808
[5] A. Foelske-Schmitz, D. Weingarth, R. Kötz, *Surf. Sci.*, 2011, **605**, 1979-1985
[6] D. Weingarth, A. Foelske-Schmitz, A. Wokaun, R. Kötz, *Electrochem. Commun.*, 2011, **13**, 619-622
[7] A. Foelske-Schmitz, D. Weingarth, A. Wokaun, R. Kötz, *ECS Electrochem. Lett.*, 2013, **2**, H13-H15
[8] D. Weingarth, PhD thesis, 2013, ETH NO. 21213

# Magnetic Circular Dichroism in Energy Loss Spectrometry

**P. Schattschneider,[1,*] and S. Löffler[2]**

*[1]Institute of Solid State Physics, TU Wien, A-1040 Wien, Austria*
*[2]Univ. Service Center for Transmission Electron Microscopy, TU Wien, A-1040 Wien, Austria*

Energy loss magnetic chiral dichroism (EMCD) is an electron-based approach to study element specific magnetic moments with highest spatial resolution. EMCD is detected as an asymmetry in the transition probability to states with positive and negative magnetic quantum numbers (chiral transitions), observed in far field electron energy loss spectrometry (EELS) [1]. The technique is similar to its well established relative - XMCD - where the asymmetry appears in the fine structure of X-ray ionisation edges of magnetic materials. Such symmetry breaking pertains in energy filtered imaging with atomic resolution, as was shown in a demonstration experiment [2], thus opening the road to mapping spins of individual atomic columns in a conventional electron microscope.

An important advantage of EMCD over XMCD is the site specificity [3], enabling the study of ferri- and antiferromagnets as well as surfaces, interfaces, and defects. One of the intriguing properties of EMCD is that the outgoing probe electrons have topological charge. Such electrons carry quantized orbital angular momentum, similar to the recently discovered vortex electrons. Vice versa, vortex electrons are a promising probe for spin mapping with atomic resolution [4]. Furthermore, such vortex electrons have been predicted to allow the investigation of the magnetic plasmon response, e.g. of metamaterials, using low energy losses [5].

The authors acknowledge funding by the Austrian Science Fund, projects no. I543-N20 and J3732-N27.

## References

[1] P. Schattschneider (ed.) *"Linear and chiral dichroism in the electron microscope"*, Pan Stanford 2011.
[2] P. Schattschneider et al., PRB **85** (2012) 134422.
[3] I. Ennen et al., J. Magn. Magn. Mat. **324** (2012) 2723.
[4] T. Schachinger et al., Ultramicroscopy, in print.
[5] Z. Mohammadi et al., Opt. Ex. **20** (2012) 15024.

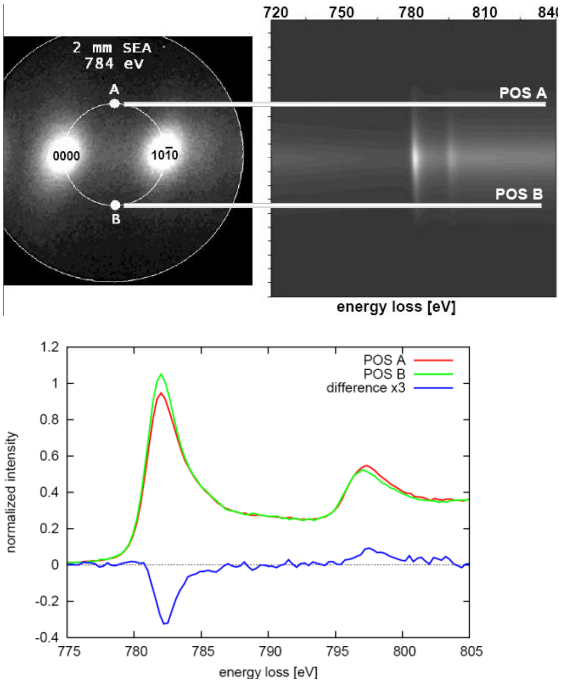


**Figure 1. EMCD with 10 nm resolution: a) far field EELS; b) magnetic signal of hexagonal Co.**

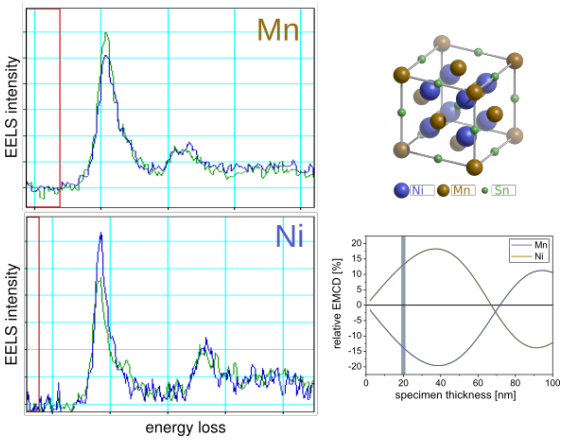


**Figure 2. Site- and chemical specificity demonstrated on a $Ni_2MnSn$ Heusler alloy.**

* E-mail: peter.schattschneider@tuwien.ac.at

# Model-based Iterative Reconstruction of Charge Density in the Transmission Electron Microscope

**Fengshan Zheng,[1,*] Vadim Migunov,[1,2] Jan Caron,[1] Giulio Pozzi[1,3] and Rafal E. Dunin-Borkowski[1]**

[1]*Ernst Ruska-Centre for Microscopy and Spectroscopy with Electrons and Peter Grünberg Institute, Forschungszentrum Jülich, 52425 Jülich, Germany*

[2]*Central Facility for Electron Microscopy (GFE), RWTH Aachen University, Ahornstrasse 55, 52074 Aachen, Germany*

[3]*Department of Physics and Astronomy, University of Bologna, Viale Berti Pichat 6/2, 40127 Bologna, Italy*

The technique of off-axis electron holography can be used to recover both the amplitude and the phase shift of an electron wave that has passed through a specimen in the transmission electron microscope. The recorded phase shift is sensitive to local variations in electrical charge density in the specimen. In principle, the second derivative of the phase shift can be used to recover the charge density distribution directly. However, this approach suffers from poor signal-to-noise ratio and artefacts.

Here, we propose an alternative model-based iterative approach that can be used to determine the charge density in a specimen from one or more recorded phase images. Figure 1a shows a phase image of a homogeneously charged sphere and its twin image simulated using known analytical solutions for the phase shift, with numerical discretization performed in real space to avoid artefacts generated by discretization in Fourier space. We use this forward model in an iterative algorithm to solve the inverse problem of reconstructing the charge density in a specimen from one or more two-dimensional phase images [1] (Fig. 1b). When this inverse modelling approach is used to determine the three-dimensional charge density distribution from a tilt series of phase images, it avoids artefacts that result from the use of standard backprojection-based tomographic techniques and allows additional constraints and known physical laws to be incorporated.

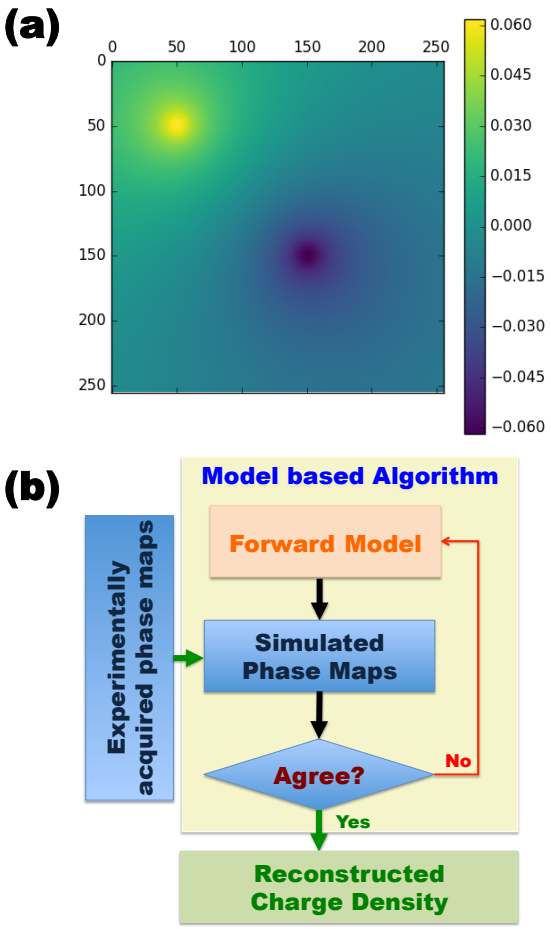


**Figure 1. (a) Electron holographic phase image simulated for a homogeneously charged sphere at (50, 50) and its twin image at (150, 150). The phase is displayed in units of radians. (b) Flow chart describing a model-based iterative reconstruction algorithm that can be used to recover a projected or three-dimensional charge density distribution from one or more recorded phase images.**

**References**

[1] J. Caron, J. Ungermann, Z.-A. Li, P. Diehle, A. Kovács, M. Riese and R. E. Dunin-Borkowski, Proceedings of the PICO 2015 Conference on Frontiers of Aberration Corrected Electron Microscopy, Kasteel Valsbroek, The Netherlands, 19-23 April 2015, PB04.

E-mail: f.zheng@fz-juelich.de

# Radiative transfer methods for electron spectroscopy

**Pavel Kaplya[1], Viktor Afanas`ev, Dmitry Efremenko[2]**
*[1]National Research University «Moscow Power Engineering Institute», Krasnokazarmennaya 14, Moscow, Russia*
*[2]Deutsches Zentrum für Luft- und Raumfahrt (DLR), Institut für Methodik der Fernerkundung (IMF), 82234 Oberpfaffenhofen, Germany*

**Synopsis** Electron spectroscopy, invariant imbedding, XPS, PES, REELS

Reflected electron energy loss spectra (REELS) and X-Ray photoelectron spectroscopy (XPS) can be modeled by using the partial intensity approach (PIA), in which a spectrum is given by the weighted sum of multiple cross-convolutions of differential inverse inelastic mean free paths (DIIMFPs) and differential surface excitation probabilities. Computations of corresponding weights (partial intensities) is still a challenging task since the multiple scattering processes should be taken into account.

$$F\left(d,\Delta,\mu_0,\mu\right)=\sum_{k=0}^{\infty}F_k\left(d,\mu_0,\mu\right)x_{in}^{k}\left(\Delta\right). \qquad (1)$$

This work gives an overview of the numerical technique [1] recently proposed for computing partial intensities. It is based on the invariant imbedding method applied to the electron transport problem. It is shown that the partial intensities satisfy Riccati and Lyapunov equations, which are solved numerically in the discrete ordinate space by using the backward differential formula. The computed partial intensities are compared to those found by the straight line approximation, the small-angle approximation and the Oswald-Kasper-Gaukler model. The performance of the proposed method is significantly higher than that of Monte-Carlo methods with the similar accuracy.

The method is applied to computations of REELS and PES for a set of samples. A good agreement is obtained between simulated spectra and measurements. It is shown that a unified approach for REELS and PES gives a framework for extracting and validating DIIMFP data [2].

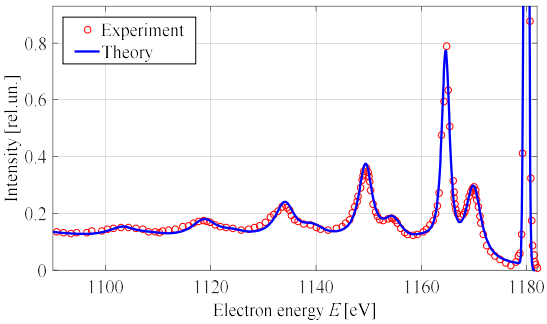


**Figure 1. Comparison of experimental REELS spectra from Ref. [3] of Al with calculated spectra. The primary electron energies is 1180 eV; the average relative difference is 6.0%.**

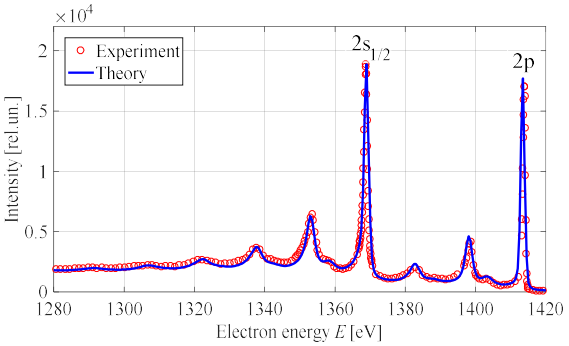


**Figure 2. Comparison of the experimental PES spectrum [4] for Al. The average relative discrepancy is 7.8%.**

**References**

1. V. Afanas`ev, D. Efremenko, P. Kaplya, JSERP **210** (2016) 16.
2. V. Afanas`ev, A. Gryazev, D. Efremenko, P. Kaplya, Vacuum. **136** (2017) 146.
3. S. Tougaard, I. Chorkendorff, Phys. Rev. B **35** (1987) 6570.
4. J. Moulder, et.al, Handbook of X-Ray Photoelectron Spectroscopy, 1995.

Email: pavel@kaplya.com

# Reflection Electron Energy Loss spectra of Highly Oriented Pyrolytic Graphite: role of anisotropic structure in plasmon excitations

**Martina Azzolini [1,2,*], Tommaso Morresi [1,2], Giovanni Garberoglio [1], Lucia Calliari [1], Yangbo Zhou [3], Hongzhou Zhang [3], Kerry Abrams [4], Nicola Stehling [4], Robert C. Masters [4], Cornelia Rodenburg [4], Nicola M. Pugno [2, 5, 6], Simone Taioli [1,7], Maurizio Dapor [1]**

*[1] European Centre for Theoretical Studies in Nuclear Physics and Related Areas (ECT*-FBK) and Trento Institute for Fundamental Physics and Applications (TIFPA-INFN), 38123 Trento, Italy*
*[2] Laboratory of Bio-Inspired and Graphene Nanomechanics, Department of Civil, Environmental and Mechanical Engineering, University of Trento, 38123 Trento, Italy*
*[3] School of Physics and CRANN, Trinity College Dublin, Dublin 2, Republic of Ireland*
*[4] Department of Materials Science and Engineering, University of Sheffield, Sir Robert Hadfield Building, Mappin Street, Sheffield S1 3JD, UK*
*[5] Ket-Lab, Italian Space Agency, Via del Politecnico snc, 00133 Rome, Italy*
*[6] School Engineering and Material Science, Queen Mary University of London, Mile End Road, E1 4NS, London, UK*
*[7] Faculty of Mathematics and Physics, Charles University, Prague, Czech Republic*

Carbon materials are attracting attention in electronics due to their outstanding physical properties. The large anisotropy in electric conductivity was already known in 1939 [1]. Graphite shows an uniaxial layered structure: the plane structure is characterized by a $sp^2$-hybridized lattice bonds. Along the plane graphite shows a small band gap and thus a higher conductivity, than in the direction normal to the surface.

In this work, we present different Monte Carlo calculations of Reflection Electron Energy Loss spectra (REELS) of Highly Oriented Pyrolytic Graphite (HOPG), in order to investigate the role of the anisotropic structure in plasmon excitations. The simulated spectra are compared with experimental data obtained in our laboratories [2].

In our model, elastic scattering between electrons and target atoms is treated with the Mott theory [3], which is based on the solution of the Dirac equation in a central field. Inelastic interactions between primary beam electrons and the electron cloud of the target result in excitation of bulk and surface plasma oscillations. An accurate description of the electron energy loss is provided by the dielectric theory developed by Ritchie [4]: the key quantity for the calculation of the inelastic cross section is the Energy Loss Function (ELF), defined as the imaginary part of the inverse of the dielectric function $\varepsilon(q, W)$, with $q$ the transferred momentum and $W$ the energy transferred during the inelastic interaction.

In our case the dielectric function was calculated in the optical limit ($q = 0$) with a full ab initio approach. Given the anisotropic structure of graphite, the dielectric function was calculated in the two main directions: q parallel to the vector c (normal to the layer direction), which accounts for inter-planar interactions, and with q perpendicular to c, which describes intra-planar excitations. The ELFs, obtained with the two dielectric functions, were fitted with the Drude—Lorentz relation in the optical limit, then the plasmon energies were expanded to momenta different from zero with a dispersion law developed in the Random Phase Approximation [4]. In Monte Carlo simulations, we modeled the anisotropic structure in three ways. In the *1st model* the electron energy loss, after an inelastic interaction, was evaluated considering only the in plane interaction [2]. The inclusion of intra-planar interaction was realized in the *2nd model*, where a linear combination of the ELFs was considered [6], by using a fixed parameter *f*. After a series of tests, it was found that setting the parameter *f* equal to 0.8, the correct influence of each component in REELS is reproduced. In the *3rd model* the linear combination of the ELF function was realized by using two functions which depend both on a fixed parameter ($f = 0.8$) and on the direction of the electron trajectory. In Fig. 1 the REEL spectra obtained with these different models are compared with experimental data.

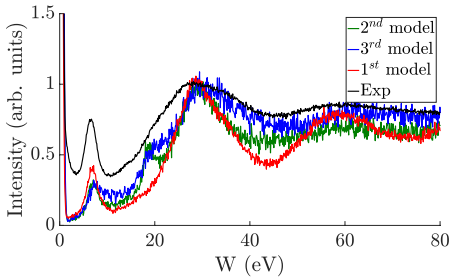


**Fig. 1: REELS of Graphite, electron beam energy was set equal to 1000 eV.**

The inclusion of inter-planar interactions (*3rd model)* leads to a closer agreement between simulated and experimental data, in particular for energy-loss values higher than 35 eV. For lower energy-loss values, surface plasmon excitations affect the spectrum: their contribution was also included in another Monte Carlo simulation [7]. Finally, the three models were applied to obtain secondary electron emission spectra and results are compared with available experimental data.

**Acknowledgments**
*N.M.P. is supported by the European Research Council PoC 2015 "Silkene" No. 693670, by the European Commission H2020 under the Graphene Flagship Core 1 No. 696656 (WP14 "Polymer Nanocomposites") and under the FET Proactive "Neurofibres" No. 732344. M.D., G.G., and S.T acknowledge funding from the Graphene Flagship (WP14 ``Polymer composites", no. 696656). This work used the ARCHER UK National Supercomputing Service (http://www.archer.ac.uk). Access to computing and storage facilities owned by parties and projects contributing to the National Grid Infrastructure MetaCentrum provided under the programme "Projects of Large Research, Development, and Innovations Infrastructures" (CESNET LM2015042), is greatly appreciated (https://www.metacentrum.cz/en/). Furthermore, we acknowledge FBK for providing unlimited access to the KORE computing facility. C.R. was funded by EPSRC (EP/N008065/1). Y.Z. and H.Z. acknowledge support from the Royal Society (grant No: IE140211).*

**References**

[1] K. S. Krishnan et al., Nature **144**, (1939) 667.
[2] M. Azzolini et al., Carbon **118**, (2017) 299.
[3] N. F. Mott, Proc. R. Soc. London Ser. **124**, (1929) 425.
[4] R. H. Ritchie, Phys. Rev. **106**, (1954) 874.
[5] H. Nikjoo et al., CRC Press, 2012.
[6] M. Dapor et al., Nucl. Instr. and Meth. in Phys. Res. B **255**, (2007) 276.
[7] D.G.F. David et al., Applied Surface Science **273**, (2013) 607.

* E-mail: mazzolini@ectstar.eu

# Very low energy STEM / TOF system

**B. Daniel,* T. Radlička, J. Piňos, L. Frank and I. Müllerová**
*Institute of Scientific Instruments of the CAS, v.v.i., Královopolská 147, 61264 Brno, Czech Republic*

Scanning low energy electron microscopes (SLEEMs) have been built at ISI for more than 25 years, either by modification of available SEMs, or completely self-built [1]. High resolution imaging is possible even below 100 eV electron landing energy, and in principle the energy can be decreased down to 0 eV. A more recent development is the use of a detector for transmitted electrons (TE) for samples below 10 nm thickness, i.e. ultrathin films and 2D materials like graphene or $MoS_2$. These TE detection capabilities will be enhanced even further with the completion of a new UHV SLEEM with a time-of-flight (TOF) energy analyzer optimized for electron energies below 100 eV.
Measurement of TE energy is expected to be helpful in better understanding of electron interactions with solids, which get increasingly complicated at low energies due to strong interaction with the density of states. The additional information allows comparison of more data for testing of simulations, which are being developed by partners at TU Vienna. The system is also expected to yield results regarding the electronic inelastic mean free path at low energies.

The TOF system, shown in the lower part of Figure 1, consists of a 630 mm magnetically shielded drift tube with two focusing electrodes to increase the acceptance angle up to 20°. The detector is a 40 mm active diameter MCP stack with copper mesh in front and a single channel metal anode mounted behind. A time-to-digital converter is used for signal timing and acquisition.
Beam pulsing with 1 ns pulse length is achieved by beam deflection with respect to a strip aperture and an octupole deflector inside the electron gun. After considering pulse length, flight path length variations and detector resolution, the energy resolution of the system will be about 1 eV at 35 eV electron energy. The lateral resolution is expected to be below 30 nm at 100 eV, including the decline caused by the active blanking system.

The SLEEM system will also have another new detector for enhanced detection of on- and near-axis electrons. Due to the implementation of the cathode lens principle for beam deceleration close to the specimen, secondary electrons are accelerated back towards the electron source. At very low landing energies this causes most of the electrons to escape though the 300 micron bore in the commonly used YAG scintillator above the specimen. While a smaller bore would reduce this signal loss, the resulting reduction of the field of view is too much of a drawback.
To detect not just these secondary electrons, but also 180° backscattered electrons, a magnetic filter has been incorporated into the gun, which deflects the electrons towards a MEDIPIX pixel detector. The use of a position sensitive detector allows not just angular sensitivity for the near-axis electrons, but also has, due to magnetic deflection, a rough capability for energy measurement that allows separation of backscattered and secondary electrons.

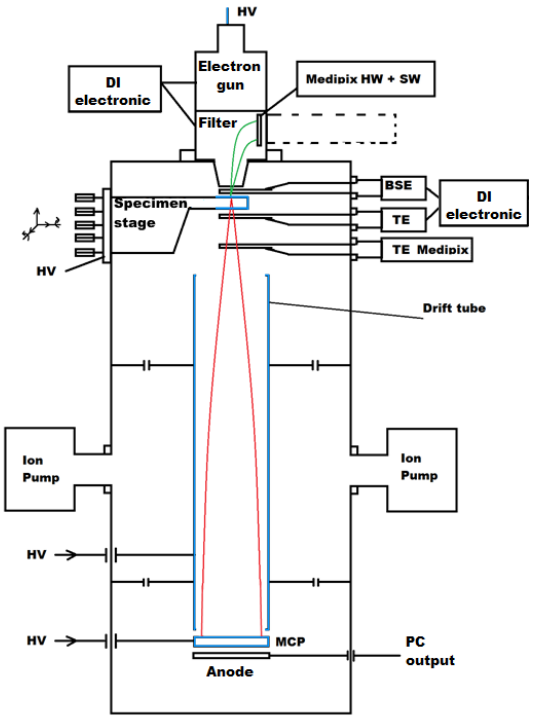


**Figure 1. Schematic view of the UHV system with paths of transmitted and reflected electrons towards the new detectors.**

## References

[1] I. Müllerová and L. Frank, Adv. Imaging Electron Phys. 128 (2003), p. 309-443.

The research was supported by SIMDALEE2 (Marie Curie FP7-PEOPLE-2013-ITN Grant # 606988) and CAS (RVO:68081731).

E-mail: bdaniel@isibrno.cz

# Electron Motion in the Electrostatic Field in the Near-Field Emission Electron Microscope

**Martin Oral[1,*], Wolfgang Werner[2], Tomáš Radlička[1], Jiří Zelinka[1], Danilo Pescia[3], Urs Ramsperger[3], Gabriele Bertolini[3]**

*[1]Institute of Scientific Instruments of the CAS, Královopolská 147, Brno, Czech Republic*
*[2]Institut für Angewandte Physik, TU Vienna, Wiedner Hauptstraße 8-10/134, Vienna, Austria*
*[3]Laboratorium für Festkörperphysik, ETH Zürich, Auguste-Piccard-Hof 1, Zürich, Switzerland*

**Synopsis:** We calculated the electrostatic field in a near-field scanning electron microscope (NFE). We developed code for calculation of electron trajectories in that field and incorporated it into an electron-solid interaction simulation program, resulting in a better understanding of signal formation in the instrument.

The geometry of the NFE scanning electron microscope comprises a sharp conductive tip placed a few nanometres above the essentially planar sample (Fig. 1). The tip apex curvature radius is a few nanometres. There is also an electron detector a few tens of millimetres away from the tip. The detector is at a positive potential with respect to the sample to attract signal electrons propagating from the sample past the repulsive part of the field near the tip. We used the first-order finite element method (FEM) to calculate the electrostatic field of the set-up. For now the field is assumed rotationally symmetric, simplifying its calculation, but it still allows for a realistic study of the phenomena involved in signal creation, as trajectory calculations are three-dimensional (Fig. 2).

The geometry presents a challenge for accuracy and precision of field calculation due to the disproportional sizes and distances of the individual electrodes (the tip, the sample, and the detector). The triangular elements are extremely small near the tip apex, where the electric field is strongly spatially dependent. The elements expand gradually further from the tip. The ratio between edge sizes of the largest and the smallest elements is about $10^6$. We used GMSH [1] to create the mesh for the geometry. We applied the Galerkin method together with the preconditioned biconjugate gradient method to solve for the values of the electric potential in the nodal points of the mesh.

For the calculation of electron trajectories we utilized our experience in charged particle optics, where the required lateral accuracy in the particle positons is in tens of picometres for trajectories a metre in length. We used the Runge-Kutta method via the GNU Scientific Library [2] to solve the equation of motion. It is possible to easily switch the variant of the RK method; we used the 4-5$^{th}$ order one, as it makes a good compromise between calculation speed and accuracy. The field interpolation in 3-D space from the mesh values is the critical and the most demanding part of the implementation which we based on an improved method from paper [3].

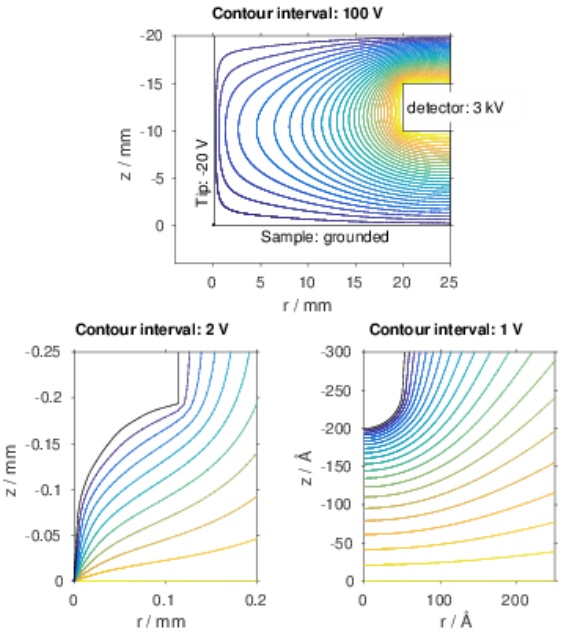


**Figure 1: The geometry of the NFE microscope and the equipotentials of the calculated field with different magnifications of the tip apex area.**

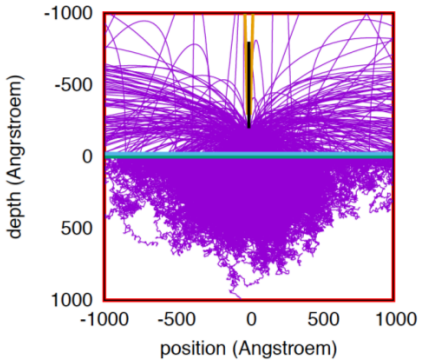


**Figure 2: Electron trajectories in the NFE microscope shown in a projection containing the tip axis. The sample is electrically conductive. Some of the secondary electrons generated in the sample, possibly after a few re-entries from vacuum into the solid and back, eventually make their way through the retarding field around the tip and hit the detector.**

## References

[1] GNU Scientific library, https://www.gnu.org/software/gsl
[2] GMSH, http://gmsh.info
[3] J. Chmelík, J. E. Barth, Proc. of SPIE **2014** (1993) p.133

*E-mail: oral@isibrno.cz

# Application of the Bandpass Filter for Secondary Electrons in SEM

**F. Mika and I. Konvalina**
*Institute of Scientific Instruments of the CAS, Královopolská 147, Brno, Czech Republic*

Through-the-lens secondary electron detector (TLD) works as a bandpass energy filter in a field emission gun SEM Magellan 400. To regulate the detected energy window the special setup of electrode potentials inside the objective lens and the positive potential on the specimen is needed [1]. During energy filtering, image contrast is changed and new information about the material can be observed [2]. Setup and functionality of the filter were successfully proved on the sample with different metal stripes made on silicon substrate [3].
We will continue and focus on another application of the filter. Help to explain image contrast between differently doped areas of semiconductor structures observable with the TLD detector. Experiments were performed on n-type doped patterns of the dopant concentration $1\times10^{19}$ $cm^{-3}$, made on an p-type Si substrate (dopant concentration $1\times10^{15}$ $cm^{-3}$). Fig. 1 shows how the different detection window of secondary electrons influenced the image contrast between heavily doped area and silicon substrate. In non-filtered secondary electron image with TLD detector (fig. 1A) n-type semiconductor is darker then p-type. This agrees with generally known theory [4]. In filtered TLD image we observe even the contrast inversion. For detected energy window 1eV to 2 eV n-type is brighter then p-type (see fig. 1B). For detected energy window 2 eV to 4 eV n-type is again darker then p-type (see fig. 1C). This very first experiment confirms that, the contrast strongly depends on energy of detected secondary electrons. For better understanding of this phenomenon further investigation with different dopant concentration and dopant types of semiconductor is needed.

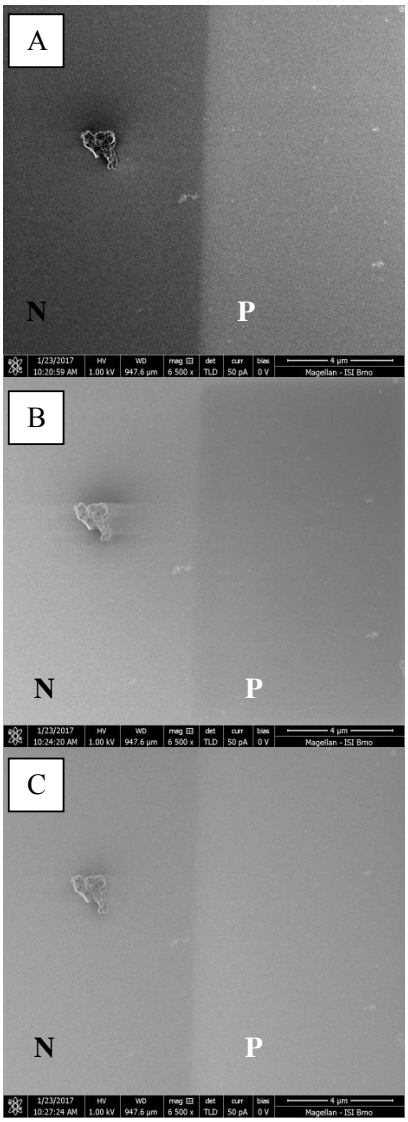


**Figure 1. N-type doped patterns (concentration $1\times10^{19}$ $cm^{-3}$) on an p-type silicon substrate (concentration $1\times10^{15}$ $cm^{-3}$). (A) Non-filtered TLD image. (B) Filtered TLD image; detected energy window is 1 eV - 2 eV. (C) Filtered TLD image; detected energy window is 2 eV - 4 eV.**

## References

[1] Konvalina I., et al., 15th International Seminar on Recent Trends in Charged Particle Optics and Surface Physics Instrumentation, Brno (2016), p. 28-29.
[2] Kazemian P, et al., Ultramicroscopy 107 (2007), p. 140-150.
[3] Mika F., et al., 15th International Seminar on Recent Trends in Charged Particle Optics and Surface Physics Instrumentation, *Brno* (2016), p. 36-37.
[4] Perovic, D. D., et al., Field - Emission SEM Imaging of Compositional and Doping Layer Semiconductor Superlattices. *Ultramicroscopy*. 1995, no. 58, p. 104-113.
[5] The work is supported by the TA CR (TE01020118),MEYS CR (LO1212), its infrastructure by MEYS CR and EC (CZ.1.05/2.1.00/01.0017) and by CAS (RVO:68081731).

E-mail: fumici@isibrno.cz

.

# Creation of entangled electrons by scattering at surfaces

Roland Feder* and Herbert Gollisch
*Theoretische Festkörperphysik, Universität Duisburg-Essen, 47048 Duisburg, Germany*

For two or more particles, entanglement of the wave function is a fundamental feature of quantum mechanics with the counterintuitive consequence that it is not possible to attribute a complete set of properties to each of the particles. This feature is at the root of currently most active theoretical and experimental research in fields like quantum computing, quantum cryptography and teleportation.

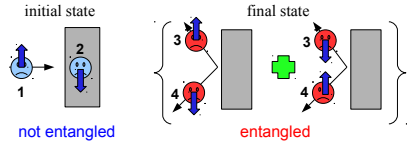


FIG. 1: Electron-induced emission of entangled electron pairs from a crystal surface.

In the following, we deal with the creation of an entangled state of two freely propagating electrons. Formally, entanglement here means that the two-electron wave function cannot be expressed as a single antisymmetrized product of two one-electron wavefunctions. As illustrated in Fig.1, such state can originate from screened Coulomb scattering of a free low-energy electron of definite spin with an opposite-spin electron bound in a crystalline surface, in a so-called (e,2e) process (cf. [1] and references therein). The numbers 1 to 4 next to the electron symbols stand for energy $E_n$ and surface-parallel momentum $\vec{k}_n^{\parallel}$ with n=1 to 4. The corresponding one-electron states are $|n\sigma_n\rangle$=$|n\rangle|\sigma_n\rangle$, where $|n\rangle$ stands for the spatial part $|E_n, \vec{k}_n^{\parallel}\rangle$, and $|\sigma_n\rangle = |\pm\rangle$ is a Pauli spinor.

The initial two-electron state is a single antisymmetrized product of the incoming and valence one-electron states $\frac{1}{\sqrt{2}}(|1\sigma_1\rangle|2\sigma_2\rangle - |2\sigma_2\rangle|1\sigma_1\rangle)$, i.e. not entangled. In the antiparallel-spin case we define $\sigma$ : $=\sigma_1=\pm$ and $\bar{\sigma}$ : $= -\sigma=\sigma_2=\mp$. The final two-electron state then has the form

$$\frac{f}{\sqrt{2}}(|3\sigma\rangle|4\bar{\sigma}\rangle - |4\bar{\sigma}\rangle|3\sigma\rangle) - \frac{g}{\sqrt{2}}(|3\bar{\sigma}\rangle|4\sigma\rangle - |4\sigma\rangle|3\bar{\sigma}\rangle), \quad (1)$$

where $f$ and $g$ are direct and exchange transition matrix elements. Consisting of two linearly independent antisymmetrized products, it is entangled. A quantitative measure of this entanglement is the von Neumann entropy

$$S = -|\tilde{f}|^2 \log_2 |\tilde{f}|^2 - |\tilde{g}|^2 \log_2 |\tilde{g}|^2, \quad (2)$$

where $\tilde{f}$=$f/(\sqrt{|f|^2+|g|^2})$ and $\tilde{g}$=$g/(\sqrt{|f|^2+|g|^2})$. S ranges from 0, if $f$ or $g$ vanish, to the maximal value 1, which is obtained if $f=\pm g$. For $f$=$g$, the final state is easily seen to become the paradigmatic Bell singlet state.

With regard to experimentally studying entanglement in (e,2e), we note that measuring spin-spin correlations and employing Bell type inequalities is beyond present-day technology. Instead, we consider the spin polarization $P$ of the electrons, which leave the surface in one direction (say 3 in Fig.1), if the primary electrons are polarized normal to the reaction plane with $\sigma_1$=$\pm$,

$$P = \sigma_1(|f|^2 - |g|^2)/I \quad \text{with} \quad I = |f|^2 + |g|^2, \quad (3)$$

where the total intensity $I$ is the (e,2e) reaction cross section. $P$ is closely related to the entropy $S$ since both are functions of the transition matrix elements $f$ and $g$. In particular, in the equal energy case ($E_3$=$E_4$) with $f$=$g$, we have the maximal entanglement $S$=1 associated with $P$=0.

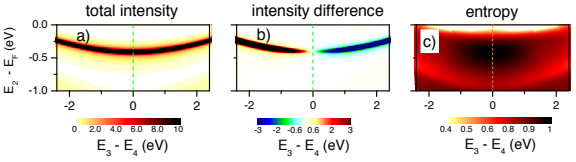


FIG. 2: (e,2e) from Cu(111): total intensity $I$, difference between spin-up and spin-down intensities ($|f|^2$−$|g|^2$) (cf.eq.3) and entanglement measure "von Neumann entropy" (cf.eq.2) as functions of valence electron energy $E_2$ and difference of the energies of the emitted electrons.

In Fig.2 numerically calculated results are shown for the Cu(111) surface, which exhibits an sp-like surface state close to the Fermi energy. This state with its parabolic dipersion is seen to manifest itself strongly in the (e,2e) intensity in Fig.2a. The difference between spin-up and spin-down intensities ($|f|^2$−$|g|^2$) in Fig.2b and thence the spin polarization $P$ (cf. eq.3) is characterized by crossing through zero at $E_3$=$E_4$. The entropy, which has the maximal value 1 for $E_3$=$E_4$, is seen in Fig.2c to remain very strong in the vicinity.

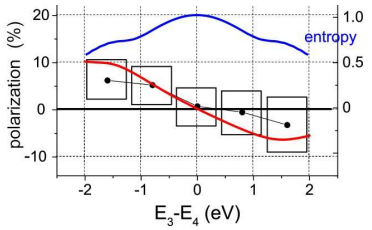


FIG. 3: (e,2e) from Cu(111): experimental spin polarization (fat dots with uncertainty rectangles) [2] and theoretical $\frac{1}{4}P$ (eq.3) (red curve) and entropy $S$ (eq.2) (blue curve) averaged over valence energy interval [-1 eV, $E_{Fermi}$].

Experimental spin polarization data are seen in Fig.3 to agree well with theory in exhibiting the zero crossing at equal energies, around which the entropy S is close to 1, which means strong entanglement.

## References

[1] R. Feder et al., Phys. Rev. B **92**, 075420 (2015).
[2] D. Vasilyev et al., Phys. Rev. B **95**, 115134 (2017).
*) **E-mail**: theophys.du1@online.de

# On the relevance of plasmon assisted generation of secondary electrons

**A. Bellissimo,[1,*] A. Ruocco,[1] M. Sbroscia,[1] S. Iacobucci,[2] G.M. Pierantozzi[1] and G. Stefani[1]**

*[1]Dipartimento di Scienze, Università Roma Tre, via della Vasca Navale 84, 00146 Roma, Italy*
*[2]CNR, Istituto Struttura della Materia c/o Dipartimento di Scienze Università Roma Tre, Italy*

**Synopsis** Time correlated electron-electron spectroscopies (e,2e) play a relevant role in establishing importance of collective excitation to the generation of secondary electrons. In particular, the relevance of spatially delocalized energy loss processes in the localized secondary electron generation is investigated. A progress report on recent results on Al(100) and HOPG is given by this communication.

Secondary electrons greatly enhance or damp crucial features of several technological devices, such as high power microwave amplifiers or charged particle detectors, just to name a few. In spite of the interest in controlling a phenomenon known from well over a century, the mechanisms responsible for secondary electron emission under charged particle bombardment are not yet fully clarified. In solids, one of the most efficient channels of electron impact energy transfer is the excitation of volume or surface plasmons. Electron-electron coincidence experiments, (e,2e), are one of the most complete ways to investigate plasmon creation and decay mechanisms[1]. Plasmon decay via interband transitions was proposed in the late 70's and recently more complex decay mechanisms have been elaborated. Two mechanisms for plasmon decay have been foreseen: the excitation of nearly free secondary electrons and the excitation of a pair of correlated free electrons[2]. In competition with these two channels, the ejection of a secondary electron due to direct scattering within a medium described by its inverse dielectric function has been proposed[3]. To establish the relative relevance of these secondary electron generation channels is of importance to many branches of fundamental and applied science but direct experimental evidences supporting either model are lacking.

The Roma Tre group has been aiming to this target by performing (e,2e) plasmon assisted experiments on Al[4,5] and Be[6] clean surfaces. The experiment on Al, performed correlating in time the energy loss suffered by a 2p photoelectron, excited by an AlKα, with secondary electrons in the 0 to 12 eV range, proposes that observed secondary electrons are emitted via a mechanism similar to photoemission with the plasmon decay playing the role of photon absorption. The experiment performed on Al at 500 eV[7] proved that surface plasmon decay accounts for roughly a quarter of the secondary electron spectrum. The recent experiment on Be[6] points to plasmon resonant (e,2e) processes as a relevant channel for secondary electron generation by plasmon decay. (e,2e) investigations on both Al and Be strictly associated a specific energy lost to the sample, with a well determined momentum transferred, with secondary electrons charecterised by well determined kinetic energy and linear momentum. The high degree of correlation existing between the two final electrons (i.e. full conservation of energy and vector momentum) can be described only via a direct coupling of the collective electron excitation (plasmon) with a single electron-hole pair of the solid valence band. This plasmon resonant channel competes with direct electron-electron impact generation of secondary electrons[8]. The Be experiment[5] performed at constant binding energy of the single particle initial state, clearly shows that the plasmon resonant channel dominates over the direct impact one in generating secondary electrons. Further support to a model that implies an integral transformation (energy and momentum) of a spatially delocalised collective excitation (plasmon) in a localized individual electron-hole pair (secondary electrons) is provided by the relevance of the bound electron density of states to the coincidence differential yield (energy and momentum) of secondary electrons. Here we present recent results on Al(100) and HOPG, obtained by a novel multichannel (e,2e) apparatus[9], that support validity of a single vertex interaction model for generation of secondary electrons in the range 0-20 eV.

**Acknowledgments** "Financial support by the FP7 People: Marie-Curie Actions Initial Training Network (ITN) SIMDALEE2 (Grant No. PITN 606988) is gratefully acknowledged"

1. F.J. Pijper and P. Kruit, Phys. Rev. B **44**, 9192
2. G.A. Bocan and J.E. Miraglia, Phys. Rev. A **71**, 024901 (2005)
3. K.A. Kouzakov and J. Berakdar, Phys. Rev. A **85**, 022901 (2012)
4. W.S.M. Werner, et al. Phys. Rev. B **78,** 233403 (2008)
5. A. Ruocco, et al. Phys. Rev. B (2017) in press
6. G. Di Filippo, et al. Phys. Rev. B **94**, 155422 (2016)
7. W.S.M. Werner, et al. Appl. Phys. Lett. **99**, 184102 (2011)
8. A. Liscio, et al. Phys. Rev. B **77,** 085116 (2008)
9. A. Ruocco et al. (2017) in preparation

[*]E-mail: bellissimo@fis.uniroma3.it

# Measurements of electronic structure of insulators

**V. Astasauskas[1], W. S. M. Werner[1], P. Kuksa[1], J. Pseiner[1], H. Kalbe[1], A. Bellissimo[2]**
*[1]Vienna University of Technology - Vienna (Austria)*
*[2]Università Roma Tre - Rome (Italy)*

It has been previously shown that it is possible to determine the band parameters of insulators using a combination of single-electron and two-electron spectroscopy. [1] A number of insulators [Calf Thymus ssDNA, CaF2, IRGANOX, SiO2, PMMA, Kapton, PE] has been measured with Reflection Electron Energy Loss Spectroscopy (REELS) and Secondary Electron-Electron Energy Loss Coincidence Spectroscopy (SE2ELCS).

SE2ELCS spectroscopy allows one to observe secondary electron spectra in coincidence with the energy loss of the primary electron. The onset of coincidences (i.e. the energy loss for which correlated electron pairs start to appear) determines the minimum energy required to promote an electron from the top of the valence band to the vacuum level. Since the energy gap (i.e. the energy difference between the valence band maximum and the conduction band minimum) can be measured with electron energy loss spectroscopy, the combination of these methods allows to determine the electron affinity. The onset of coincidences is equivalent to the maximum energy of a correlated electron pair.

The band gap and electron affinity of the above mentioned insulators have been measured. A deconvolution algorithm has been applied to the REELS spectra to acquire the optical constants of the materials. [2] It was found that the optical constants of organic insulators are very similar. Inelastic mean free path of the materials were calculated from the optical constants.

**Acknowledgement**

Financial support by the FP7 People: Marie-Curie Actions Initial Training Network (ITN) SIMDALEE2 (Grant No. PITN 606988) is gratefully acknowledged

**References**

[1] S. Samarin et al, Measurements of insulator band parameters using combination of single-electron and two-electron spectroscopy, 129 Solid State Commun 389-393 (2004)

[2] Wolfgang S.M. Werner et al, Simple algorithm for quantitative analysis of reflection electron energy loss spectra (REELS), 604 Surf. Sci 290-299 (2010)

E-mail: astasauskas@iap.tuwien.ac.at

# SIMDALEE2017 Abstracts

# Friday, September $22^{th}$

# Low-secondary electron emission yield of polarized surfaces

**I.Montero, L. Olano, M.E.Dávila, I.Bretos, L. Calzada, R. Jiménez,**

*Instituto de Ciencia de Materiales de Madrid (ICMM), CSIC. Calle Sor Juana Inés de la Cruz 3. 28049-Madrid. Spain.*

**Synopsis** Secondary electron emission properties of metal/polyimide were studied under different temperature and surface polarizations.

Research on low secondary electron emission coatings is essential for the design and manufacture of space high-power RF devices without multipactor discharge. This electron avalanche phenomenon appears for a determined power, frequency and electrode or wall distance and may destroy a RF equipment working in vacuum. Research on low-secondary electron emission surfaces is essential for the design and manufacture of space high-power RF devices. The electron multiplication due to high secondary electron emission yields (SEY) from a dielectric surface is one of the main causes for the multipactor. This effect induces not only discharging but also excess surface heating, leading to localized surface melting caused by excess electron bombardment. For this reason, SEY at high temperature is important for understanding the actual electron discharge process. The SEE yield of platinum coated polyimide (a super-heat resistant polyimide film produced from biphenyl tetracarboxylic dianhydride monomers), and anti-multipactor coatings, such as rough silver (Fig.1) and graphene carbon coatings having low-SEE yields, were measured in the SEY laboratory of CSIC. SEY can effectively be determined by continuous (total dose 42.5 nC/mm$^2$) and pulsed (1.1 fC/mm$^2$/pulse) electron irradiation methods. In this pulsed method one single pulse is used for each primary energy. The pulse time is 180 ns. The macroscopic behavior of the induced inner polarization in the polyimide was investigated by SEY measurements. The difference of intrinsic SE emission coefficients depending on the orientation was studied. The upward polarization "domains" show a lower SE emission ability. The results indicate that the total SE emission of this metal/polyimide can be altered by changing the bulk polarization, which provide an avenue for device design with this kind of materials. The time-dependent electron emission process from Pt/polyimide was clarified with the help of exciting electron pulses of variable duration. The electron emission of Pt/polyimide was strongly influenced by the electric field distribution on the sample surface. The time-resolved analysis gives insight into the SEY results and the polarization switching in the system.

**References**

[1] I.Montero, L.Aguilera, M.E.Dávila, V.Nistor, L.Galán, D.Raboso, Applied Surface Science, 291 (2014) 74.
[2] I. Bretos, R. Jiménez, C. Gutiérrez-Lázaro, I. Montero, and M. L. Calzada, Applied Physics Letters, 104 issue3 (2013) 091105.
[3] E. Bronchalo, Á. Coves, R. Mata, B. Gimeno, I. Montero, L. Galán, V. E. Boria, L. Mercadé, E. Sanchís-Kilders, IEEE Transactions on Electron Devices, 63 (2016) 3270.

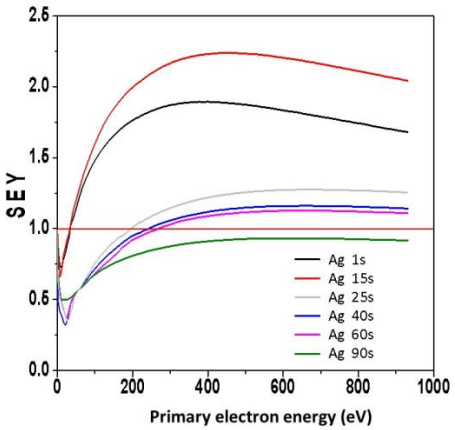


**Figure 1. Low-SEY silver coatings under different surface treatment conditions. SEY as a function of the primary electron energy.**

E-mail: imontero@icmm.csic.es

# Measurement of electron backscattering yield at low incident energies

**M. Belhaj,[1,*] S. Dadouch,[1] Th. Gineste[1], J. Puech[2]**
*[1] ONERA-the French Aerospace-Lab , 31055 Toulouse, France*
*[2]CNES, 31055 Toulouse, France*

The backscattering electron yield (BSEY) is defined as the number of emitted backscattered electrons (BSEs) to the number of incident electrons. The knowledge on BSEY at low incident electron energy is needed in many applications (electrons spectroscopy, electron microscopy, modeling of plasma walls interactions, modelling of the multipactor effect in RF hardwars, etc.). Unfortunately, the BSEY experimental data at relatively low incident energy (< 1 keV) and for a quite scarce variety of incident angles . Therefore, we have recently developed a simple and useful original technic to measure the BSEY. A schematic sketch describing the basic principle of the method is given in Figure 1. The sample was grounded and a metallic plate surrounding it was negatively biased. The negative isopotential generated by the metallic plate retract back to the sample surface electrons emitted with low energies (secondary electrons: SEs). Only electrons with energies higher than 50 eV (conventionally BSE) could be emitted. One important advantage of this experimental arrangement is that the negative isopotential acts as a shield against low energy tertiary electrons generated by BSE on the tank. Indeed, the tertiary electrons could disturb the measurement if they are collected by the sample. In the present configuration, the energy cut-off was set to approximately to 15 eV and not 50eV. Electrons emitted with a lower energy than 15eV were repelled to the sample as it is attested by the energy distributions of the emitted electrons shown in the Figure 2. Indeed, the SEs peak vanishes progressively when the negative metallic plate bias is increased. The BSEY yield as function as the incident electron energy is deduced from the measurement of the sample current and the incident current as BSEY= $(I_0-I_S)/I_0$. An example of the BSEY measured on silver sample as function of the incident energy and incidence angle is shown also in Figure 3. The incidence angle of 0° correspond to electron beam normal to the surface.

The aim of our contribution is to present this BSEY measurement technic to discuss its capabilities' and limits. New results on a variety of electrical conductive samples will be also presented

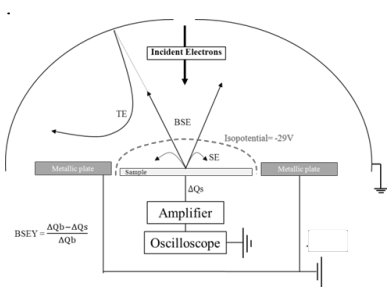


**Figure 1. Experimental setup and measurement principle .**

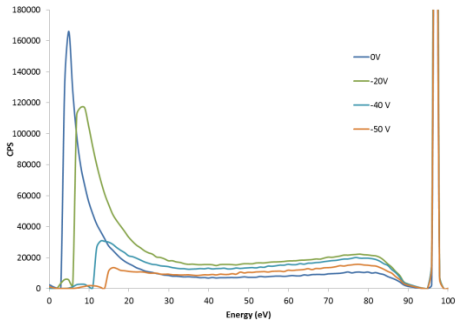


**Figure 2. Energy distribution of the emitted electrons under 100 eV electron irradiation as function of the ring bias.**

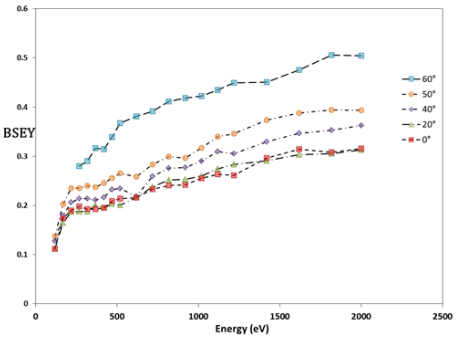


**Figure 3. BSEY of silver as function of electron the incidence energy and incidence angle .**

E-mail: Mohamed.Belhaj@onera.fr

# GEANT4 Study of the effect of the surface roughness on the Secondary Emission Yield

**C. Inguimbert[1], J. Pierron[1], M. Raine[2], M. Belhaj[1], J. Puech[3]**
*[1]Onera, 2 av. Edouard Belin Toulouse, France*
*[2]CEA DAM DIF, Bruyères-le-Châtel Arpajon, France*
*[3]CNES, 18 av. Edouard Belin Toulouse, France*

## Synopsis

The goal of this paper is to provide a better understanding of low energy Electron Emission Yield (EEY) thanks to some Monte Carlo simulations [1-3].
As it is well known, the secondary emission yield is closely dependent on the surface properties, such as contamination, oxidation, roughness or surface morphology [4-6]. The aim of this work is to study the effect of surface morphology on the EEY by simulating the transport of low energy electrons [ev, keV] in 3D geometries including surface structures.
For that purpose the GEANT4 [3] toolkit has been improved to allows the transport of low energy electrons down to few eV. GEANT 4 is a C++ toolkit assembled by an international collaboration, for describing radiation interaction with matter [3]. The low energy electron transport model MicroElec [7] of the open access code Geant4 [3] was initially dedicated to the transport in silicon target down to 16 eV. For the purpose of the study of secondary electron emission, the MicroElec module has been extended down to ~ 10 eV for silicon, aluminum and silver target materials. The model has been validated for aluminum, silver and silicon from 10 eV to 2 keV by means of comparisons with experimental measurements of EEY performed in an ultrahigh vacuum facility on Ar-etched samples [4, 8].
An application using a fully parameterized geometry allowing the simulation of the transport of low energy electrons in 3D surface structures of different shapes (rectangular or groove patterns) has been developed.

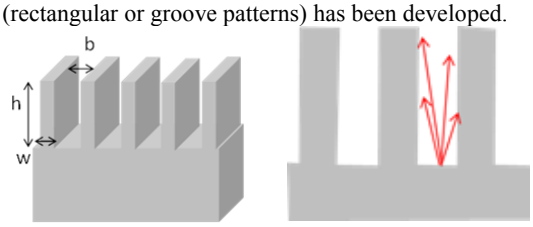


**Figure 1. Shape of the 3D geometrical structure used in the Monte Carlo simulations**

In this work, a sample is modeled by a bulk volume capped with four small customizable rectangular patterns periodically located to simulate the roughness. The shape parameters of these structures (height *h*, width *w* and distance b between two patterns (Figure 1)) have been varied and the effects on the EEY have been analyzed. The studied typical dimensions range from 20 nm up to 80 µm.
It is demonstrated that the surface asperities cause a decrease of the EEY due to electrons emitted near a rough area recrossing the surface (shadowing effects).

It is shown that the EEY is minimized when the ratio height over width is maximized.

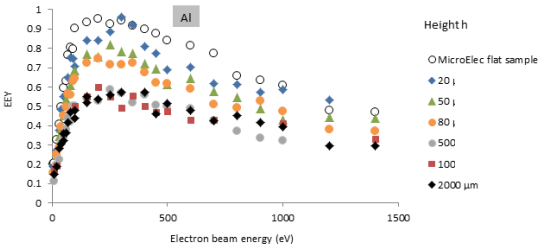


**Figure 2. EEY for a sample of aluminum with a surface with grooved patterns of width w=b=50 µm and different heights h of 0, 20, 80, 500, 1000 and 2000 µm.**

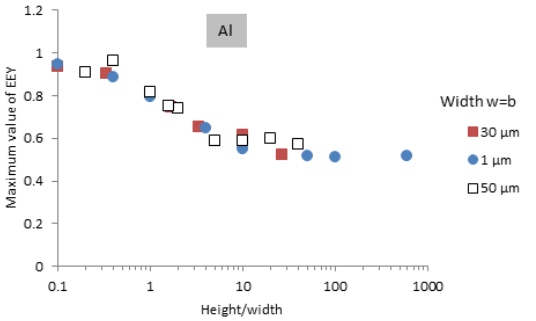


**Figure 3. Maximum values of the EEY for aluminum in function of the aspect ratio height/width for different widths w=b of 1 µm, 30 µm, and 50 µm..**

## References

[1] J. Roupie, O. Jbara, T. Tondu, M. Belhaj, and J. Puech, J. Phys. D. Appl. Phys., vol 46, no. 12, pp. 125306, Feb. 2013.
[2] J. Pierron, C. Inguimbert, M. Belhaj, M. Raine, and J. Puech, to be published in IEEE trans. Nucl Sci. 2017.
[3]Geant4[Online]: https://geant4.web.cern.ch/geant4/
[4] T. Gineste, M. Belhaj, G. Teysedre, and J. Puech, Appl. Surf. Sci., vol. 395, pp.398-404, Dec. 2015.
[5] C. Inguimbert, J.Pierron, M. Belhaj, and J. Puech. (2016, July). "Extrapolated range expression for electrons down to ~10 eV". Presented at IEEE NSREC conference.
[6] K. Nishimura, T. Itotani, and K. Ohya, Jpn. J. Appl. Phys., vol. 33, no. 8, pp. 4727-4734, Aug. 1994.
[7] A. Valentin, M. Raine, J.-E. Sauvestre, M. Gaillardin, and P. Paillet, Nucl. Instr. Meth. Phys. B., vol. 288, pp. 66-73, Oct 2012.
[8] Pierron J. & al.2016 RADECS2016Conference Germany to be published in IEEE Trans.nuc. sci. 2017

E-mail: Christophe.Inguimbert@onera.fr

# TESCAN S8000G
## and novel Orage™ FIB column

*Anticipating the future, expanding your possibilities today*

TESCAN
PERFORMANCE IN NANOSPACE

### Orage™ FIB column: Prepare for the new level in sample preparation

- Next generation of Ga source FIB column and a guarantee of world-class quality in sample preparation
- Cutting-edge ion beam optics delivering improved resolution at low beam energies for damage-free ultra-thin TEM specimens
- High ion beam currents up to 100 nA enabling fast sputtering rates for maximum throughput and minimum time-to-result

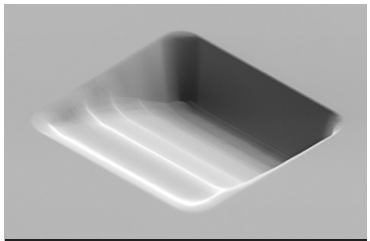

Cross-section 50 µm wide prepared with an ion beam current of 85 nA.

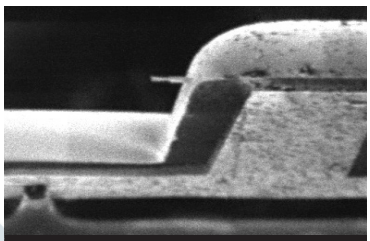

1 keV FIB image of a lamella on the TEM grid.

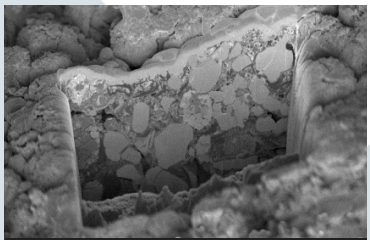

50 µm-long cross-section prepared in a Li-ion battery cathode.

A.P.E. Research
NANOTECHNOLOGY

# The company

Tools for Microscopy and Nanotechnologies

***...we are a dynamic company with over 15 years experience in ADVANCED INSTRUMENTATION for NANOTECNOLOGY***

**Since 1999 A.P.E. Research** is an SME active in the following sectors:

- design and developing of innovative SPM microscopes
- development of new methods in biology and physics based on use of probe microscopes
- development of scientific instrumentation for surface science physics
- development of new software for real-time microscopy

**A.P.E. Research has SPM customers in 10 nations (EUROPE and ASIA)**


## PARTNERSHIPS:

- **CNR IOM** former INFM – TASC
  From 1998 APE is an official Spin-Off company CNR
- **AREA Science Park**
- **Sincrotrone ELETTRA Trieste**
- **Università Trieste**
- **IISc Bangalore**

European Commission

**FP7 SIMDALEE2**

FP7-PEOPLE-2013-ITN Grant # 606988

MARIE CURIE ACTIONS

# SIMDALEE2017 Notes

# SIMDALEE2017 Notes

# Author index

Flamingo
HOTEL RESORT
Flamingo ★★★★ MarePineta ★★★ i Nidi ★★★★★

## HOTEL FLAMINGO RESORT

### PISCINA / SWIMMING POOL
12 Piscina adulti / Adult's pool
14 Piscina bambini / Children's pool

### RISTORANTI / RESTAURANTS
10 I Coralli
11 Le Lanterne
29 Wild Duck sul parco / Park restaurant pool

### BENESSERE / WELLNESS
3 Centro benessere / Wellness Centre Ippocampo

### SPORTS
2 Palestra / Gym
23 Mini Golf
24 Campo da tennis / Tennis couts

### SERVIZI
1 Parcheggi / Parking
5 Ricevimento / Reception
9 Bar
6 Boutique
7 Sala TV / TV Room
8 Centro congressi / Conference center
30 Anfiteatro / Amphiteatre
15 Sdraio / Sun-beds

### SPAZI VERDI / GARDENS
31 Parco di Eucalipti / Eucalyptus Park

### CAMERE / ROOMS
SUPERIOR
4 da-a / from - to 101-136

STANDARD
16 da - a / from - to 137 - 152
18 da - a / from - to 153 - 168
19 da - a / from - to 169 - 184
20 da - a / from - to 185 - 200
21 da - a / from - to 201 - 218
22 da - a / from - to 219 - 234

I NIDI
25 da - a / from - to 501 - 518
26 da - a / from - to 519 - 534
27 da - a / from - to 535 - 550
28 da - a / from - to 551 - 566

32 Villa Margherita
33 Villa Margherita II

## HOTEL MARE PINETA

### PISCINA / SWIMMING POOL
39 Piscina adulti / Adults' pool

### RISTORANTI / RESTAURANTS
44 - 45 Ristorante / Restaurant

### SPORTS
40 Campo da tennis / Tennis couts

### SERVIZI
41 Sala TV / TV room
42 Ricevimento / Reception
43 Bar
46 Ombrelloni / Beach umbrellas

### SPAZI VERDI / GARDENS
38 Pineto / Pinewood

### CAMERE / ROOMS
34 da - a / from - to 20 - 53
35 da - a / from - to 54 - 65
36 da - a / from - to 66 - 79
37 da - a / from - to 80 - 83

# Sources, Interaction with Matter, Detection and Analysis of Low Energy Electrons 2017 (SIMDALEE2017)

| | Monday<br>September 18th | | Tuesday<br>September 19th | | Wednesday<br>September 20th | | Thursday<br>September 21st | | Friday<br>September 22nd |
|---|---|---|---|---|---|---|---|---|---|
| | | 08:30 – 10:00 | 2.1 IMFP/SEY<br>**C.T. Chantler**<br>K.T. Arat<br>I. Mullerova | 3.1 SFM<br>**A. Schlenhoff**<br>J.P. Xanthakis<br>U. Ramsperger<br>C.J. Edgecombe | 4.1 PE<br>**G.Schoenhense**<br>A. Khursheed<br>A. Foelske-Schmitz | 5.1 SEY<br>**I. Montero**<br>M. Belhaj<br>C. Inguimbert | |
| | | 10:00 – 10:30 | **Coffee Break** | | | | | |
| | | 10:30 – 12:00 | 2.2 SEY<br>**R.Cimino**<br>V.Petit<br>P.Riccardi<br>A.M.M.G. Theulings | 3.2 Bio-nano<br>**A. Bass**<br>M. Sauer<br>H. Kalbe | 4.2 REELS/TEM<br>**P. Schattschneider**<br>F. Zheng<br>P. Kaplya<br>M. Azzolini | **Discussion** | |
| 12:00 – 13:00 | **Lunch** | 12:00 – 13:00 | **Lunch** | | | | | |
| 13:00 – 14:00 | **Free time** | 13:00 – 14:30 | 2.3 SPM<br>**L. Grill**<br>V. S. Milosevic<br>M.Lorenzo<br>B.J. Murdoch | **Excursion** | 4.3 SEM/INSTR.<br>B. Daniel<br>M. Oral<br>F. Mika | | | |
| 14:00 - | Start Registration | | | | | | | |
| 14:30 - 16:00 | SIMDALEE2-meeting | 14:30 – 15:00 | **Coffee Break** | | **Coffee Break** | | | |
| 16:30 -17:00 | **Welcome reception** | 15:00 – 16:30 | 2.4 COI<br>**F. O. Schumann**<br>A.H. Weiss<br>G. Rohringer | | 4.4 COI<br>**R. Feder**<br>A. Bellissimo<br>V. Astasauskas | | | |
| 17:00 - 17:10 | **Opening** | | | | | | | |
| 17:10 - 17:20 | **Welcome Address EC** | | | | | | | |
| 17:20 - 18:30 | **Plenary talk: E. Bauer** | | **Flash Poster Presentations** | | | | | |
| 18:30 – 19:30 | **Free time** | 16:30 – 19:30 | **Free time** | | | | | |
| 19:30 – 20:30 | **Dinner** | 19:30 – 20:30 | **Dinner** | | **Dinner** | | | |
| 20:30 – 22:30 | **Get together & Whisky degustation** | 20:30 – 22:30 | **Poster session** | **Conference Dinner** | | | | |